Soot Surface Growth Mechanisms in Stationary Combustion Systems

by

Scott Macadam

B.Sc. (Chemical Engineering), University of Natal (Durban), South Africa, 1991

M.S. (Chemical Engineering Practice), Massachusetts Institute of Technology, 1993

Submitted in partial fulfillment of the requirements for the degree of

DOCTOR OF PHILOSOPHY

at the

Massachusetts Institute of Technology

June 1997

Signature of Author _____

Department of Chemical Engineering
June 1997

Certified by _____

János M. Beér
Professor Emeritus of Chemical and Fuel Engineering
Thesis Supervisor

Certified by _____

Adel F. Sarofim
Lammot du Pont Professor of Chemical Engineering Emeritus
Thesis Supervisor

Accepted by _____

Robert E. Cohen
St. Laurent Professor of Chemical Engineering
Chairman, Committee for Graduate Students

Abstract

Due to their adverse effects on human health, both soot and polycyclic aromatic hydrocarbons (PAH) are classified as hazardous combustion-derived pollutants. Because of this, it is in our interest to develop combustion control strategies that minimize their formation. To meet this objective, it is imperative that we fully understand the chemical and physical processes controlling their formation in practical flames. This thesis comprises three projects that fall within the realm of soot and PAH formation : 1) soot surface growth mechanisms 2) the effect of flue gas recirculation on soot/PAH formation and 3) PAH isomerization reactions in pyrolytic environments.

In order to accurately model the formation of soot, it is necessary to understand the processes by which carbon is added to the surfaces of growing soot particles. The two pathways thought to be responsible for post-nucleation soot surface growth are i) acetylene (C_2H_2) addition and ii) PAH addition. However, there is some uncertainty as to which pathway is more dominant and which conditions favor each pathway. To empirically determine the relative contributions of acetylene and PAH to soot surface growth, soot was produced in a Jet-stirred/Plugflow Reactor (JS/PFR) under acetylene-rich and acetylene-lean conditions with ethylene (C_2H_4) as the fuel. The JS/PFR is an enclosed premixed flame combustor operated at atmospheric pressure and over a temperature range of 1400-1700K. Since PFR acetylene levels increase with fuel equivalence ratio (ϕ), an acetylene rich PFR environment was generated by operating the JSR at a high ϕ of 2.2. The acetylene lean environment was reached by operating the reactor slightly fuel rich (ϕ = 1.3) and injecting benzene into the PFR to enhance soot and PAH formation. The feed to the JSR was a ethylene/air/nitrogen stream and the two temperatures were chosen to be 1580K and 1650K.

Because of the relatively low acetylene concentrations in the ϕ = 1.3 + benzene experiments, the acetylene addition pathway was ruled out in favor of the PAH pathway for these cases. For the 1580K cases, the calculated soot/PAH collision efficiencies, or probablities of a collision resulting in a reaction, declined from 0.11 to 0.03 with increasing residence time (8 to 25 ms), while at 1650K they declined from 0.24 to 0.08. These calculations rested on the assumption that all the observed soot growth occurred via PAH addition alone. The apparent soot/PAH collision efficiencies for the acetylene rich cases were factors of 3-4 higher than those of the acetylene-lean cases. This was interpreted as an indication that, in the acetylene rich cases, the *apparent* soot/PAH collision efficiencies did not equal the *true* soot/PAH collision efficiencies i.e. the assumption that all soot growth occurred by PAH addition was not valid. This suggested that, in the acetylene rich cases, acetylene played a major role in the soot growth. In fact, it was found that it contributed towards 65-75% of the observed soot growth. Soot/acetylene collision efficiencies were found to decline from $5x10^{-4}$ to $3x10^{-4}$. The tendency of collision efficiencies to decrease with residence time was attributed to declining radical concentrations in the PFR.

The effect of flue gas recirculation (FGR) on soot and PAH formation was investigated. This was done by introducing flue gas diluents (nitrogen and carbon dioxide) into the JS/PFR feed and monitoring the effects of diluent *type* and dilution *rate* on soot/PAH levels. To maintain constant fuel equivalence ratios and temperatures, the feed was preheated to compensate for the thermal

effects of the different diluents. For a ϕ of 2.2 and at a temperature of 1580K, increasing the nitrogen dilution rate from 13.5% to 21% was found to decrease soot concentrations by 30% and PAH levels by 20%. This was attributed to the dilution of acetylene, the major PAH and soot growth agent. Substituting the 13.5% nitrogen dilution stream with a 5.5% N_2 + 8% CO_2 stream resulted in a 30% drop in soot levels at 1580K and a 45% drop at 1650K. This was confirmed by Chemkin modeling results which predicted lower PAH and acetylene levels for the case of CO_2 dilution. This was attributed to the reaction of CO_2 with H atom to yield CO and OH. Since OH is a significant hydrocarbon oxidizing agent, its higher concentrations resulted in lower acetylene, PAH, and soot levels. And since this reaction is endothermic, its effects are more noticeable at higher temperatures.

The pyrolysis of 2 and 3 ringed PAH follows three distinct steps : i) biaryl formation ii) cyclodehydrogenation (condensation) to form fluoranthenes and iii) internal rearrangements to form pyrenes. From the results of previous pyrolysis studies, the first two steps are reasonably well understood. The focus of this study was on the role of isomerization reactions in the distribution of the MW 302 and 352 compounds formed in the pyrolysis of naphthalene, anthracene, and phenanthrene. The motivation behind this study is the fact that since mutagenicity is compound specific, isomerization reactions may play a crucial role in the conversion of non-mutagenic species to mutagenic species.

A methodology was developed to qualitatively predict the relative distributions of the condensation products of the naphthyl-anthracene and bianthryl isomers. Both the relative concentrations of the biaryl precursors and steric effects were found to be significant. The latter effects were especially noticeable for the cases of non-planar molecules such as dibenzo[a,l]fluoranthene. Most of the biaryl condensation products (primary fluoranthenes) are believed to undergo Scott-Roelofs rearrangements to form secondary fluoranthenes, thereby almost doubling the number of fluoranthene pyrolysis products. Due to the relatively low energy barriers of this type of isomerization, concentrations were near their equilibrium levels. Using the most direct fluorathene-to-pyrene isomerization pathway, the various pyrene products were identified. The associated energy barriers were estimated by calculating thermodynamic properties for all species. These data were then used to determine the most favorable pathways in the pyrolysis of naphthalene/anthracene, naphthalene/phenanthrene, anthracene/phenanthrene, anthracene, and phenanthrene. In this way, the most probable pathways which convert two and three ringed PAH to various mutagenic six ringed PAH were identified.

Thesis Supervisors : János M. Beér, Professor Emeritus of Chemical and Fuel Engineering

Adel F. Sarofim, Lammot du Pont Professor of Chemical Engineering Emeritus

Acknowledgments

During the course of my 5.3 years at MIT I had the opportunity to meet and interact with a long list of remarkable people, most of whom deserve my heartfelt thanks.

I was incredibly fortunate to have had such supportive and considerate thesis supervisors. Professor Adel Sarofim, with his brilliant intellect and concern for others, was a constant inspiration, both on a personal and an academic level. Professor János Beér, was both incredibly understanding and a useful resource when it came to practical combustion issues. I am grateful to both my thesis advisors for giving me the independence to tackle issues I thought were interesting and for steering me in the right direction when my rudder wasn't functioning. My thesis committee members also deserve a special mention. Professor Jack Howard, a valuable councilor in all matters related to soot and PAH, always responded to my questions in a thorough and timely fashion. Professor John Longwell, the inventor of the Jet-stirred/Plugflow Reactor, was of enormous assistance when I needed help with the reactor.

My education at MIT would be incomplete without the wealth of experience I gained from working with others in the combustion group. The person who deserves the most thanks is Carlo Procaccini, a fixer of computer problems; teacher of fluid mechanics, electronics, applied math, Italian history, and other applied disciplines; and fellow caffeine addict and practical joker. Giovanna Gambi, with her friendliness and wonderful sense of humour, was a pleasure to work with. She taught me a great deal about optical diagnostics, HMMS's, and Neapolitan slang. I was also lucky to have worked with two *diplomarbeiter* from the University of Karlsruhe, Germany. Arne Hoffmann and Cord Manegold were both incredibly motivated individuals who were willing to spend long hours in the lab to obtain the results we sought. Other 66-053 and 66-153 inhabitants who made my life more bearable include Dr. Angelo Kandas, Dr. Alex Diaz, Dr. Jon Allen, Lt. (Dr. to be) Bill Grieco, Dr. Mike Masonjones, Dr. Guido F. Sacchi, Dr. (Prof. to be) Chris Pope, Dr. (to be) Tim Benish, Dr. (to be) Matt DiPippo, Dr. (to be) Joanna DiNaro, Dr. (to be) Brian Phenix, Dr. Shakti Goel, Dr. Henning Richter, Dr. Hiroshi Saito, Dr. (to be) David Kronholm, and Dr. Rich Shandross.

I am indebted to Emmi Snyder, Bhengy Jackson, Craig Abernathy, and Kathy Brownell for taking care of things on the administrative side. Tony Modestino was invaluable whenever lab equipment needed to be found/replaced/fixed/moved/removed. I am also grateful to the Core Lab people (Art Lafleur, Elaine Plummer-Turano, Koli Taghizadeh, and K.C. Swallow) for their analytical expertise and extraordinary ability to detect and quantify so many of the unpleasant yet interesting compounds we made in the reactor. Thanks also go to Lenore Rainey for her TEM analyses of my soot samples.

I would like to mention a few of the many Ashdown folk I met during my earlier years at MIT. They include : Paul Fieguth, who taught me all I know about character building; John Keen, taught me all I know about organizing ski-trips; Stefan ter Haar, taught me all I know about the virtues of organic food and the strengths/weaknesses of the German auto industry; and Rob Pensalfini, taught me all I know about crustaceans that live on asteroids.

I thank my parents Joe and Gail Macadam as well as my sister Dawn Gubb for their undying support and encouragement, despite the 8,000 mile gap between us. After many years working with soot, I can now tell my father that his son has the credentials to qualify as a chimney sweep.

Finally, for their financial assistance, I would like to acknowledge the EPA Center on Airborne Organics, the Electric Power Research Institute (EPRI), Ente Nazionale per l'Energia Elettrica (ENEL), and the National Institute of Environmental Health Sciences (NIEHS).

Table of Contents

List of Figures

List of Tables

Chapter 1. Introduction

1.1 Problem Statement

Two centuries after the start of the industrial revolution, combustion systems remain a significant source of undesirable air pollutants. From a health effects standpoint, one class of compounds which has created a great deal of concern are the PAHs (polycyclic aromatic hydrocarbons) since the results of numerous studies have indicated that many of these compounds are significant mutagens and carcinogens. A related issue is the fact that polycyclic aromatic hydrocarbons are typically produced with and deposited on carbonaceous particulates or soot. Not only are particulates themselves possible mutagens but they aggravate the problem by playing an active role in the transport of the PAH into the lungs, and as a result increase the likelihood of the species inducing mutations.

If society decides to remain committed to using fossil fuels to meet so much of its energy needs, it has to take steps to reduce emissions of hazardous compounds such as PAH and soot. To meet this objective, we have to improve our understanding of the processes controlling the formation of these species since any improvement in our knowledge puts us in a stronger position to develop effective combustion control strategies.

In order to improve our understanding of the *chemical* aspects of soot and PAH formation, it is advantageous to study soot/PAH formation under conditions where mass transfer effects are minimal. This is due to the fact that mixing phenomena increase the degree of complexity of the soot and PAH formation processes and make it difficult to assess the roles of the various precursor species. Thus, from an experimental standpoint, it is more desirable to study soot and PAH formation under the homogeneous conditions of a premixed flame than

under the conditions of a diffusion flame. Therefore, the experimental strategy selected for this study was one which entailed the production of PAH and soot in a near isothermal, unidimensional premixed flame combustor. Although most practical burners rely on diffusion flame combustion, there are regions in the post flame zones of these combustors that display a similarity to premixed flames. The most relevant example is the case of homogeneous fuel-rich pockets found downstream of fuel-lean diffusion flames that not only resemble fuel-rich premixed flames but are important sources of PAH and soot. This is especially true for situations where imperfect mixing or rapid flue gas cooling prevents the fuel-rich, soot/PAH containing pockets from undergoing sufficient oxidation.

With regard to the specific problem of soot surface growth, a great deal of uncertainty remains as to the precise mechanism by which carbon is added to the soot particles. The two viewpoints are i) acetylene (C_2H_2), due to its abundance in fuel rich flames and its ability to participate in the aromatic ring building process, is the major soot growth agent and ii) PAHs, due to their active role in soot nucleation, continue to act as surface growth agents once the nuclei are formed. If the relevant contributions of these two growth agents to soot surface growth under different conditions are known, existing soot and PAH models may be refined.

Of the various techniques used to reduce pollutant formation in combustion systems, one of the most common is flue gas recirculation (FGR). This is particularly relevant to the problem of NOx (nitrogen oxide) reduction. However, there are indications that i) FGR and ii) the addition of various diluents may also reduce soot and PAH formation. If this phenomenon is better understood, it increases the potential of FGR as an effective control strategy.

Like the soot formation process, the PAH molecular weight growth process may take place via two mechanisms i) the sequential addition of light hydrocarbons such as acetylene and ii) the combination of smaller PAH via aryl-aryl reactions into larger species. Since mutagenic

properties appear to be limited to specific PAH, it is in our interest to understand the mechanisms by which these specific PAH compounds are formed. These said species may be built up via the addition of light hydrocarbons or they may be formed via the rearrangement (isomerization) of other less harmful species. Any improvement in our understanding of how these isomerizations take place and where they are most applicable will be of value.

1.2 Objectives

The specific objectives of this thesis are :

1. Determine the relative contributions of acetylene (C_2H_2) and PAH to soot surface growth in an experimental combustor. The desire is to monitor soot formation in an environment where mass transfer and mixing effects are minimal, and to *empirically* determine the relative importances of C_2H_2 and PAH as soot growth agents.

2. Calculate collision efficiencies for soot/acetylene and soot/PAH interactions. This information will be valuable from a soot modeling standpoint since it can be implemented in kinetic models. Also, it will provide more quantitative information on the role of soot particles as a PAH sink.

3. For a fixed temperature and a fixed fuel equivalence ratio, determine the effects of diluent *type* and diluent *rate* on soot and PAH formation in the experimental combustor. This will allow us to gain an understanding of how flue gas recirculation (FGR) may suppress soot and PAH formation in large scale combustors.

4. Develop a methodology for estimating the relative adundances of the condensation products formed during the cyclodehydrogenation of biaryl species. The biaryls in question are the

products of naphthalene, anthracene, and phenanthrene pyrolysis. The methodology will be based on how steric and statistical factors affect the distribution of condensation products.

5. Identify the possible isomerization reactions which may convert biaryl condensation products (fluoranthenes) into other PAH species. Calculate energy barriers associated with the various reactions, and use that information to determine the most important pathways.

Chapter 2. Literature Review

Soot has been studied for well over a century. Of the early investigators, one of the most memorable was Sir Michael Faraday, the discoverer of benzene and the first to discover that the familiar yellow luminosity of flames is caused by radiation from soot particles. In a series of simple but enlightening experiments, he inserted wires (nowadays know as thermopheretic probes) into a candle flame to collect soot at different regions of the flame [Faraday 1988]. Innumerable papers have been published since then, yet many issues have remained unresolved to this day. McKinnon [1989] summarized this phenomenon by generating an interesting plot of the number of soot publications per year for the period 1962-1988. He noticed a sharp increase in the number of publications around 1980, which he attributed to the fuel shortage of that time. With renewed interest in synthetic fuels came the realization that their greater aromatic content meant greater sooting tendencies. On a more recent note, studies linking elevated particulate levels with mortality from respiratory and cardiovascular disease have put soot in the spotlight once again [Dockery *et al.* 1992, Samet *et al.* 1995]. Of most concern are the fine aerosol particles which are too small to be filtered or impacted in the human nasal passage and upper reaches of the lung and thus are able to penetrate the alveoli. Schwartz *et al.* [1996] suggest that particles less than 2.5 microns in diameter are specifically responsible for the observed associations with premature mortality. From atmospheric sampling, these fine aerosols appear to be made of *inter alia* aqueous droplets, organic droplets, and solid soot aggregates [Katrinak *et al.* 1995].

The field of soot formation has been reviewed periodically by various authors. These include Street & Thomas [1955], who summarized the literature of soot formation prior to that year; Palmer & Cullis [1965], who summarized the main experimental observations on carbon formation from gaseous fuels and included a survey of kinetic mechanisms; and Haynes &

Wagner [1980], who presented an updated review of soot formation as it occurs in premixed, diffusion, and spray flames as well as soot oxidation and the influence of additives. Traditionally research has been more focused on soot formation than on polycyclic aromatic hydrocarbon (PAH) formation. However, this has changed in the last 15 years, largely because of improvements in PAH identification and quantification techniques, and an increased interest in the health effects of mutagenic PAH species.

2.1 Combustion Systems

All experimental investigations into the soot and PAH formation processes have been based on the strategy of i) generating soot and PAH in a bench or pilot scale combustion system and ii) collecting samples for chemical analysis or using optical techniques for *in-situ* analysis. The following survey briefly reviews some of the experimental systems which have been used in these studies.

2.1.1 Laminar Flat Flames

In a pioneering study by Bonne, Homann, & Wagner [1965], a 20 torr laminar flat flame was sampled using a molecular-beam/mass spectrometry system. This allowed quantification of both stable and radical chemical species found in the acetylene, ethylene, propane, benzene, and ethanol flames studied. Concentration profiles were obtained for fixed gases, as well as light hydrocarbons and polyacetylenes up to $C_{12}H_2$. They observed that soot was first formed in the region where polyacetylene concentrations were high, and that the number concentration of soot particles was constant in the region where polyacetylene concentrations were fairly constant. This prompted them to claim that polyacetylenes played a vital role in soot formation.

In a later publication, Homann & Wagner [1967] included PAH in their growth scheme. They studied benzene flames and found a high concentration of PAH in the oxidation zone where soot first appeared. They concluded that PAH could add to "bulky reactive radical intermediates" in the oxidation zone, and proposed three classes of compounds important to carbon formation. These are 1) acetylene and the polyacetylenes 2) unreactive PAH without sidechains and 3) reactive PAH with sidechains. Thus, in the benzene flame, the class 3 compound scould add to the growing polyacetylene polymer.

Tomkins & Long [1969] studied acetylene/oxygen flat flames and characterized their measurements into three classes of compounds, namely total polymeric material, chloroform insoluable material, and chloroform soluable material. They found two distinct regions of PAH formation. The first was characterized by a sharp increase followed by a sharp decrease at the end of the oxidation zone. The second was in a region of the flame where the temperature was 1170K to 973K, and where PAH levels gradually increased. They concluded that the PAH formed in this second zone via the pyrolysis of residual acetylene. Because the PAH formed in the primary zone went through a maximum where incipient sooting occurred, they concluded that PAH may be important in the formation of soot.

Bittner & Howard [1981] used a molecular beam/mass spectrometry sampling system to study 20 torr benzene flames under non-sooting (ϕ = 1.8) and sooting (ϕ = 2.0) conditions. The mass spectrometer was operated as a high pass filter by collecting molecules above a certain cut-off mass (700 a.m.u.). They observed that the peak concentration for the high moleular weight material was two orders of magnitude higher in the sooting case than in the non-sooting case. Since the formation of soot is the balance between growth reactions and oxidation or destruction reactions, the high molecular weight material which forms at lower burner heights may not be completely destroyed passing through the oxidation zone and thus will form soot in the secondary zone. Another observation was the fact that lower molecular weight material peaked

at a lower position in the flame than higher molecular weight material, which suggests sequential growth of smaller compounds into larger compounds.

2.1.2 Flow Reactors

Early flow reactor studies concentrated on the pyrolysis of hydrocarbon fuels in an inert carrier gas. A great deal of work has been done in this area by Badger *et al.* [1958-67], but their studies were confined to temperatures below 973K, with long residence times. Hou & Palmer [1965] pyrolyzed diacetylene and benzene in a high temperature, atmospheric pressure reactor (up to 1523K) with residence times of 30-250 ms. It was found that the decomposition of diacetylene demonstrated a similarity to that of acetylene. The decomposition of benzene, however, appeared to be a mixed order reaction. This was attributed to the first order benzene decomposition due to wall effects and the second order combination of two benzenes to yield biphenyl and hydrogen.

2.2 Formation of Polycyclic Aromatic Hydrocarbons

2.2.1 Formation of the First Aromatic Ring

The importance of the first aromatic ring in PAH formation lies in the obvious role of benzene as a platform for further aromatic growth. This was demonstrated by Scully & Davies [1965] who concluded that aromatic fuels had a greater propensity to soot than non-aromatic ones. Furthermore, benzene was identified as the key bottleneck to overall molecular weight growth [Bittner 1981, Cole 1982]. For this reason, attention was directed toward identifying the aliphatic species which participate in benzene synthesis.

Cole [1982] initially proposed that this sequence occurs via the addition of acetylene to the 1,3-butadienyl radical (reaction 2.1). This was supported by the shock-tube work of Colket [1986] and the diffusion flame study of Bartok & Kuriskin [1988].

$C_4H_5 + C_2H_2 \Rightarrow$ (lin) C_6H_7 (reaction 2.1)

(lin) $C_6H_7 \Rightarrow$ cyclohexadienyl

cyclohexadienyl => benzene + H

Based on shock tube pyrolysis work, Frenklach *et al.* [1984, 1985] postulated the addition of acetylene to the vinylacetylene radical (reaction 2.2). This mechanism was supported by Harris *et al.* [1988] who found it to be the only route that could possibly account for their observed benzene synthesis rate in an atmospheric premixed C_2H_4/O_2 flat flame.

$C_4H_3 + C_2H_2 \Rightarrow$ (lin) C_6H_5 (reaction 2.2)

(lin) $C_6H_5 \Rightarrow$ (cyclo)C_6H_5

The third sequence (reaction 2.3) was proposed by Alkemade & Homann [1989], Stein *et al.* [1990], and Miller & Melius [1992]. In this mechanism, the formation of benzene takes place via the direct combination of two propargyl radicals :

$C_3H_3 + C_3H_3 \Rightarrow$ fulvene (reaction 2.3)

fulvene => benzene

2.2.2 The PAH Molecular Weight Growth Process

The acetylene addition hypothesis holds that sequential acetylene addition to aryl radicals is the key polymerization reaction responsible for the formation and growth of PAH and soot.

This idea was initially proposed by Frenklach [1983] and Frenklach *et al.* [1985] following their shock-tube pyrolysis studies. The hypothesis was supported by the results of several molecular beam/mass spectrometry probing studies [Bittner 1981, Cole 1984, Westmoreland 1986] and a quartz microprobe study [Smyth & Miller 1987]. Thus the acetylene addition mechanism has reached the status of a widely accepted pathway [Frenklach 1988], [Glassman 1987]. However, the precise mechanism by which acetylene attaches itself to an aromatic substrate has not conclusively been determined. Frenklach *et al.* [1984] asserted that PAH growth proceeded along the following pathway (reaction 2.4), regardless of the size of the aromatic substrate involved.

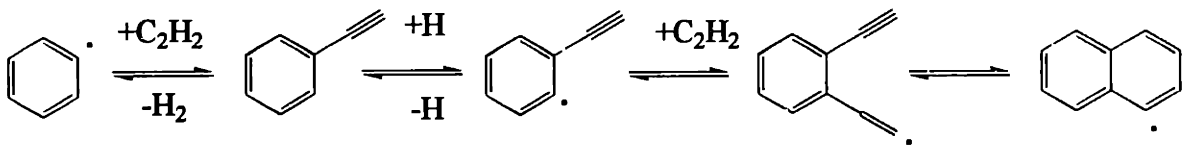

(reaction 2.4)

This mechanism has since been advanced as the dominant pathway for the buildup of aromatic species [Frenklach *et al.* 1986, Frenklach & Warnatz 1987, Brezinsky *et al.* 1988, Frenklach 1988, Harris *et al.* 1988]. An alternate route (reaction 2.5) was put forward by Bittner [1981] and Bittner & Howard [1981].

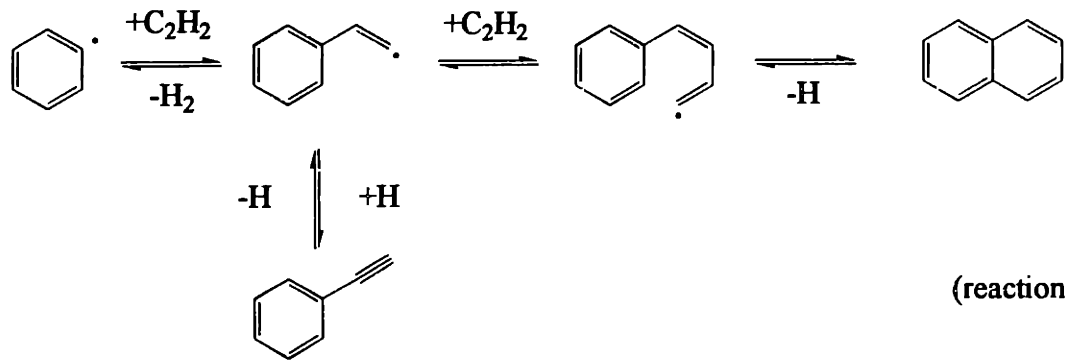

(reaction 2.5)

Frenklach *et al.* [1984] determined that reaction 2.4 is significantly faster than reaction 2.5. This conclusion was based on the notion that the first intermediate adduct (phenyl-CH=CH•) of the latter mechanism is so unstable that stabilization via loss of a hydrogen atom is faster than the C_2H_2 addition step. One would expect that the formation of a stable molecule followed by its reactivation by hydrogen atom abstraction would be slower than a radical-reactant interaction. However, in the case of consecutive reversible reactions such as these two sequences, this does not hold true.

Reaction 2.4 was applied to the growth of larger polycyclics, including fused ring compounds Frenklach *et al.* [1984]. The formation of pyrene via this route is represented by reaction 2.6.

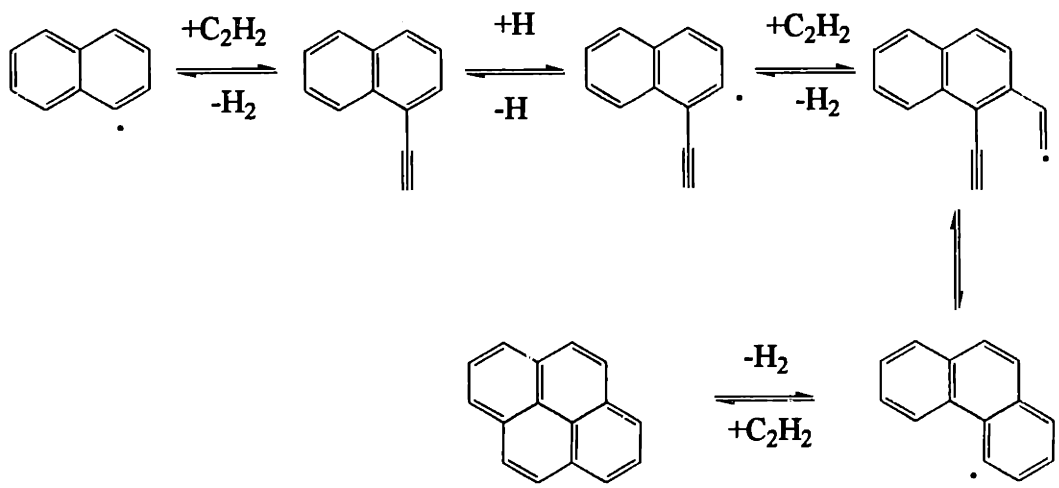

(reaction 2.6)

This mechanism may continue into the formation larger compounds such as anthanthrene and coronene. One characteristic of this addition sequence is that both radical and molecular intermediates are formed. Several molecular intermediates (e.g. acenaphthalene, pyrene, coronene) tend to have high thermodynamic stabilities, and fomation reactions which are

practically irreversible. They can therefore be considered unreactive sideproducts and are found in abundance in flame samples [Marr *et al.* 1992, Benish *et al.* 1996, Macadam *et al.* 1996].

2.2.3 Aryl-Aryl Reactions

This class of reactions encompasses PAH polymerizations such as dimerizations, trimerizations etc. [Badger 1965]. Dimerization reactions have been found to prevail in the pyrolysis of aromatics [Wornat *et al.* 1992, Mulholland *et al.* 1992, Mukherjee 1993, Masonjones 1995] and in the combustion of benzene [McKinnon 1989]. The significance of these reactions is the fact that they essentially bypass acetylene addition in the PAH molecular weight growth process, thereby providing a "short cut" to the formation of larger species. An example would be the combination of naphthalene and anthracene to form dibenzo [a,j]fluoranthene (reaction 2.7).

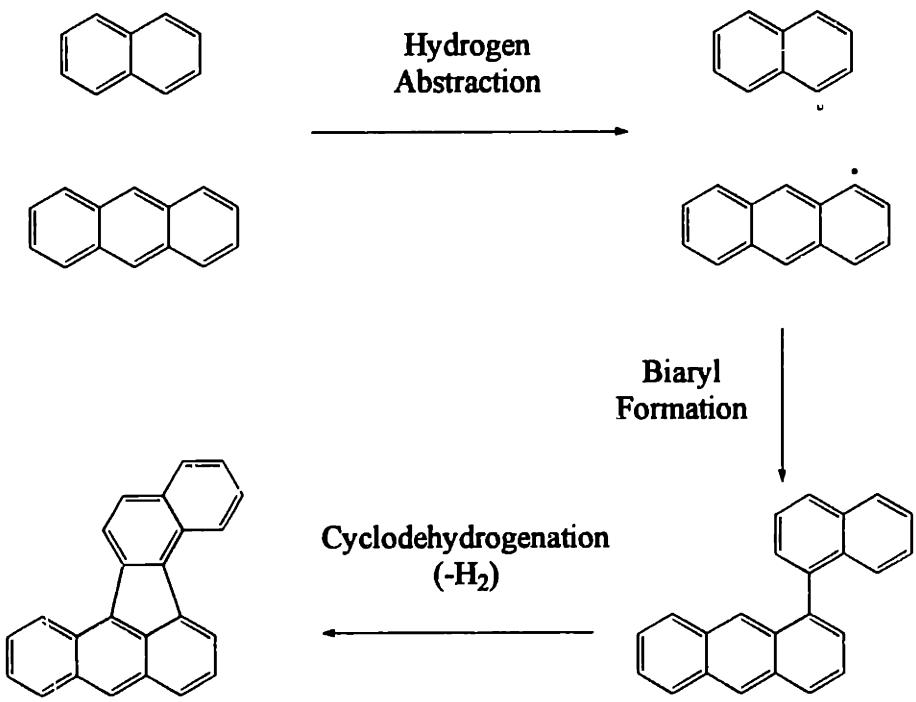

(reaction 2.7)

This sequence consists of i) aryl radical formation by hydrogen abstraction ii) radical-radical combination of the two aryl radicals iii) cyclodehydrogenation of the biaryl to form a dibenzofluoranthene. The latter step is a condensation reaction involving the loss of two hydrogen atoms and the formation of a five membered ring. Dimerization reactions may also be accompanied by acetylene addition, for example the phenanthrene formation sequence indicated by reaction 2.8.

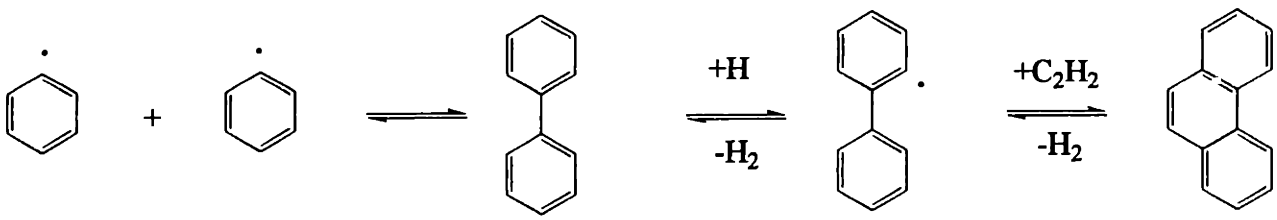

(reaction 2.8)

Aryl-aryl reactions are of particular importance in the formation of PAH > 500 amu. Due to the shear size of these molecules, there is some doubt as to whether their formation occurs by sequential acetylene addition since the number of steps (and length of time) involved is unrealistically high [McKinnon *et al.* 1992]. A one-step dimerization reaction, on the other hand, may lead to the formation of e.g. a 600 amu molecule from two 300 amu reactants. Another aspect of PAH polymerization is the fact that the polyarenes by nature have higher H/C ratios than the fused ring compounds resulting from acetylene addition. The H/C ratios observed for large PAH and young soot particles match polyarenes more closely than they do fused aromatics, and provide further support for the polymerization mechanism.

2.2.4 PAH Oxidation

Polycyclic aromatics are subject to oxidation by the various radical species present in the PFR environment, most notably OH. In his study of PAH oxidation by OH, Lam [1988] extended Vaughn's [1988] benzene oxidation pathway to polycyclics such as naphthalene, phenanthrene, and pyrene (reactions 2.9a - 2.9c).

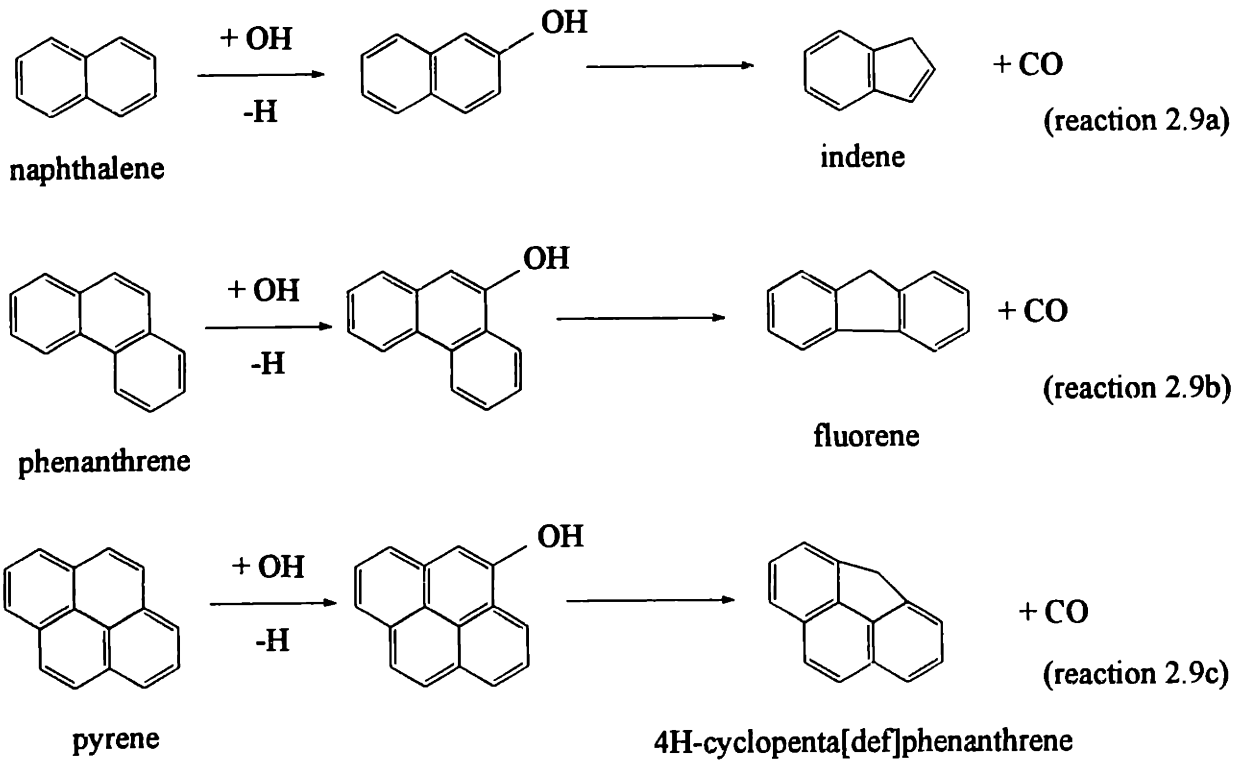

In these reactions, the hydroxyl radical displaces a hydrogen and then removes a carbon (in the form of CO) to leave behind a five membered ring. An alternative mechanism is the sequence proposed by Mauß *et al.* [1994] and Frenklach *et al.* [1994], in which OH fractures a

ring to leave an ethynyl group attached, which is in turn removed by further OH attack (reaction 2.10).

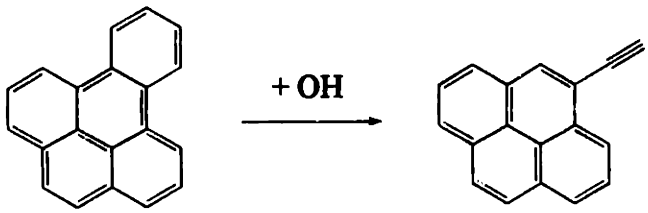

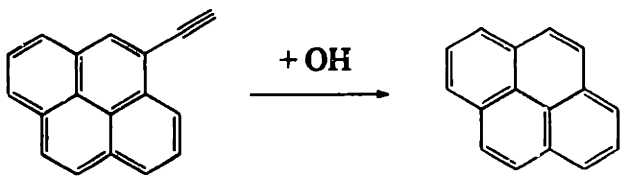

(reaction 2.10)

This ring removal sequence is essentially the reverse of the HACA addition mechanism.

2.3 PAH Isomerizations

Of the various classes of PAH isomerizations, one of the most throughly studied is the conversion of acephenanthrylene and aceanthrylene to fluoranthene [Scott & Roelofs 1987]. This four-centered rearrangement involves breaking one C-H and one C-C bond while forming one C-H and one C-C bond. This results in a five membered ring exchanging places with an adjacent six membered ring. Although kinetic data is lacking, thermodynamic calculations have shown that these reactions are equilibrated within the 15 ms residence time of the original PFR [Howard *et al.*

1995]. Based on experiments with C^{13} labeled benzene [Scott *et al.* 1987], naphthalene [Scott & Agopian 1977], and pyrene [Scott *et al.* 1982], Scott *et al.* concluded that PAH structures are rather flexible at flame temperatures. They in fact asserted that, at elevated temperatures, the conventional hexagonal representation of the benzene molecule is a simplification. A second type of PAH isomerization is the Stone-Wales [1986] four-centered rearrangement. This involves the concurrent breaking and forming of two C-C bonds, as is indicated by reaction 2.11.

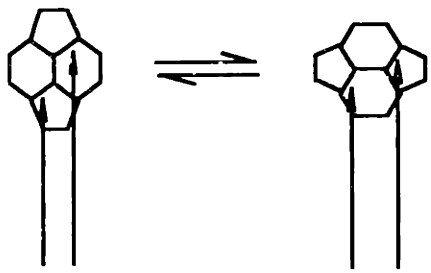

severed C-C bonds newly formed C-C bonds

(reaction 2.11)

This rearrangement is important in fullerene formation [Pope *et al.* 1993]. With regard to PAH's, its relevance lies in the fluoranthene-pyrene isomerization since a four centered Stone-Wales carbon-carbon shift is the step which directly converts an azulene compound to pyrene (after two consecutive Scott-Roelofs rearrangments convert fluoranthene through aceanthrylene to the azulene). This type of rearrangement is a relatively slow one. In fact Howard *et al.* [1995] demonstrated that the fluoranthene:pyrene ratio observed in PFR samples deviates from the equilibrium ratio by several orders of magnitude.

2.4 Soot Formation

2.4.1 Soot Nucleation

It is generally agreed upon that polycyclic aromatic hydrocarbons are active participants in the soot inception (nucleation) process. PAH formation has been found to preceed soot formation, and PAH concentrations decline rapidly as soot levels rise [Bonne *et al.* 1965, Homann & Wagner 1967, Bittner 1981, McKinnon & Howard 1992]. Since PAH molecules in the 500-800 amu size range are large enough for van der Waals attractions to be important [Pope 1988, Miller 1990], they may be held together long enough for chemical bonds to form. This process, termed reactive coagulation, may result in the formation of a 2000 amu molecule (or soot nucleus) following several PAH-PAH collisions [McKinnon & Howard 1992]. Several hypothetical soot precursor molecules which have been conceptualized by Howard [1990] appear in Figure 2.1.

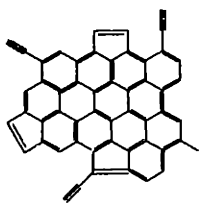

$C_{54}H_{18}$
666 g/mol
H/C = 0.33

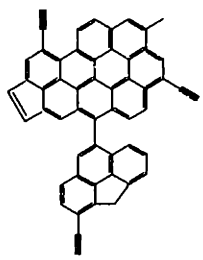

$C_{54}H_{24}$
672 g/mol
H/C = 0.44

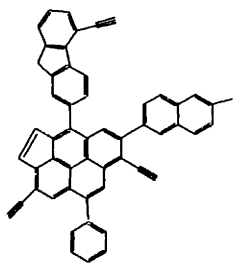

$C_{54}H_{30}$
678 g/mol
H/C = 0.56

(figure 2.1)

Harris and Weiner [1989] attributed soot nucleation to the coagulation of high molecular weight PAH molecules. They proposed that large PAH may be divided into three classes. Class

A contains molecules greater than 1000 amu, Class B is between several hundred and 1000, and Class C is smaller than several hundred. Due to high van der Waals forces, collisions between Class A and any other molecule can lead to sticking. Class B can stick to itself or Class A, and Class C can only stick to Class A. In their dynamic scheme, Class B molecules are scavenged from the system by collisions with themselves and Class A. These are the collisions which form soot nuclei. Once the Class B inventory is depleted, nucleation will stop but mass growth will continue as Class A molecules continue to scavenge Class C molecules.

The work of D'Alessio *et al.* has indicated that these large soot precursors may consist of many two or three ringed subunits joined together by aliphatic bonds. This is based on their observation that these high molecular mass structures display the same UV fluorescence properties as C2 compounds but, according to scattering measurements, have an average size of 2 nm (2500 amu) [D'Alessio *et al.* 1992]. Their results suggest that at higher residence times and C/O ratios, these structures undergo an internal rearrangement leading to particles with more condensed aromatic rings and with a more compact three dimensional shape. These newly created particles then serve as soot nuclei and begin to undergo surface growth.

2.4.2 Soot Surface Growth

Following nucleation, the infant soot particles react with surrounding hydrocarbons and further increase in size. This deposition of soot mass through the reactions of gaseous species with the soot particle surface is responsible for most of the soot mass growth [Haynes & Wagner 1982]. Experimental studies have shown that in the case of laminar premixed flames, the surface growth rate is proportional to the acetylene concentration [Harris & Weiner 1985], hinting that acetylene is the prime soot surface growth agent. Frenklach [1996] proposed that surface growth occurs via H-abstraction-C_2H_2-addition involving arm-chair sites on the soot surface (reaction 2.12).

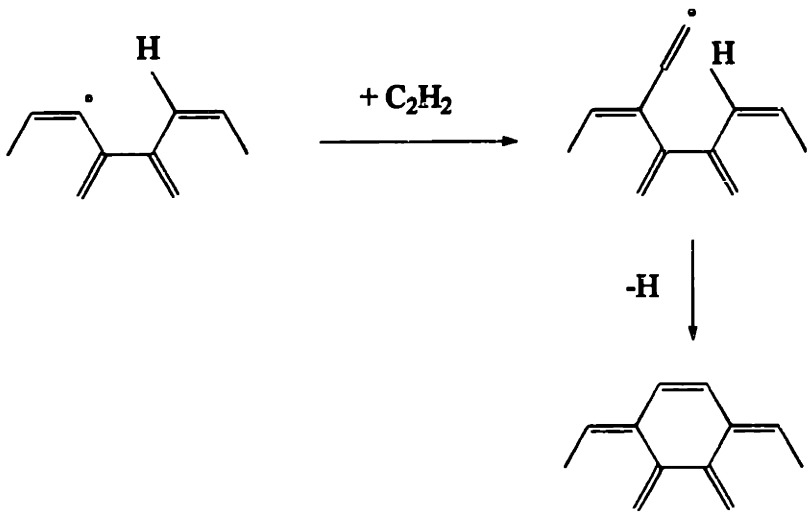

(reaction 2.12)

This mechanism continues until a new layer of aromatic rings is formed. In this way, sustained acetylene deposition results in the build up of the soot surface. Extensive experimentation has revealed that the specific soot surface growth rate decreases with residence time [Harris 1983]. This is described by the first order differential equation (equation 2.1)

$$\frac{df_v}{dt} = k_{sg} (f_{v\infty} - f_v) \qquad \text{(equation 2.1)}$$

where k_{sg} is a fitted surface growth rate constant and $f_{v\infty}$ is a fitted parameter representing the ultimate amount of soot formed [Wagner 1981]. The rate constant k_{sg} fits well to an Arrhenius form with an activation energy of 43 kcal/mol and an A factor of 1.56×10^7 s^{-1} [Baumgärtner *et al.* 1985]. The ultimate soot fraction has a maximum around 1600K [Böhm *et al.* 1988]. The declining specific rate constant is not believed to be a result of temperature changes in the flames. This suggests that the surface reactivity declines with age, possibly due to an "annealing" process which results in the loss of active sites [Woods & Haynes 1991]. However, Frenklach's [1996] modeling results indicated that the surface growth rate actually increases with time, provided the H atom concentration is constant. He therefore asserted that the observed decline in reactivity may (partly) be attributed to declining H levels.

The alternate surface growth mechanism involves direct PAH addition to the soot particles [Lam *et al.* 1988, Marr *et al.* 1994, Benish *et al.* 1996]. Although PAH concentrations in premixed flames are typically orders of magnitude lower than acetylene levels, soot-PAH collision efficiencies are orders of magnitude higher than soot-acetylene collision efficiencies. This compensates for the relatively low PAH levels, and suggests that PAH may play a significant role in surface growth, perhaps dominating it [Marr *et al.* 1994, Benish *et al.* 1996]. Soot-PAH collision efficiencies strongly depend on the density of radical sites on both the soot particles and the PAH molecules. Benish *et al.* [1996] proposed that PAH with five membered rings on their periphery more readily form radicals. This is based on the fact that the vinyl C-H bond dissociation energy is lower than that of the aryl C-H dissociation energies [Howard 1990]. This implies that PAH containing five membered rings are inherently more reactive surface growth agents.

2.4.3 Soot Particle Coagulation and Agglomeration

Carbon deposition from surface growth produces soot particles with final sizes in the 20-40 nm range [Palmer *et al.* 1965]. Samples taken from combustor systems as well as from the atmosphere have revealed that soot aggregates are composed of spherical primary particles linked together in chainlike structures, a result of particle agglomeration. A distinction may be made between coagulation and agglomeration. Coagulation refers to the process which occurs when two liquid droplets or two solid particles with high internal mobility collide to form a new particle. Due to their liquid-like properties, the parent particles lose their original shape. Agglomeration refers to the process where two solid particles collide and stick together but retain their original shapes. This is more likely true for older soot particles while coagulation would occur in the case of large PAH or young soot particles [Wagner 1980]. The effect of coagulation on the soot number density may be represented by the Smoluchowski equation (eqn 2.1) :

$$\frac{dN}{dt} = -k_c N^2 \qquad \text{(equation 2.1)}$$

where N is the soot number density and k_c is the coagulation rate constant. Prado *et al.* [1983] integrated this equation and found that, at sufficiently high soot volume fractions, the number density is independent of the initial value. Gay & Berne [1986] conducted a theoretical study to support the observation that particles can stick on collision. They found that the translational energy of the colliding particles can be dissipated as thermal energy in the lattice of the newly formed double particle. This calculation was done by computing the molecular dynamics of two clusters of 135 hard spheres each. Assuming that the spheres had Leonard-Jones potential surfaces, the simulation showed that the potential energy of the two separated clusters was rapidly converted to thermal energy. They contend that this energy accomodation can account for the high sticking efficiency seen in submicron aerosols.

2.4.4 Soot Oxidation

Fenimore & Jones [1967] studied the oxidation of soot by OH in a double-burner premixed ethylene flame. A lower burner produced a supply of soot which was then cooled, mixed with more oxidant, and burned out in a secondary burner. The OH concentration was determined assuming partial equilibrium of the reaction $O + H_2O = 2OH$. O concentrations were determined from the rate of $O + N_2O = 2NO$, where N_2O was added to the flame. The removal rate of carbon by OH was found to have a collision efficiency of 0.1. Page & Ates [1978] also found that OH was the main oxidizing agent of the soot produced in an ethylene flame and computed a collision efficiency of 0.25. Neoh [1980] conducted a careful study of the burnout rate of soot produced in a methane flame. H atom was measured by using an optical absorption method which involved doping the flame with lithium, see also Marr [1993]. O and OH were calculated assuming partial equilibrium. Of the possible oxidants (O, OH, O_2, H_2O, CO_2), it was found that only OH gave a reasonable collision efficiency (i.e. greater than unity). The reaction efficiency was found to be in the range 0.13-0.27. Higher in the flame, Neoh noticed that the soot particles began to break up. This was ascribed to less reactive O_2 having time to diffuse into the pores before reaction and then reducing the structural integrity of the spherule to the point of rupture.

2.5 Fluegas Recirculation

The recirculation of part of the fluegas (exhaust) stream exiting an industrial combustor has been proven to be an effective technique for reducing NO_x levels [Garg 1994, Das & Mathur 1993]. This is due to the fluegas lowering both the peak flame temperature and the average oxygen concentration. However, both fluegas recirculation and the introduction of certain diluents have been found to reduce soot levels in an oil burner [Cooper *et al.* 1964]. In this study, it was discovered that H_2O and CO_2 are more effective than N_2, Ar, and He at curtailing

soot formation. This was ascribed to the fact that the former two molecules are more effective third body colliders in radical-radical recombination reactions and therefore act to reduce the size of the radical pool. Since soot growth is so reliant on radicals and radical sites, a consequence of any radical pool depletion is a reduction in soot levels.

Haynes *et al.* [1982] investigated the influence of a series of gaseous additives on soot formation in premixed ethylene/air flames. They found that CH_4, C_2H_4, and CH_3NH_2 enhance soot formation while O_2, NO, NH_3, H_2S, SO_2, and SO_3 curtail it. However, none of the additives was found to affect either particle coagulation or the specific surface growth rate. Müller-Dethleefs & Schlader [1976] investigated the role of steam in carbon formation in premixed ethylene and propane flames. The heat released by the water vapor was found to partly offset the cooling effect of the steam, and a shift of the carbon limit toward higher C/O ratios was observed. The latter effect was attributed to OH (a direct product of H_2O decomposition) inhibiting soot formation. In their laminar diffusion flame study, Schug *et al.* [1980] mixed SO_2 ,CO_2, and H_2S with the fuel stream and used the smoke point to gauge sooting propensities. Although the diluents were found to be effective in reducing soot levels, these observations were attributed solely to the thermal effects of the diluents.

Chapter 3. Experimental Methodology

3.1 Jet-stirred/Plugflow Reactor

The Jet-stirred/Plugflow Reactor is a well characterized bench scale combustor operated at atmospheric pressure (Figure 3.1). It was developed by Nenniger and a complete description of its design and construction has been given [Nenniger 1983]. In its early years, the JSR was used to study PAH and soot formation with $C_2H_4/O_2/N_2$ and toluene/O_2/N_2 feed mixtures [Nenniger 1983]; and $C_2H_4/O_2/N_2$, C_2H_4/toluene/O_2/N_2, and C_2H_4/benzene/O_2/N_2 mixtures [Vaughn 1988]. Sun [1985] studied NO_x chemistry by adding NH_3 to the $C_2H_4/O_2/N_2$ JSR feed. More recently, soot and PAH formation in the PFR section has been investigated. Lam [1988] studied PAH and soot formation for fuel-rich $C_2H_4/O_2/N_2$ mixtures with and without benzene injection into the PFR, while Marr [1993] conducted a similar study with naphthalene injection. These experiments were made possible by incorporating a fuel additive vaporizer unit into the system. This unit, which permitted the injection of a prevaporized additive into the PFR, has subsequently been replaced by a portable vaporizer [Manegold 1995].

The Jet-stirred Reactor (JSR) is a toroidal shaped chamber cast out of alumina ceramic. This chamber has an outer diameter of 12 cm and a volume of 250 cm^3. Ethylene (Grade 2.5 supplied by BOC Gases), is premixed with laboratory air and diluent nitrogen at a point upstream of the JSR. All flowrates are set by rotameter control. The JSR temperature is measured by a Type R Pt-Pt/Rh thermocouple (Omega) placed within the chamber while a series of heating tapes around the feed line ensures a measure of control over the inlet temperature. The feed stream is introduced to the JSR through 32 stainless steel jets located around the periphery of the toroidal chamber. These jets are oriented at an angle so as to promote a swirling, well-mixed flow inside the reactor. This allows the JSR to be modeled as an ideal well-stirred reactor.

Under normal conditions, the JSR residence time is 6 ms. Upon leaving the JSR, the combustion gases pass through 8 exit ports and enter a flow-straightener which directs the flow 90° upwards into the PFR tube. Since earlier flow visualization studies revealed a spiral PFR flow pattern, the flow straightener was designed to eliminate the angular momentum imparted by the JSR. It is an 8 vane wheel which divides the flow into equally spaced sectors (Figure 3.2). It is machined from a 2.5 cm (height) x 5 cm (diameter) cylindrical plug of Zircar alumina and is inserted into the top section of the JSR. The PFR tube abuts the flow straightener, holding it firmly in place, thus completing the JSR-PFR transition.

The 50cm long plugflow reactor is comprised of 4 concentric alumina cylinders (Zircar AL-30). The length of the PFR was increased from its original 30cm to provide more residence time for the study of PAH and soot growth. The PFR is unique in that it emulates the post-flame zone of a premixed flat flame. It lends itself to kinetic studies due to its near-isothermal and plugflow-like characteristics. Lam [1988] took thermocouple measurments at various positions in the PFR to test the plugflow assumption. In these data it was found that the average thermocouple reading did not change appreciably across the PFR diameter. The location of a thermocouple 5 cm above the top of the flow straightener revealed a temperature of 1626±5K for fuel-rich $C_2H_4/O_2/N_2$ combustion at 1630K. This verified the isothermal assumption. In another test, Brouwer [1993] performed hot wire anemometer measurements in the PFR under coldflow conditions, ensuring that the flow velocity gave the same local heat transfer coefficient as the faster flowing, less dense gas at 1630K. The velocity profiles at heights of more than 5 cm above the flow straightener exhibited flat plugflow character (Figure 3.3).

Since there was a need to inject prevaporized aromatics into both the aformentioned PFR and the PFR used by Brouwer [1993], a portable vaporizer was designed and constructed [Manegold 1995], also see Figure 3.4. The principle of operation is identical to that of the fuel additive vaporizer injection (FAVI) system used by Lam [1988] and Marr [1993]. A volume of

liquid additive (benzene or toluene) is stored in a cylinder, where it is maintained at a given temperature by an Omega controller. Nitrogen is bubbled through a sparger immersed in the liquid and the additive/nitrogen stream flows along a heated line to the injector tube. A reservoir tank ensures that the liquid level does not drop appreciably during a run. The nitrogen flowrate is set by rotameter control and is not varied from run to run. The aromatic feedrate to the PFR is set by chosing the appropriate liquid temperature. Tests have shown that the aromatic flowrate is within 10% of the rate calculated by assuming saturation of the nitrogen (see Figure 3.5).

The PFR injector tube is a 3/8" alumina thermocouple protection sheath (Omega) with 8 equally spaced 1/32" holes drilled 1/4" from the closed end. Aromatic additives have shown a tendancy to undergo significant pyrolysis and coking within the injector tube. To mimimize this undesirable phenonemon, the injector is retracted to position where the holes lie about 8mm below the bottom of the flow straightener. This ensures that only the top 1/2" of the tube lies within the reactor, thereby reducing problems associated with additive preheat. The location of the injector in this "low" position and the allignment of the 8 holes with the flow straightener vanes ensures optimum mixing of the additive with gases leaving the JSR. Using a radial sampling probe, Manegold [1995] demonstrated that under coldflow conditions the radial distribution of benzene in the PFR is strongly dependent on the injector position. Figure 3.6 shows the flat benzene radial profile with the injector in the "low" position, and the Gaussian-like profile with the injector in a "high" position above the flow straightener. To examine the quality of mixing under hotflow conditions, Neon was added as a tracer to the benzene/nitrogen stream leaving the vaporizer. With the JSR running at a ϕ of 1.3, gaseous samples were taken from 9 sampling points along the PFR axis. Neon concentrations, obtained from GC-TCD analysis (Supelco Molecular Sieve 5A column) appear in Figure 3.7. Since the variation in Neon concentration was well within experimental error, these data indicate that mixing is uniform under hotflow conditions, provided the injector is in the proper position.

3.2 Gas Sampling and Analysis

Samples were withdrawn from the PFR via a water-cooled stainless steel probe with a 5 cm outer diameter. By nature of its relatively large diameter and considerable cooling effect, this probe significantly influences the flowfield downstream of the sampling point. However, since samples are only taken along the centerline and since the PFR flowfield is uniform, the probe is not expected to influence the section of the PFR upstream of the sampling point. The positions of the 5 selected sampling points appear in table 3.1.

Table 3.1 PFR Sampling Point Positions

Sampling Point ‡
4.0 cm
15.0 cm
26.0 cm
37.0 cm
48.0 cm

‡ distance above top of flow straightener

The position of the sampling probe was set by placing a 1/4" stainless steel rod of desired length between the probe head and the bushing connecting the probe to the PFR.

Gas samples were taken by inserting 250 ml collection jars (Supelco 2-2162M) into the sampling line. After a nominal sampling time, the vacuum pump (Cenco Hyvac) was turned off and the jar valves closed. To minimize leaks, analysis was carried out within 24 hours of sampling. For fixed gases such as CO, CO_2, O_2, N_2, analysis was carried out using an HP5890

Series II gas chromatographer with a packed Carboxen-1000 column (Supelco 1-2390). 500 microliter injections were made, after which the peak areas were compared to those from the injection of an appropriate standard (Scotty Mixture #216). For light hydrocarbon analysis, injections were made into the split/splitless inlet of the GC. This inlet was connected to an Astec GasPro GSC column, which separates C1-C4 hydrocarbons and monocyclic aromatics. An oven temperature program consisting of a 10°C/min ramp from 40°C to 200°C was selected. A Scotty Mixture #64 standard was used to identify and quantify these compounds.

3.3 PAH Sampling and Analysis

In the case of PAH sampling, fixed volumes of gas (usually 0.4 ft^3 or 11 liters) were withdrawn from the PFR. Volume measurements were made by inserting a wet-test meter (Precision Scientific Co.) downstream of the sampling apparatus. Typical gas flowrates through the PAH sampling system were 0.3 ft^3/min (8.5 liters/min). The flowrate was varied by adjusting a valve along the line. A prewashed disposable filter unit (Balston DFU 9933-05-DQ) was placed in the line to trap soot particles. Since PAH and soot would otherwise be deposited along the inside of the probe, a teflon probe liner was inserted for each sample. This liner was removed after each sample was collected and washed with dichloromethane (DCM) to remove the PAH and soot. Due to the range in vapor pressures of constituent PAH compounds, heavier PAH's condense inside the disposable filter, inside the teflon probe liner and along the transfer line while more volatile PAH's remain in the vapor phase and are discharged unless trapped. To capture these more volatile compounds, a series of two 250ml glass traps (Pyrex # 1760-250) was placed in the sample line. These traps are partly filled with glass beads and dichloromethane solvent. The solvent extracts PAH from the gas stream while the beads act to break up bubbles and increase the surface area of the gas-liquid interface. Previous studies with this assembly established the PAH capture efficiency to be nearly 100% [Lam 1988]. The extract was then combined with the washings from the disposable filter, probe liner and transfer line, and passed

through a prewashed analytical filter (Pallflex T60A20) to remove particles. The 200-400ml of extract was placed in a 500ml Kuderna-Danish apparatus with a 10ml receiving ampule, connected to a Snyder condensation column. The sealed vessel was heated in a waterbath at 55-60°C for a period of approximately 2 hours, until the volume was contained within the receiving ampule. The high number of theoretical plates of the column ensures little PAH loss during the DCM evaporation. The concentrate was filtered through a prewashed disposable 0.2 micron syringe filter (Micron Separations) to remove any remaining solid particles which may damage instrumentation during the subsequent analysis.

A portion of the filtered concentrate was allocated to "Total Tar" measurements [Lafleur *et al.* 1986]. This technique is based on the principle that if the DCM solvent in a specific volume of sample is left to evaporate, the mass of the remaining residue is a measure of the concentration of "Total Tar" or DCM-soluable material. In practice, a 100 microliter sample of concentrate was taken, deposited on a preweighed aluminum foil cup, and left for 5 minutes. The cup plus residue was then weighed on a Mettler balance. To minimize errors, the procedure was done in triplicate. Drawbacks of this procedure include losses of lighter PAH by evaporation, although it was shown that the losses are minimal for compounds larger than naphthalene [Marr 1993], and contributions to the Total Tar residue from contaminants in the extract such as the phthalate compounds typically found in plastics.

Once the Total Tar analyses had been carried out, the concentrate volumes were reduced further by blowing a stream of nitrogen over each liquid surface. Upon reaching a volume of approximately 1ml, the solvent was exchanged. This involved adding 0.5ml of dimethyl sulphoxide (DMSO), and blowing additional nitrogen to remove the remaining DCM. By replacing the solvent with the less volatile DMSO, volume losses by solvent evaporation are minimized. Additional safeguards were taken by storing the samples in a refrigerator until they were ready for analysis by high performance liquid chromatography (HPLC-UV/DAD), gas

chromatography/flame ionization detection (GC-FID), and gas chromatography/mass spectroscopy (GC-MS). With GC/FID, the identification and quantification of the individual PAH compounds was carried out by comparing retention times to those of calibrated standards. For lower molecular weight aromatics (78 to 128 amu), analysis was done using a Hewlett-Packard 5890A GC fitted with a Megabore capillary column (J & W Scientific, Quadrex 0.53mm). The oven temperature was ramped from an initial 40°C to 200°C at 10°C/min. For PAH in the 102 to 252 amu range, the same GC was fitted with DB-5 capillary column (J&W Scientific). In that case, the oven temperature was ramped at 10°C/min from 50°C to 300°C, and held at the maximum temperature for 20 minutes. With HPLC-UV, peaks were identified by comparing the UV spectrum of each compound with the spectra contained in an appropriate library. Compounds from naphthalene (128 amu) to ovalene (398 amu) were identified this way.

3.4 Soot Sampling and Analysis

The soot sampling procedure was similar to the PAH procedure in that measured volumes of gas were withdrawn from the PFR with a vacuum pump. Typical flowrates were 0.6 ft^3/min (17 liters/min) while the volumes collected ranged from 0.2 ft^3 (5.7 liters) to 2 ft^3 (57 liters) depending on the soot loading. The disposable filter unit and glass traps used to collect PAH were replaced with a glass filter holder (Ace Glassware) containing an analytical filter (Pallflex T60A20). Before an experiment, each filter was rinsed with DCM to extract soluable material and to wash off loose fibers. After drying in an oven at 60°C for 45 min, the filters were stored in a dessicator and weighed on a Mettler H20 balance (accuracy of $\pm 10^{-5}$g). Static electricity was found to influence the balance readings, especially during the cold, dry winter months. To counter these effects, a method was developed to allow the filters to be suspended from the hook at the top of the balance [Procaccini 1996]. By inserting a wire hook through a hole near the edge of each filter and hanging it onto the balance hook, the filter did not come into contact with the pan and as a result did not have the opportunity to bias the readings. To further reduce

measurement errors, four separate readings were taken for each filter. After the initial measurements, the filters were placed between Vycon gaskets (custom made by Greene Rubber) and fastened in the filter holder for sampling. After each run, the probe liners and transfer lines were rinsed with DCM to remove soot and PAH. These washings were then passed through the filters, which were finally rinsed with DCM to extract all remaining tar. This separation technique was used previously to remove tars from carbon [Lam 1988, Vaughn 1988, Mulholland 1992, Marr 1993]. Washed filter papers varied in color from beige to black depending on the soot levels at the particular sample point. After drying at 60°C for another 45 min, the filters were weighed as they were before the experiment, and the quantities of soot determined by difference. Typical soot yields were in the range of 1-5 mg per filter.

3.5 Soot Size Analysis

The objective of this analysis was to deposit the soots collected in the various experiments onto TEM (transmission electron microscope) grids and obtain images of the aggregates. This would then allow us to measure diameters of the primary particles observed in the images.

Filter papers collected from soot sampling were sonicated in methanol to dislodge the soot aggregates. The liquid was then passed through a micro syringe filter to remove unwanted strands from the filter paper. Using a dropper, a small volume of the liquid was dropped onto a 3.0 mm diameter 200 mesh copper grid, and the solvent allowed to evaporate. The instrument used was a JOEL 200CX, which is a 200 KeV high resolution microscope equipped with a high brightness electron source and free lenses control. The filament was a high resolution LAB_6. Typical magnifications were in the 60,000-200,000 range.

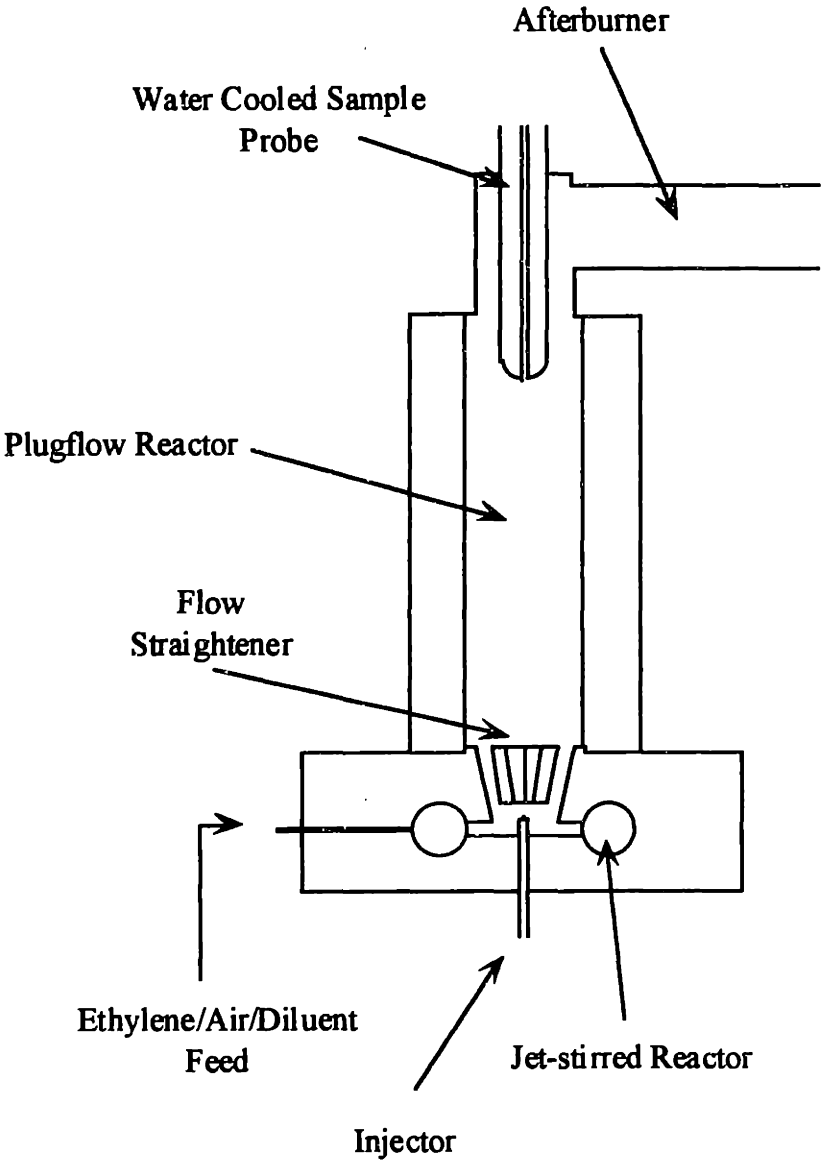

Figure 3.1 The Jet-stirred Plugflow Reactor (JS/PFR)

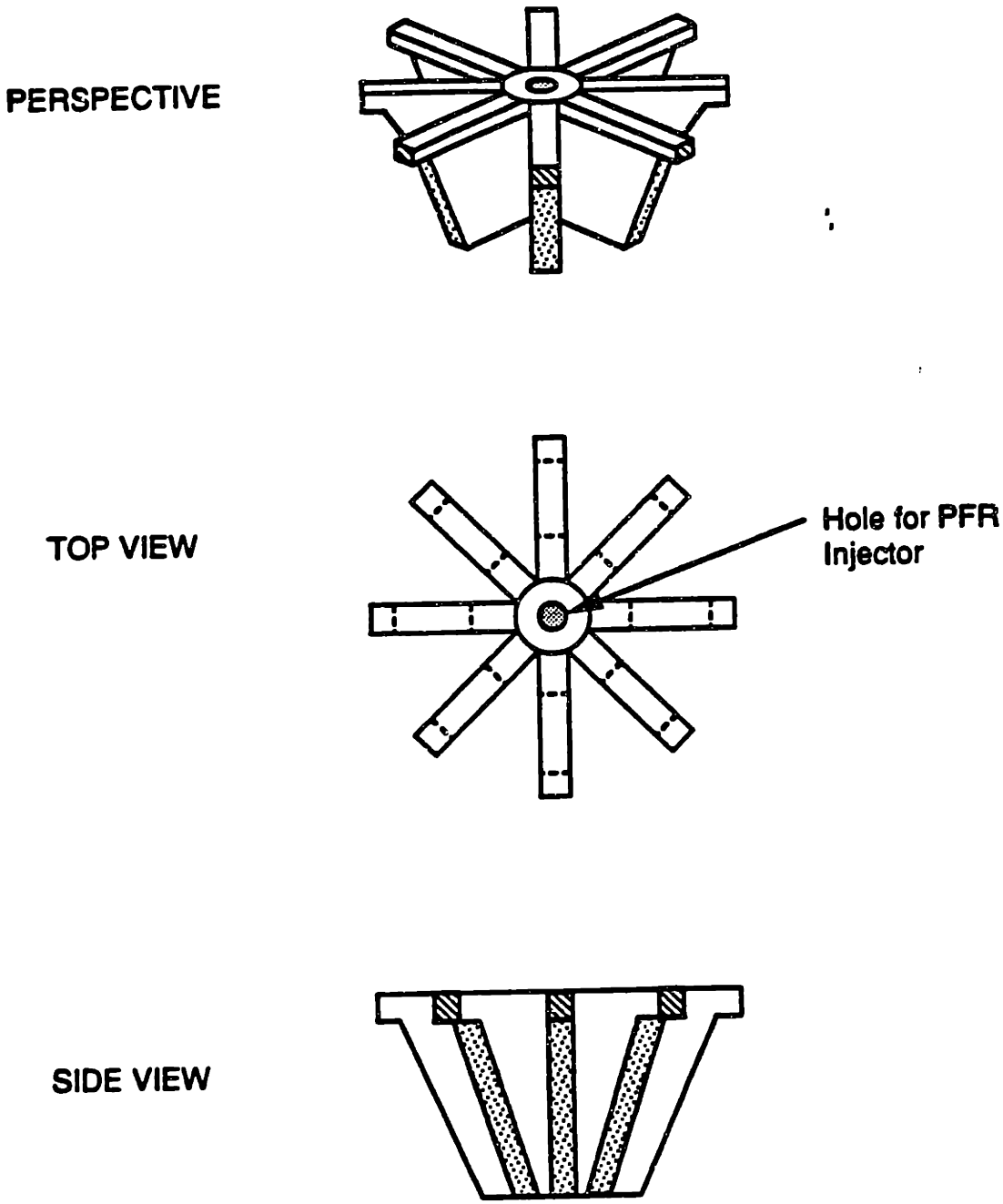

Figure 3.2 Flow Straightener for JS/PFR System

from Marr [1993]

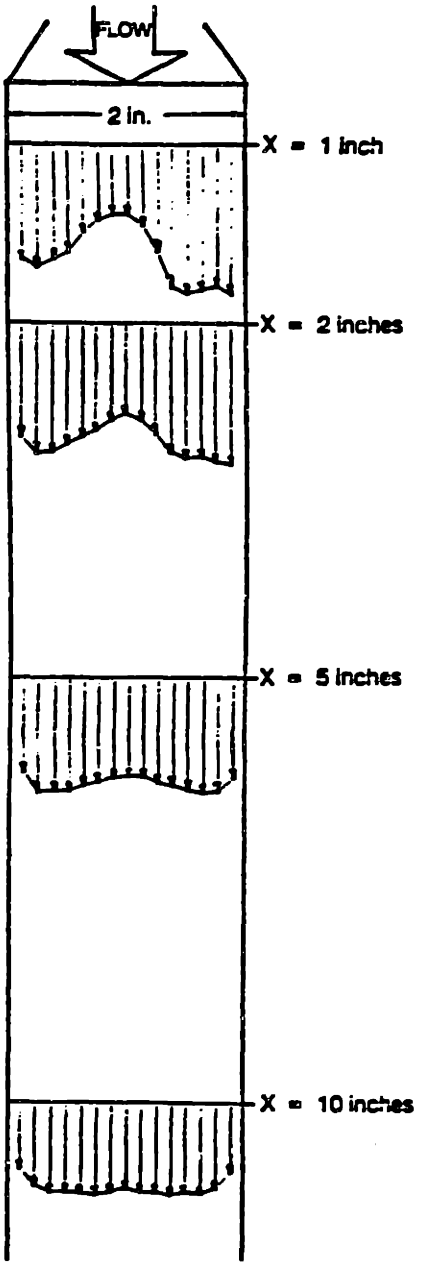

Figure 3.3 Velocity Profiles in PFR

as measured by hot-wire anemometry [Brouwer 1993]

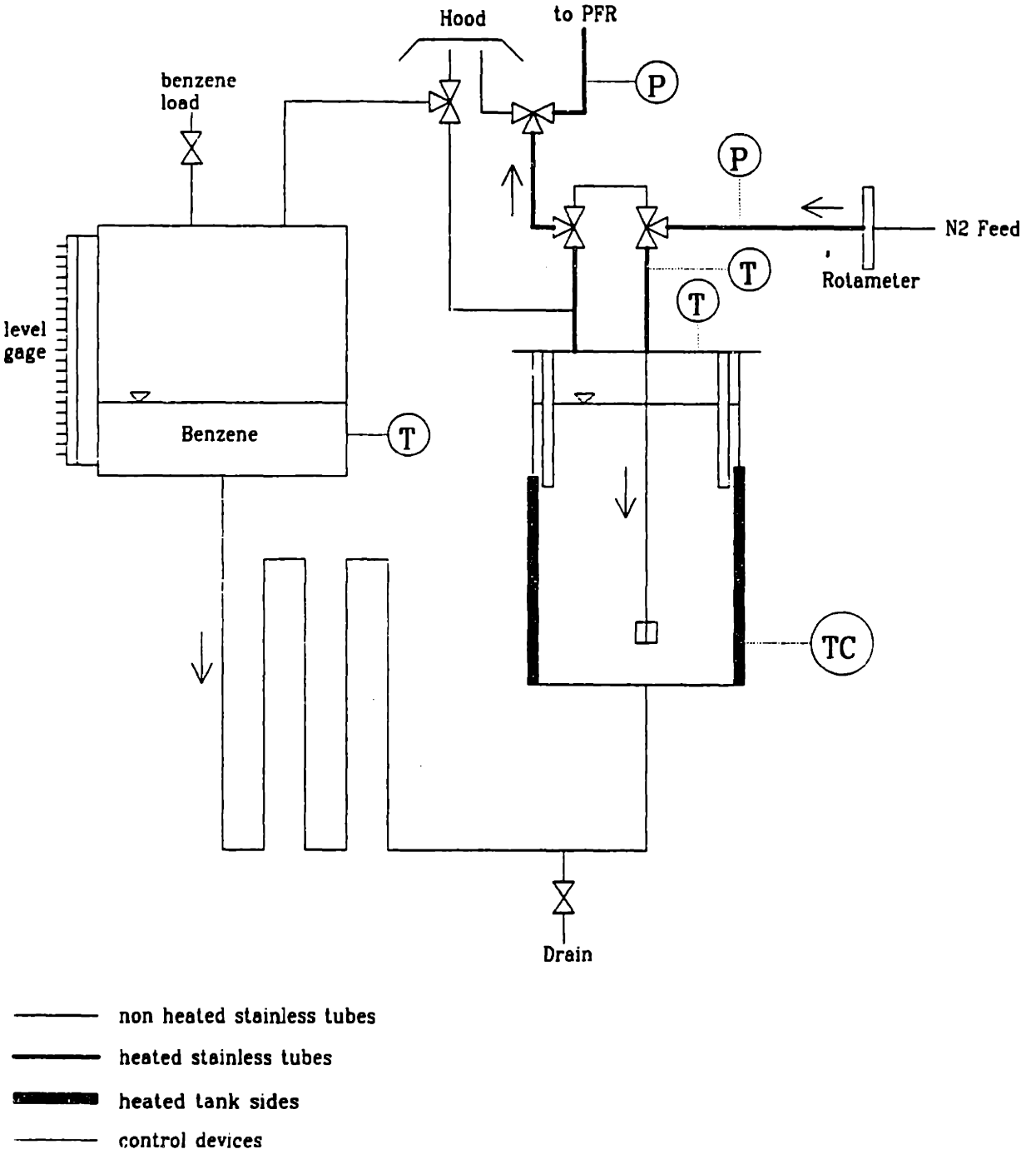

Figure 3.4 The Portable Benzene Vaporizer

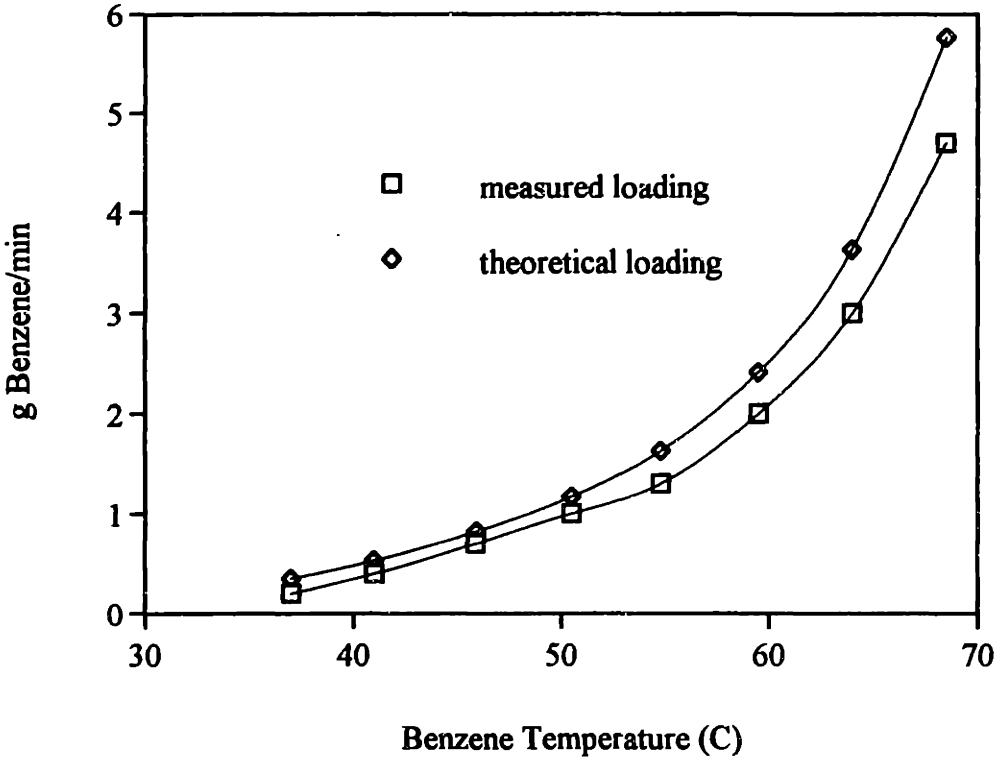

Figure 3.5 Benzene Vaporizer Calibration Curve

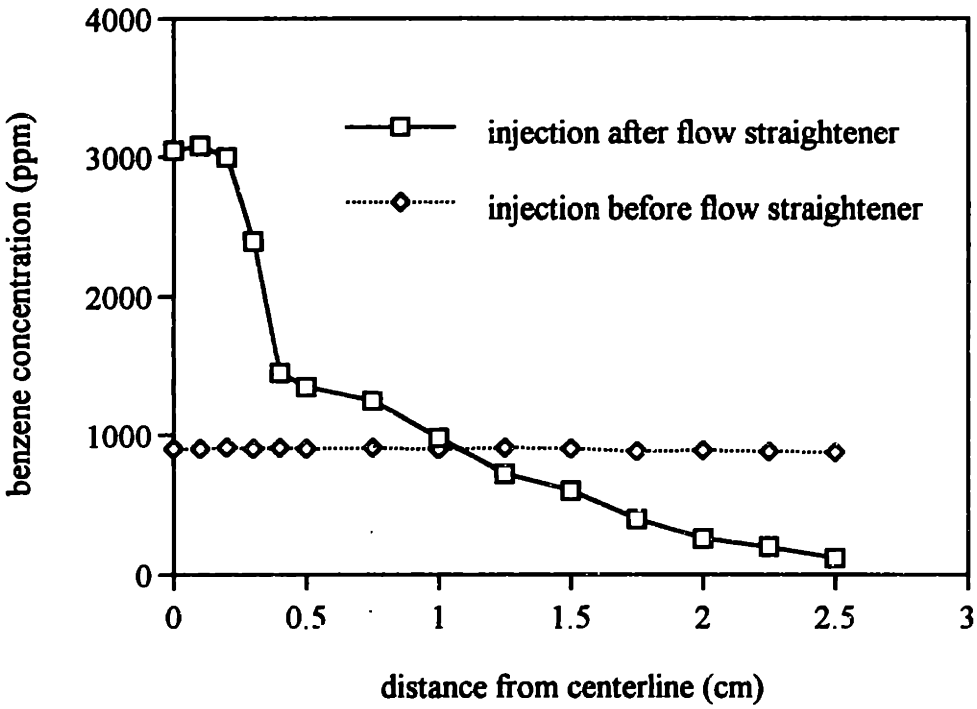

Figure 3.6 Coldflow Benzene Injection Results

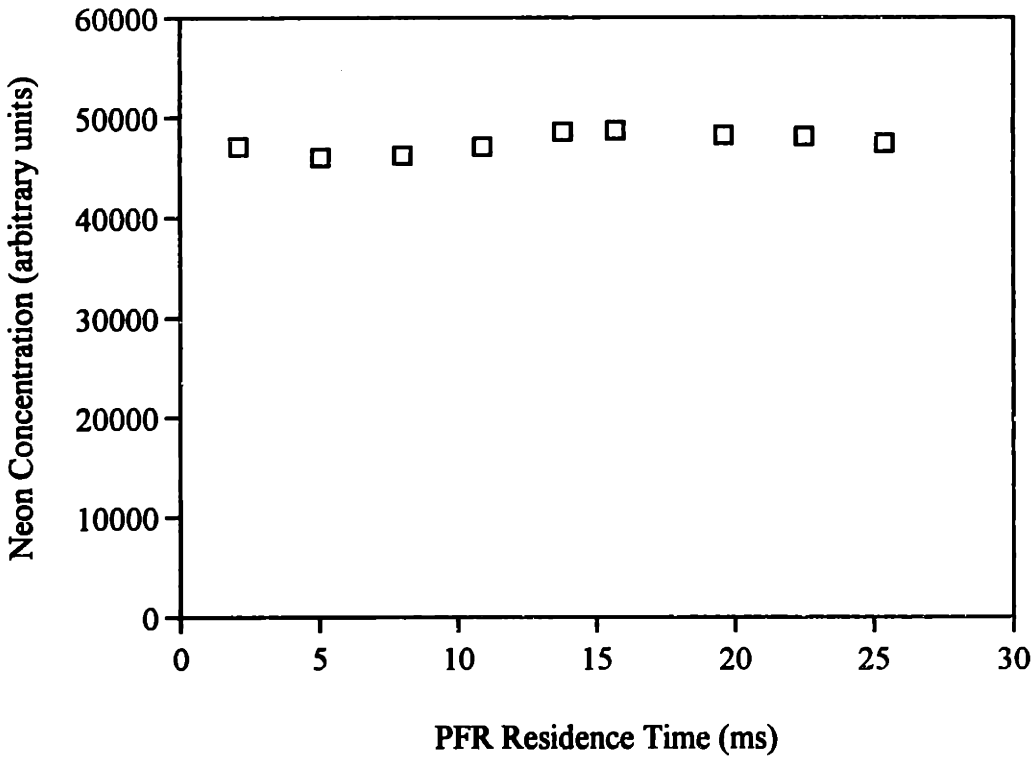

Figure 3.7 Measured Neon Concentrations along Centerline of PFR
ϕ = 1.3 + 4.2 g/min benzene, T = 1580K
(neon injected with benzene)

Chapter 4. Soot Surface Growth Pathways

The focus of this chapter is on the roles of acetylene and PAH as soot surface growth agents. The underlying goal is to meet the first two objectives of section 1.2 i.e. to empirically determine to the relative contributions of acetylene and polycyclic aromatics to post-nucleation soot surface growth.

4.1 Experimental Approach

To determine the relative contributions of PAH and acetylene to soot surface growth by using soot, PAH, and C_2H_2 data alone, *a priori* knowledge of soot-PAH and soot-C_2H_2 collision efficiencies is required. These collision efficiencies can then be used in conjunction with collision frequencies to calculate carbon addition rates via the two pathways. However, in view of the significant uncertainties in collision efficiency values, this technique is somewhat risky.

The technique used in this study is based on the idea that soot can be generated in the JS/PFR under acetylene lean conditions by operating the JSR at a slightly fuel-rich baseline and injecting an aromatic compound through the ceramic injector into the PFR [Marr *et al.* 1994]. In this way, PAH and soot formation is promoted without introducing large quantities of acetylene. Under these conditions, the low acetylene levels in the PFR virtually guarantee that the soot surface growth occurs primarily via the PAH addition route. Since PAH dominate surface growth in this case, the soot-PAH collision efficiencies may be calculated by relating the observed soot growth rates to the collision frequencies and collision efficiencies. These collision efficiencies may then be applied to other experimental cases, especially those in which acetylene is believed to play a more substantial role in particle gowth. With the current JS/PFR set-up, the most convenient acetylene rich experiment is the case where the JSR is operated at a high

equivalence ratio and where no aromatics are injected. The fuel rich conditions ensure that there is an abundance of acetylene (in the order of 1%) in the PFR. Lam [1988] found that if ethylene is injected into the PFR under fuel rich baseline conditions ($\phi = 2.2$) the bulk of it is converted to acetylene. Therefore, under fuel rich conditions, any incremental increase in the ϕ will raise the acetylene concentration. For this acetylene rich case, the relative contributions of acetylene and PAH may then be determined by comparing the apparent soot-PAH collision efficiencies (i.e. calculated by assuming all soot growth occurred by PAH addition) with those from the acetylene lean cases.

4.2 Soot Surface Growth at 1580K

4.2.1 Acetylene Lean (Benzene Injection) Cases

In the acetylene lean, benzene injection experiments, the JSR fuel equivalence ratio was set to 1.3, which resulted in the acetylene levels reported in Figure 4.1. The four chosen benzene injection rates appear in Table 4.1. These rates were attained by varying the temperature of the liquid benzene in the vaporizer, while maintaining a constant nitrogen flowrate.

Table 4.1 Benzene Injection Rates for 1580K Acetylene-Lean Cases

Benzene Temperature	Benzene Injection Rate	% of Carbon from Benzene
59.6°C	3.4 g/min	12%
62.1°C	4.2 g/min	15%
67.1°C	6.4 g/min	21%

Nitrogen (carrier gas) flowrate = 1.5 liters/min

The soot concentrations measured for these three cases appear in Figure 4.2 while the corresponding total PAH concentrations appear in Figure 4.3. Total PAH refers to the sum of the PAH concentrations measured by HPLC or GC-FID, see Appendix B for a listing of the individual species concentrations. Total tar measurements were not carried out for these cases because of the significant levels of phthalate contaminants in the samples. Since "Total Tar" is defined as all DCM soluable material, no distinction can be made between those compounds generated in the PFR and those originating in the sampling apparatus and dissolved by DCM during sampling and concentrating. The source of these contaminants was finally identified as the disposable filter units used in the PAH sampling train. The problem was solved by rinsing the filter units several times with DCM before use.

As anticipated, both soot and PAH levels rose as a result of an increasing benzene injection rate, with soot demonstrating a stronger dependence.

4.2.2 Acetylene Rich Case

For the 1580K acetylene rich case, the fuel equivalence ratio was set to 2.2 and no aromatic injected into the PFR. This gave rise to relatively high acetylene yields, as is seen in Figure 4.1. The soot concentrations for this case appear in Figure 4.4 while the PAH and "Total Tar" concentrations appear in Figure 4.5. The latter plot indicates that detectable PAH constituted approximately 50% of the total tar.

4.3 Soot Surface Growth at 1650K

The purpose of these experiments was to assess the effect of temperature on the relative contributions of acetylene and PAH to soot surface growth. The strategy followed was identical to that of the 1580K experiments. In these cases, the higher JSR temperature was reached by

preheating the feed (and maintaining a constant dilution rate) as opposed to decreasing the N_2 dilution rate. This ensured that the diluent effects were minimized, and that all the differences observed at the higher temperature were purely thermal in nature. These runs comprise one acetylene lean experiment (ϕ = 1.3 + 4.2 g/min benzene) and a ϕ = 2.2 acetylene rich (non injection) experiment.

4.3.1 Acetylene Lean (Benzene Injection) Case

The soot concentrations measured for the acetylene lean run appear in Figure 4.6 while the total PAH and total tar data are plotted in Figure 4.7. When compared to the lower temperature results (Figures 4.2 and 4.3) these data indicate that the higher temperature led to an order of magnitude increase in soot levels and a moderate decrease in PAH concentrations.

4.3.2 Acetylene Rich Case

The soot concentrations for this ϕ = 2.2, 1650K case appear in Figure 4.8 and the PAH and "total tar" data in Figure 4.9. The higher temperature resulted in a factor of two increase in soot levels (with respect to the 1580K case) and a factor of two decrease in PAH and total tar levels.

4.4 Characterization of PAH and Soot

4.4.1 Detected PAH Species

Figure 4.22 contains the structural formulae of all the PAH species detected in the PFR samples by HPLC or GC-FID analysis. A comprehensive listing of the individual PAH concentrations for all experimental cases appears in Appendix B. As these data indicate, the

relative abundances of specific PAH decline as the molecular weight increases. In fact the most prevalent compounds are the 2 ringed species acenaphthylene and naphthalene. This pattern is evidence of the sequential addition mechanism that is thought to be the prevailing pathway to molecular weight growth [Frenklach *et al.* 1989].

Another general observation is the fact that the PAH profiles for the acetylene lean (benzene injection) and acetylene rich cases display a similarity (see Figures 4.14 and 4.15 for PAH profiles). But several differences in individual compound concentrations do exist, and these are presented in the following section.

For the 1650K acetylene rich cases, the high molecular weight species (MW $\geq$ 300) make up a larger fraction of the total PAH inventory than in the acetylene lean case. Specifically, the sum of the coronene, cyclopenta[cd]coronene, and naphtho[8,1,2-abc]coronene levels comprises 2-3% and 0.3-0.5% of total PAH in the acetylene rich and acetylene lean cases respectively. This may be attributed to the higher acetylene concentrations in the former case, which would have resulted in a higher formation rate of compact PAH such as coronene via the HACA (hydrogen abstraction acetylene addition) mechanism.

It is also of interest to compare concentration ratios of known isomer pairs. A familiar Scott-Roelofs pair is fluoranthene/acephenanthrene, which have been found to be well equilibrated after 5 ms at 1620K in the original PFR [Howard *et al.* 1995]. For our acetylene rich cases, this ratio lies between 1.5 and 1.8 while for the acetylene lean cases it lies between 2.5 and 2.9. These results are in good agreement with the theoretical ratio of 1.7-2.7. The theoretical fluoranthene/pyrene ratio is considerably lower (0.02-0.05) due to the greater stability and lower Gibb's free energy of pyrene. The measured fluoranthene/pyrene ratios, however, are far from their equilibrium values. Howard *et al.* [1995] attributed this to the large number of steps and high energy barriers required for this transformation. The acetylene rich fluoranthene/pyrene

ratios were found to be 0.6-0.7 while the acetylene lean ratios were 0.7-2.4. All these results point to a more active fluoranthene formation route in the acetylene lean cases.

Two competing fluoranthene formation sequences are reaction 4.1 [Bittner & Howard 1981] and reaction 4.2 [Marr 1993]

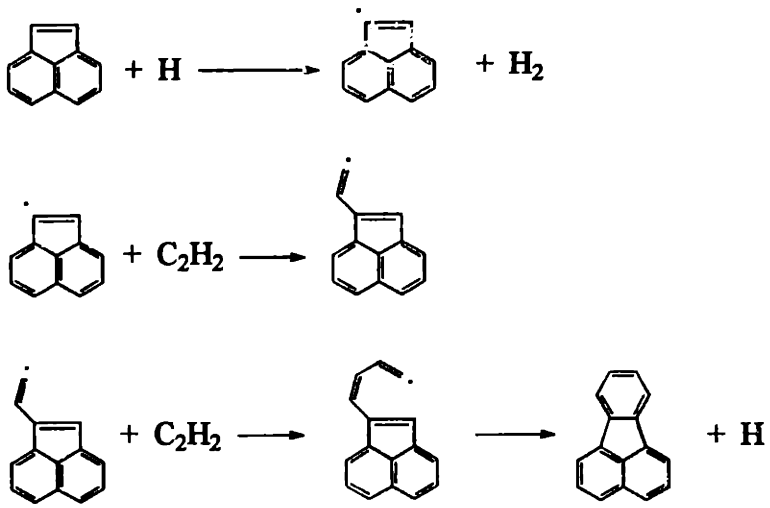

(reaction 4.1)

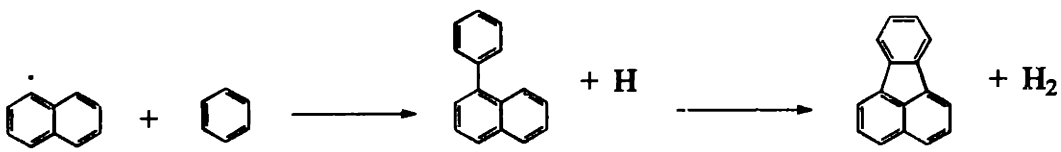

(reaction 4.2)

It stands to reason that reaction 4.2 will be favored by the high levels of benzene in the acetylene lean (benzene injection) experiments, which could potentially explain the high fluoranthene yields relative to the acetylene rich cases.

Another compound which is more prevalent in the acetylene lean cases than in the acetylene rich cases is indeno[1,2,3-cd]pyrene. Due to its structural similarity to fluoranthene, a potential formation pathway may well be a reaction analogous to reaction 4.2, but involving benzene and pyrene rather than benzene and naphthalene.

4.4.2 Characterization of Soot

In order to obtain particle size information necessary for carrying out the collision efficiency analysis, transmission electron microscopy (TEM) images were taken of the sampled soot. The initial set of TEM images was of the soots collected on filter papers during the 1580K acetylene rich and lean experiments. The soot agglomerates observed in these samples resemble the structures seen in Figures 4.23 and 4.24. Figure 4.25, for comparison, is an image of one of the few "classical aggregates" observed in the PFR soot. It is evident that most of our PFR soot aggregates lack the classic "necklace" structure, but rather appear to be composed of amorphous carbon deposited into large "plates". Since it is doubtful that these "plates" actually existed in the PFR, they must have been formed during the sampling. The question is why were these unusual structures seen in our samples while "normal" looking soots are frequently collected from other experimental flames?

This puzzle was partially solved when the PFR images were compared to TEM micrographs taken of a soot sample collected from a benzene pyrolysis reactor [Prado & Lahaye 1981]. These soots, which appear in Figure 4.26a & b, seem to have the same structure as the "plates" observed in the PFR samples. Prado & Lahaye proposed that the "carbonaceous residue" found in their benzene pyrolysis samples differed in structure from classical soot aggregates because, under their conditions, the soot primary particles were not solid particles but viscous tar droplets. They asserted that these droplets coagulated into large amorphous structures upon sampling. However, at higher residence times (Figure 4.26c & d), their soot

agglomerates appeared to be made up of solid primary particles. Their hypothesis was that "tar droplets" will be found at low temperatures and low residence times since these are conditions which do not favor dehydrogenation and graphitization. At higher temperatures, viscous tar droplets may well be present in the early stages of soot growth but they rapidly lose hydrogen to solidify into primary particles. Jander [1997] also observed "plate-like" structures in certain flat flame soot samples. One such aggregate (see Figure 4.27) was collected from a ϕ = 2.0, atmospheric pressure ethylene/air flame and clearly resembles the PFR structures.

The unusual structures of the PFR soot aggregates made it difficult to discern the individual primary particles, which in turn made it difficult to obtain reliable particle size information. However, a few isolated samples proved to contain enough primary particles for a rudimentary size analysis. These data appear in Appendix B. The soot number densities calculated by using the average diameters and measured concentrations are similar to the value used by Marr [1993] i.e. $1x10^{15}$ particles/m^3.

4.5 Collision Efficiency Analysis

4.5.1 Soot/PAH and Soot/C_2H_2 Interactions

The soot, PAH, and acetylene data coupled with soot particle size information enabled us to calculate apparent soot-PAH collision frequencies for all experiments. Equation 4.1 was used for this purpose.

$$\frac{d[soot]}{dt} = \gamma_{soot,PAH} \frac{\sigma_{soot/PAH}^2}{4} \left(\frac{8\pi RT}{\mu_{soot/PAH}} \right)^{0.5} N_{soot} [PAH] \qquad \text{(equation 4.1)}$$

where $\mu_{soot/PAH} = (M_{soot} \cdot M_{PAH})/(M_{soot} + M_{PAH})$, the reduced soot/PAH molecular weight. Due to the large molecular weight difference between soot and PAH, this was approximated as M_{PAH}. Likewise, $\sigma_{soot/PAH}$ was approximated as σ_{soot} on account of the large size difference. This global collision technique has been used in similar studies by Lam [1988] and Marr [1993, 1994].

Soot growth rates were obtained by fitting a polynomial equation to each set of soot concentrations, and then differentiating the equation to yield growth rates as a function of PFR residence time. This technique, which "smoothes" out variations in the data points introduced by errors in the measurements, is very similar to Marr's "ROSG" (rate-of-soot-growth) method [Marr 1993]. In most cases, the data closely fit second order polynomials. In the few cases where second order polynomials were inaccurate, third order polynomials gave good agreement. Using the soot growth information, the apparent soot-PAH collision efficiencies were then calculated for each residence time. As is evident from equation 4.1, all soot growth is assumed to occur via PAH addition. The following assumptions were also made :

i) soot oxidation is negligible

ii) the soot number density is constant with residence time

The apparent soot/PAH collision efficiencies for the 1580K experimental cases appear in Figure 4.10. As this plot indicates, the collision efficiency values for the benzene injection cases are remarkably similar for all benzene injection rates. For this range of injection rates, the soot levels varied by a factor of four and the PAH levels by a factor of three. This suggests that the mechanism by which PAH adds to soot is similar for all acetylene lean cases, regardless of the absolute soot and PAH concentrations. The apparent soot/PAH collision efficiencies for the 1650K acetylene lean case appear in Figure 4.11. These values exceed those of the 1580K cases by a factor of approximately two. This difference is ascribed to the higher radical concentrations

which are expected at higher temperatures. A larger radical pool would enhance the formation of PAH radicals, which would in turn increase the probablity of a PAH/soot collision resulting in the formation of a bond.

Because of the relatively low acetylene levels in the PFR, the assumption that all soot growth occurs by PAH addition and very little occurs via acetylene addition should be valid for these cases. Thus, the apparent collision efficiency values are likely to be close to the true values.

The apparent soot-PAH collision efficiencies for both the 1580K and 1650K acetylene rich cases appear in Figures 4.10 and 4.11. The most interesting feature indicated by these plots is that the acetylene rich values exceed those of the acetylene lean values by a factor of 3-4. There are two explanations for this discrepancy. Firstly, the high apparent collision efficiencies for the acetylene rich cases may be a result of the different PFR environments in the $\phi = 2.2$ and the $\phi = 1.3$ + benzene experiments. The high apparent collision efficiencies could be explained by i) higher temperatures or ii) higher radical concentrations in the acetylene rich case. With regard to temperature differences, thermocouple readings were taken in all experiments and errors are expected to be less than 30K. The 1580K and 1650K acetylene lean data reveal that the effect of raising the temperature by 70K led to a two fold increase in PAH/soot collision efficiencies. In light of this, a 30K variation could not account for the observed 3-4 fold difference. Higher apparent PAH/soot collision efficiencies in the acetylene rich experiments could also arise from higher PAH radical levels in these cases. Should the concentrations of PAH radicals (relative to total PAH levels) be higher, then the expected probability of a soot/PAH collision resulting in a reaction (or formation of a bond) would be higher. Howard [1990] proposed that larger PAH molecules, by virtue of their greater resonance stability, are expected to have more radical sites per carbon atom than smaller PAH. Also, PAH containing 5 membered rings on their edges are more likely to have H atoms abstracted since bond dissociation energies are lower for vinyl C-H

bonds than for aryl C-H bonds. These factors could be significant if the profiles of PAH are sufficiently different for the acetylene lean and acetylene rich cases i.e. if there is a greater abundance of larger PAH and/or PAH with five membered rings in the acetylene rich case. Figure 4.12 shows the profiles of PAH (expressed as fraction of total PAH vs carbon number) for the 1650K acetylene lean and acetylene rich cases at the lowest residence time (2.5 ms) while Figure 4.13 contains the same information for the highest residence time (30 ms). These graphs indicate that a large fraction of the total PAH is composed of 2 ringed aromatics such as naphthalene and acenaphthylene (the most abundant compound) and that this trend is common to all cases. Since the graphs show a general similarity between the acetylene rich and lean cases, it is unlikely that PAH radical concentrations are significantly higher in the former case.

In view of the arguments presented above, there is insufficient evidence to suggest that the acetylene rich and lean PFR environments are different enough to explain the discrepancy in soot/PAH collision efficiencies. Therefore, the second explanation must be true i.e. in the acetylene rich cases, the assumption that soot growth occurs only via PAH addition is not valid. If indeed it is not valid, then there must be another important soot surface growth agent other than PAH for these cases. Since this experiment is by definition acetylene rich, the most likely soot growth agent must therefore be acetylene.

The exact contribution of acetylene to soot growth at a given residence time may be estimated by using the ratio of the apparent collision efficiency to the true collision efficiency, where the true collision efficiency was assumed to equal the average collision efficiency for the acetylene lean cases. For example, should the apparent:true collision efficiency ratio equal four, then 75% of the observed soot growth would occur by acetylene addition and 25% by PAH addition.

Using this technique, the relative contributions of PAH and acetylene to soot surface growth were calculated for the 1580K and 1650K acetylene rich cases. The results, which appear in Figure 4.14, indicate that the acetylene contribution to soot growth was in the 65-75% range for both cases. Thus, it would appear that soot surface growth was dominated by acetylene in the $\phi = 2.2$ cases and by PAH in the $\phi = 1.3$ + benzene cases. The findings for the $\phi = 2.2$ case are in agreement with the numerical results presented by Frenklach *et al.* [1991], who studied one of Harris & Weiner's [1985] atmospheric premixed ethylene flames, and concluded that acetylene (via the HACA mechanism) dominated soot growth in that case. At first glance the results may imply that the soot surface growth which occurs in fuel rich premixed flames is dominated by acetylene in the case of aliphatic fuels and by PAH in the case of aromatic fuels. However, since only two specific conditions were investigated, these findings may not be applicable to all cases.

With the relative acetylene contributions, the soot-acetylene collision efficiencies were calculated for the $\phi = 2.2$ cases. These results appear in Figure 4.15. From this plot, it can be seen that the soot-acetylene collision efficiencies varied between 5×10^{-4} and 3×10^{-4}. These values are 2-3 orders of magnitude lower than the soot/PAH values. This is attributed to the fact that an acetylene molecule will only collide and stick to a soot particle if it encounters a radical site upon collision. A PAH molecule, on the other hand, is larger and may itself contain a radical site. Both of these factors will increase its probability of sticking to a soot particle.

Armed with knowledge of the apparent soot-PAH collision efficiency values, the assumption of soot oxidation not being significant was investigated. As Figure 4.3 indicates, total PAH concentrations were in the order of 100 mg/m^3 (at 1580K) for the acetylene lean experiments. This corresponds to a mole fraction of 6×10^{-5}. The OH levels for these experiments, calculated by applying the Miller-Bowman mechanism [1989] to a PSR/Senkin model of the JS/PFR, lie in the region of 2×10^{-6}. For comparison, Marr [1993] reported a figure of 1×10^{-6} for his 1630K, $\phi = 2.2$ case. As is seen in Figure 4.10, apparent soot-PAH collision

efficiencies for the 1580K cases varied between 0.11 and 0.03 depending on the PFR residence time. With regard to soot-OH collision efficiencies, Neoh [1980] obtained values of 0.13 at 1780K and 0.27 at 1830K. It has been customary to use the average of these two values, i.e. 0.20. An additional factor is the number of carbons added/removed by each collision. A 200 amu PAH molecule is capable of adding 15 carbons to a soot particle while an OH radical can only remove a single carbon. With this concentration and collision efficiency information, the expected removal rate of carbon due to OH oxidation would be at least 50 times smaller than the addition rate of carbon by PAH. This effectively rules out soot oxidation as a major sink. This assumption, however, may not apply to PAH oxidation since PAH/OH collision frequencies, by virtue of the higher PAH number densities, are expected to be considerably higher than soot/OH frequencies.

All collision efficiency values show a decline with increasing PFR residence time, a trend seen in other sooting premixed flames e.g. [Harris *et al.* 1983]. In the case of PAH-soot collisions, the probability of a PAH adding to the soot particle is significantly higher if the PAH is a radical rather than a parent molecule. If it is assumed that the collision efficiency between a PAH radical and a soot particle is unity and the collision between a parent PAH and a soot particle is very low, then the measured soot-PAH collision efficiencies may be correlated with the fraction of PAH species present as radicals. Since we lack the capability of measuring radicals directly in the PFR, and do not have a radical scavenging system in operation, we have to resort to estimating radical species by assuming partial equilibrium. The abstraction process is represented by reaction 4.3.

$$PAH + H\cdot = PAH\cdot + H_2 \qquad \text{(reaction 4.3)}$$

PAH and H_2 concentrations are available for each experimental case. H concentrations were estimated using a Chemkin package [Kee *et al.* 1989]. The equilibrium constant for the reaction involving each significant PAH was estimated using the THERM package [Ritter & Bozzelli 1991]. Equilibrium constants were calculated for primary aryl, secondary aryl, and vinyl radicals [Howard 1990]. H/H_2 ratios and total PAH radical concentrations (the latter expressed as fractions of the total PAH concentrations) are plotted in Figure 4.16 along with the soot-PAH collision efficiencies for the $\phi = 1.3 + 4.2$ g/min benzene case. The PAH radical fractions appear to approximate the soot-PAH collision efficiency values and display the same downward trend with increasing residence time. The driving force for this decrease appears to be a declining H/H_2 ratio. If reaction 4.3 is not valid, i.e. the species in question are not in equilibrium, it is more likely that the PAH radical concentrations will be higher than their equilibrium values than lower. This is due to the fact that PAH radicals are intermediates in the PAH growth process, in particular the hydrogen abstraction acetylene addition (HACA) growth mechanism [Frenklach *et al.* 1984]. Therefore, with increasing residence times, the PAH radical levels will approach equilibrium and decline in relative terms. This will contribute further to the decreasing PAH•/PAH ratios.

4.5.2 PAH/C_2H_2 Interactions

The pathways leading to the formation and destruction of PAH may be may be represented by the following global collision model (equation 4.2).

$$\frac{d[PAH]}{dt} = \gamma_{C2H2,PAH} \cdot Z_{C2H2,PAH} - \gamma_{soot,PAH} \cdot Z_{soot,PAH} - \gamma_{OH,PAH} \cdot Z_{OH,PAH}$$

(equation 4.2)

Where each γ represents a collision efficiency and each Z a collision frequency. To simplify analysis, all PAH were lumped together in one bin, and no distinction was made between the

different reactivities of differently sized PAH. According to this equation, mass is added to the PAH bin by the reaction of acetylene to existing PAH. This is based on Frenklach's HACA mechanism [Frenklach 1996] which stipulates that acetylene is the prime PAH growth agent. PAH mass is removed from the bin by reactive coagulation between soot and PAH (a soot surface growth mechanism) and by OH oxidation. This model was developed by Lam [1988] and has been used extensively by both Lam and Marr [1993, 1994] to interpret JS/PFR data. However, their approach was to solve equation 4.2 in conjunction with the analogous equation for soot growth. Since this is a system of two equations and three unknowns ($\gamma_{C2H2,PAH}$ $\gamma_{soot,PAH}$ and $\gamma_{C2H2,soot}$), they made the assumption that $\gamma_{C2H2,soot} = \gamma_{C2H2,PAH}$ to reduce it to a 2x2 system. In our study, it was decided to solve for these three unknowns by exploiting our knowledge of the relative contributions of acetylene and PAH to soot growth.

The net PAH growth rates are available from experimental data, all collision frequencies may be calculated using gas collision theory (equation 4.1), and the 3 unknowns are $\gamma_{C2H2,PAH}$, $\gamma_{soot,PAH}$ and $\gamma_{OH,PAH}$. It was decided not to apply this methodology to the acetylene lean data because, in these cases, PAH formation occurred via benzene decomposition and may not be accurately represented by the HACA mechanism. However, the HACA mechanism is probably valid for the acetylene rich cases. As was described in section 4.4.1, the apparent soot/PAH collision efficiencies obtained from the acetylene lean data are believed to be more reliable than those obtained directly from the acetylene rich cases, so these were used. Regarding the OH/PAH collision efficiency, the most reliable value for this parameter is the average of Neoh's [1980] two soot/OH values i.e. 0.20. By using the $\gamma_{soot,PAH}$ values from the acetylene lean experiments and by assuming a $\gamma_{OH,PAH}$ of 0.20, values for $\gamma_{C2H2,PAH}$ were obtained for the acetylene rich experimental cases. The results (with and without oxidation) for the 1580K case appear in Figure 4.17 while those for the 1650K case appear in Figure 4.18. Since oxidation seems to play a significant role in the PAH growth process, the calculated acetylene/PAH collision efficiencies will be sensitive to the chosen PAH/OH collision efficiency.

It is of interest to compare the PAH/C_2H_2 collision efficiencies with the corresponding soot/C_2H_2 values. Figures 4.15, 4.17 and 4.18 indicate that the soot/C_2H_2 values exceed the PAH/C_2H_2 ones by roughly one order of magnitude. This would suggest that the probability of an acetylene/soot collision resulting in a reaction is higher than the probability for an acetylene/PAH collision. This is consistent with the findings of Frenklach *et al.* [1989, 1996], who asserted that reactions between acetylene and PAH should be much slower than those between acetylene and soot. They explained this phenomenon by claiming that reaction reversibility is more significant in gaseous systems such as the C_2H_2/PAH one, represented here by reaction 4.4.

$$A_i\bullet + C_2H_2 = A_iC_2H + H \qquad \text{(reaction 4.4)}$$

Where A_i is an i-ring aromatic. Soot particles, on the other hand, have large reactive edges, which effectively eliminate the rate-limiting dependence on reversible ring cyclization.

4.6 Benzene Injection with $\phi = 1.6$ Baseline (1580K)

In this case, the experimental parameters were chosen to allow the contributions of both soot growth mechanisms to be significant. The feed to the JSR was set at a moderately high but non-sooting fuel equivalence ratio of 1.6 while the JSR temperature was set to 1600K (PFR temperature ~ 1580K). The fuel equivalence ratio ensured that the PFR was supplied with relatively high quantities of acetylene while benzene was injected into the PFR to promote PAH formation. The soot and PAH concentrations measured in this case appear in Figure 4.19. From this plot, it is evident that substantially more soot was formed than in the $\phi = 1.3$ + 4.2 g/min benzene case. This is attributed to the higher rates of formation of PAH (and consequently soot)

which resulted from benzene being injected into an environment relatively rich in acetylene. The combination of aromatics and C2 "building blocks" was perfect for the growth of higher molecular weight PAH. The concentration of PAH, unlike the ϕ = 1.3 + 4.2 g/min case, increased initially, peaked, and then decreased at higher residence times. This was ascribed to the increased role of soot as a PAH sink due to the higher soot levels. This kind of behavior is seen extensively in flat flames e.g. [McKinnon *et al.* 1992] and is what one would expect to see in the ϕ = 1.3 + benzene cases at higher residence times.

In order to estimate the relative contributions of acetylene and PAH to soot growth in this case, collision efficiency information is required for either the soot-acetylene or soot-PAH interactions. Since this is unavailable for this particular case, soot-acetylene collision efficiency values calculated for the ϕ = 2.2 were used. Equation 4.1 was then used to calculate the portion of the observed soot growth originating from acetylene addition. Table 4.2 contains the results of this analysis.

Table 4.2

Contributions of PAH and Acetylene to Soot Growth for ϕ = 1.6 + 4.2g/min benzene Case

PFR Residence Time	Contribution from PAH	Contribution from C_2H_2
7.9 ms	79 %	21 %
13.8 ms	78 %	22 %
19.6 ms	48%	52%
25.4 ms	18 %	82 %

These results illustrate how the role of PAH in soot surface growth decreases in importance once PAH concentrations decline. Since acetylene levels are more constant with residence time, acetylene becomes more dominant (in relative terms) at later stages of the growth process. This

idea of PAH controlling soot growth in the early stages and acetylene controlling growth in the later stages has been proposed by other workers e.g. Harris & Weiner [1988]. It is based on the fact that, at higher soot concentrations, the removal of PAH by collisions with soot particles is sufficient to reduce PAH levels to the point where they no longer dominate soot growth.

4.7 Toluene Injection Runs

In a series of experiments carried out in the MIT Combustion Research Facility [see description in Appendix C], a fuel-lean natural gas flame was fired and aromatic additives injected into the secondary combustion chamber of the furnace [Thijssen *et al.* 1994]. The objectives of this study were to determine the effect of i) fuel type and ii) temperature on the formation and oxidation of PAH under turbulent conditions. The two additives were chosen to be benzene and toluene and the two temperatures 1350K and 1550K. Since the natural gas flame may be treated as a "blackbox" generator of combustion gases and the secondary chamber as a PFR, this system is essentially a larger, more complex version of the JS/PFR. Because of this interesting similarity, it was decided to carry out a series of four JS/PFR experiments comprising two temperatures and two aromatic additives and matching, as closely as possible, the CRF test parameters. The experimental conditions appear in Table 4.3. Here the baseline ϕ was 1.3, and the additive injection rate 4 g/min.

Table 4.3 Experimental Parameters of CRF Comparison Tests

Additive	PFR Temperature
benzene	1520K
benzene	1650K
toluene	1520K
toluene	1650K

The tests were run at temperatures somewhat higher than those of the CRF experiments since very little soot is observed in the PFR below 1450K. To compensate for diluent effects, the feed was preheated in the 1650K cases while maintaining a constant N_2 dilution rate.

Initially the JSR fuel equivalence ratio was chosen to match the $\phi = 0.9$ conditions of the CRF natural gas flame. However, under these conditions, very little soot was formed in the PFR with benzene injection while no soot at all was formed with toluene injection. In the CRF runs, however, substantially more soot and PAH was produced with toluene injection than with benzene injection (see Appendix D). The CRF results were attributed to the greater ease with which toluene loses a hydrogen (to form benzyl radical) than does benzene (to form phenyl radical). A major difference between the two sets of experiments is that in the JS/PFR experiments the additives were prevaporized while in the CRF runs they were injected as liquids. The mixing problems associated with liquid droplet injection would explain the higher yields of soot and PAH in the CRF experiments. In other words, when injecting a spray, the local fuel equivalence ratio will significantly exceed the mean value. And since hydrogen atoms may be abstracted more readily from toluene than from benzene, toluene may be more easily oxidized in fuel-lean environments such as the $\phi = 0.9$ baseline. Therefore, the discrepancy between the CRF and JS/PFR results is very likely due to mixing phenomena. This is similar to the results of a series of jet-stirred reactor experiments [Kowalik *et al.* 1981] in which soot formation was studied with i) the toluene fuel injected as a liquid spray and ii) the fuel prevaporized and injected as a gas. It was found that substantially more soot was formed in the liquid spray cases, precisely because of the locally fuel rich pockets that arose from imperfect mixing.

The low JS/PFR soot levels motivated the shift to a slightly fuel-rich baseline (ϕ = 1.3) since this has been demonstrated to yield relatively high soot and PAH concentrations. The soot levels for the four experiments appear in Figures 4.20 and 4.21. They indicate that significantly more soot was formed with toluene injection than with benzene injection, and that the toluene vs. benzene difference diminishes as the temperature increases. At 1520K, soot levels for the toluene injection case were a factor of five higher than those of the benzene case, whereas at 1650K they were a factor of three higher. This may be explained in terms of activation energy differences between radical reactions involving benzene and toluene. Some of the more important reactions of this type are reactions 4.5-4.8 [Colket & Seery 1994].

$C_6H_6 + H = C_6H_5 + H_2$	Ea = 16.0 kcal/mole	(reaction 4.5)
$C_7H_8 + H = C_7H_7 + H_2$	Ea = 8.4 kcal/mole	(reaction 4.6)
$C_6H_6 + CH_3 = C_6H_5 + CH_4$	Ea = 16.0 kcal/mole	(reaction 4.7)
$C_7H_8 + CH_3 = C_7H_7 + CH_4$	Ea = 11.1 kcal/mole	(reaction 4.8)

Reactions 4.5 and 4.6 indicate that the activation energy for the reaction in which hydrogen atom abstracts hydrogen from benzene to produce phenyl is 7.6 kcal/mole higher than the comparable reaction for toluene. Likewise, the reaction involving CH_3 radical has a 4.9 kcal/mole higher activation energy for benzene than for toluene. Assuming that soot levels are strongly dependent on aromatic radical concentrations, one would expect soot levels from the toluene case to exceed those of the benzene case by a factor of 5-12 at 1520K and 4-10 at 1650K. This approximates the experimentally determined ratios of 5 at 1520K and 3 at 1650K.

As expected, the effect of increasing the temperature from 1520K to 1650K was to increase soot levels by a factor of 10 for the toluene injection cases and by a factor of 15 for the benzene inejction cases. This is in qualitative agreement with the CRF results.

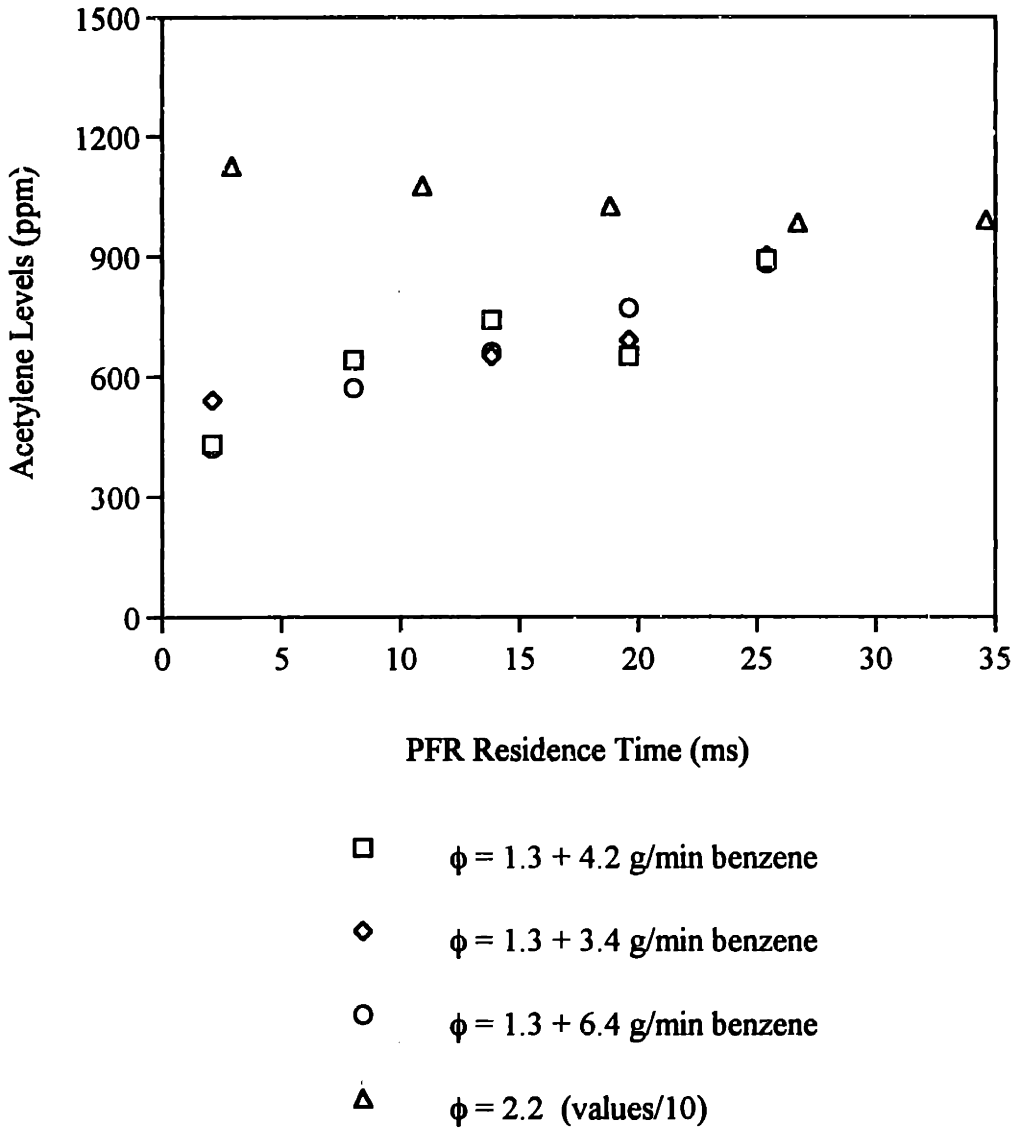

Figure 4.1 Acetylene Concentrations for 1580K Cases

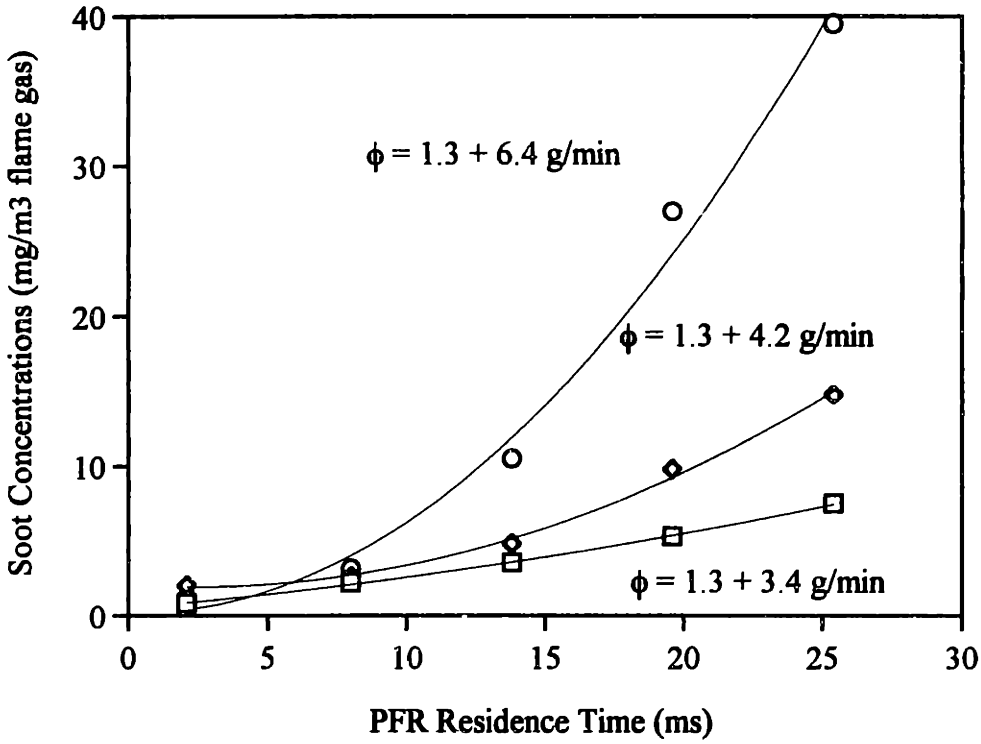

Figure 4.2 Soot Concentrations for 1580K Acetylene Lean (Benzene Injection) Cases

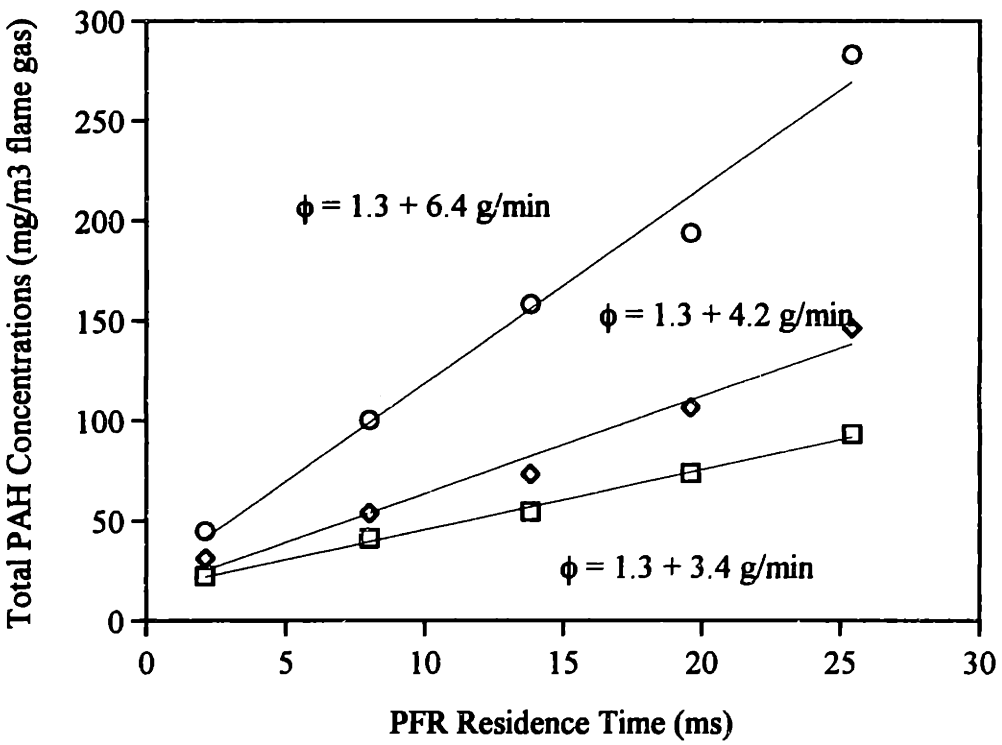

Figure 4.3 Total PAH Concentrations for 1580K Acetylene Lean (Benzene Injection) Cases

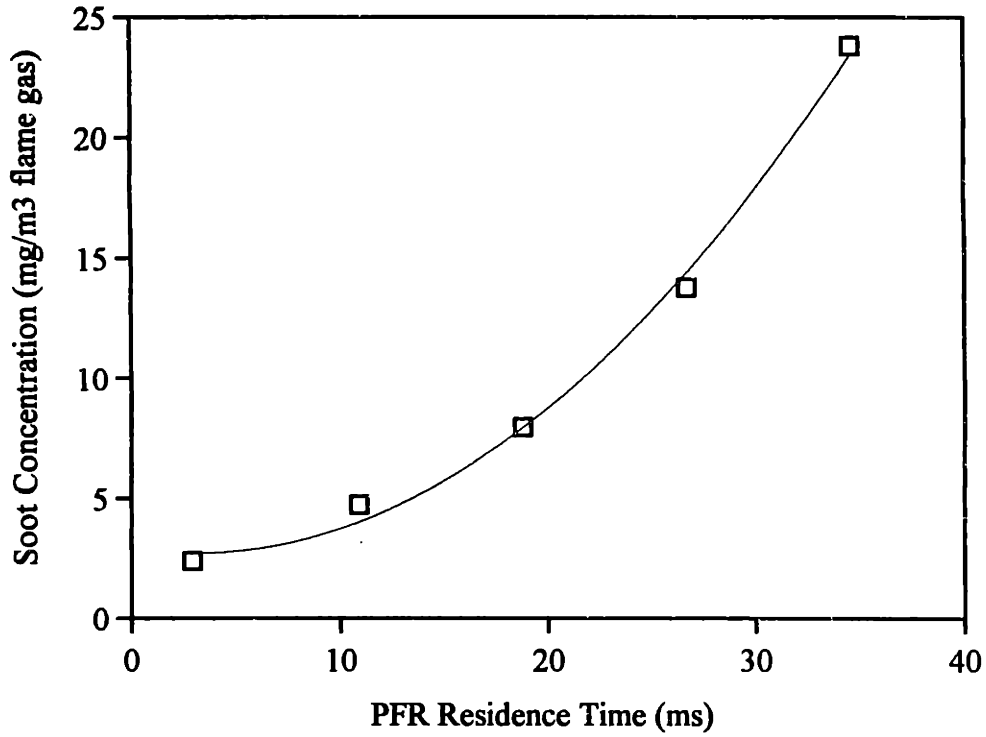

Figure 4.4 Soot Concentrations for 1580K Acetylene Rich Case

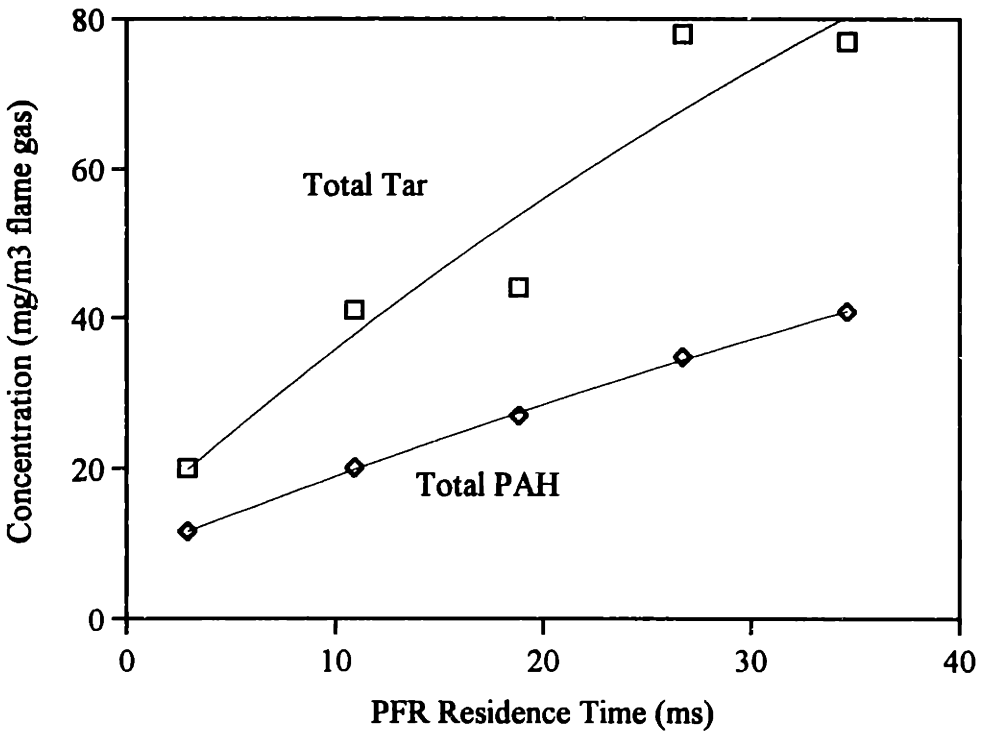

Figure 4.5 Total Tar and PAH for 1580K Acetylene Rich Case

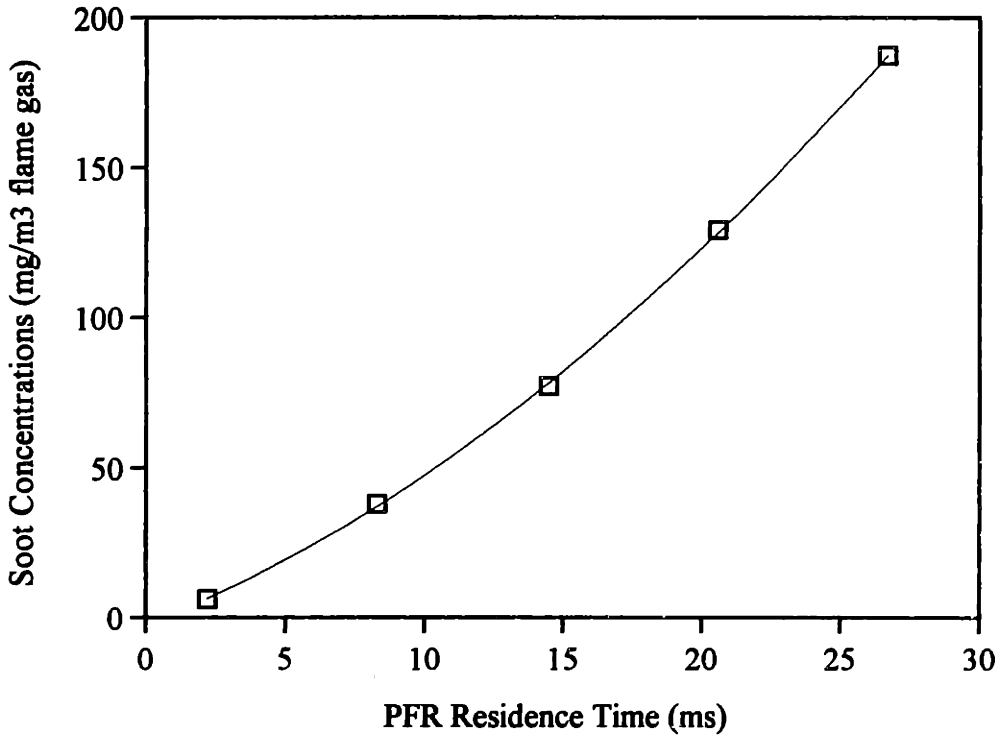

Figure 4.6 Soot Concentrations for 1650K Acetylene Lean Case
ϕ = 1.3 + 4.2 g/min benzene

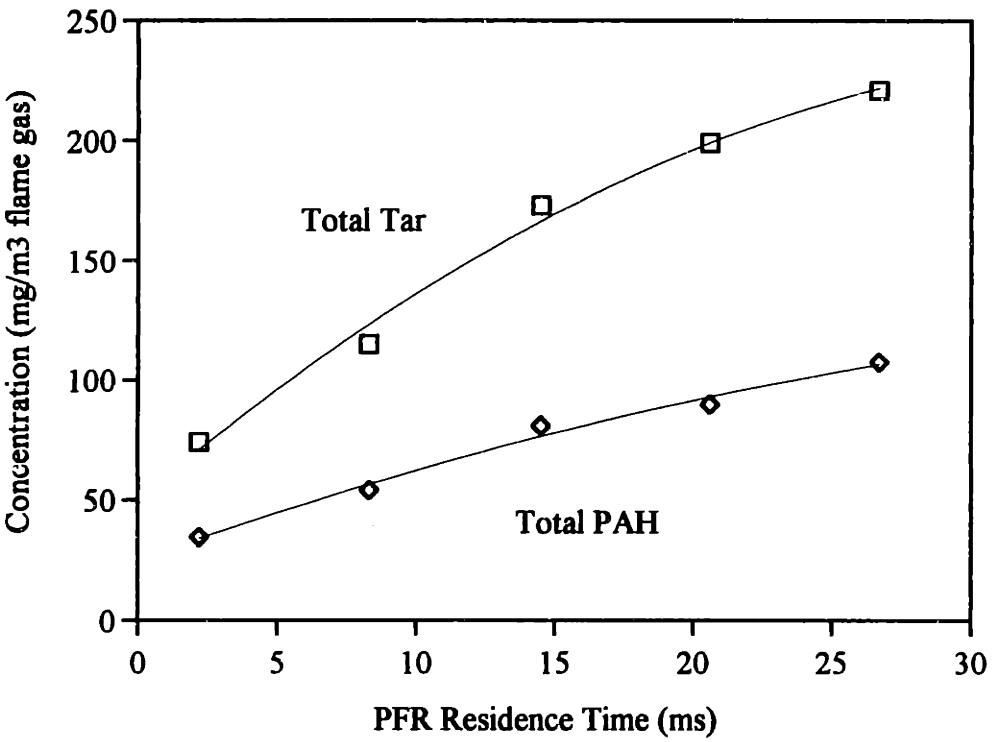

Figure 4.7 Total Tar and PAH Concentrations for 1650K Acetylene Lean Case
ϕ = 1.3 + 4.2 g/min benzene

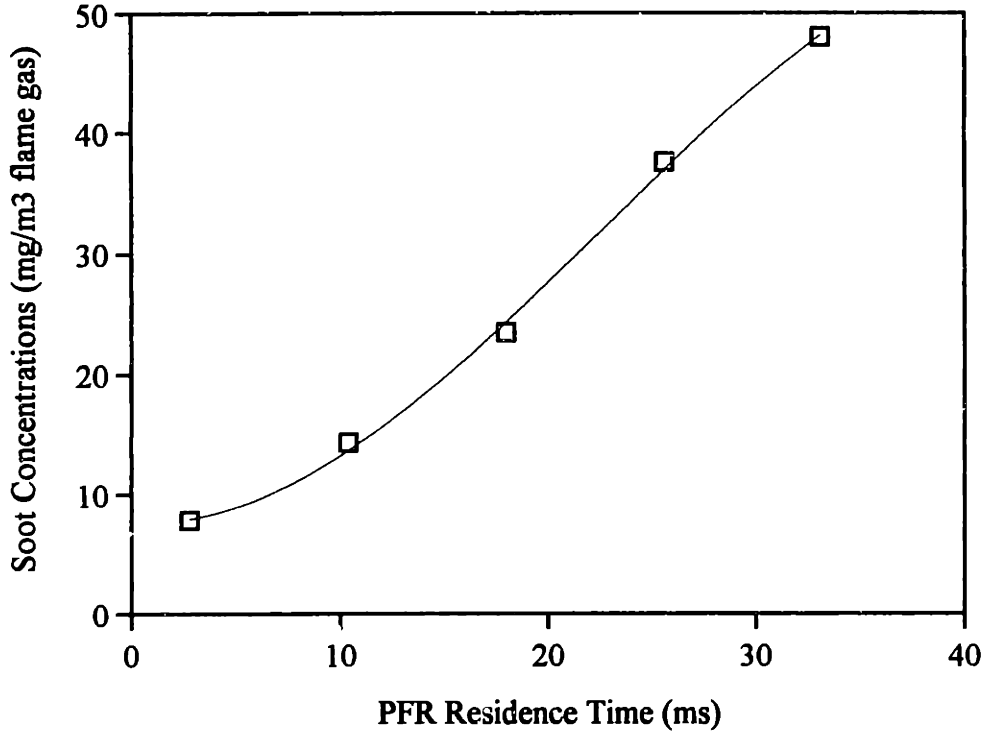

Figure 4.8 Soot Concentrations for 1650K Acetylene Rich Case

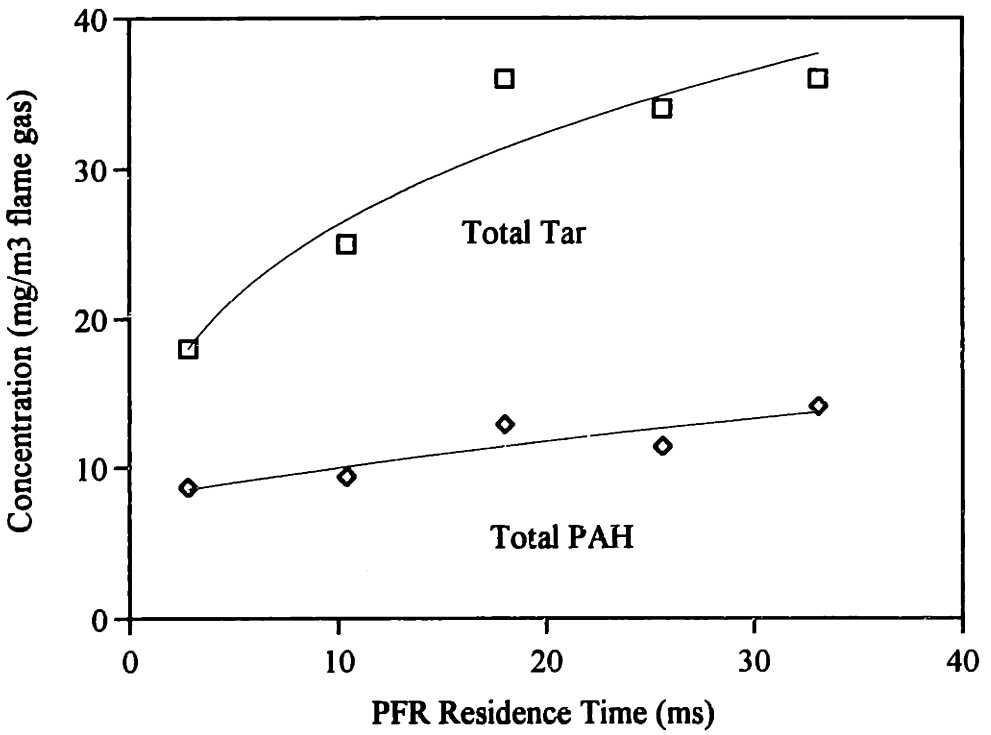

Figure 4.9 Total Tar and PAH Concentrations for 1650K Acetylene Rich Case

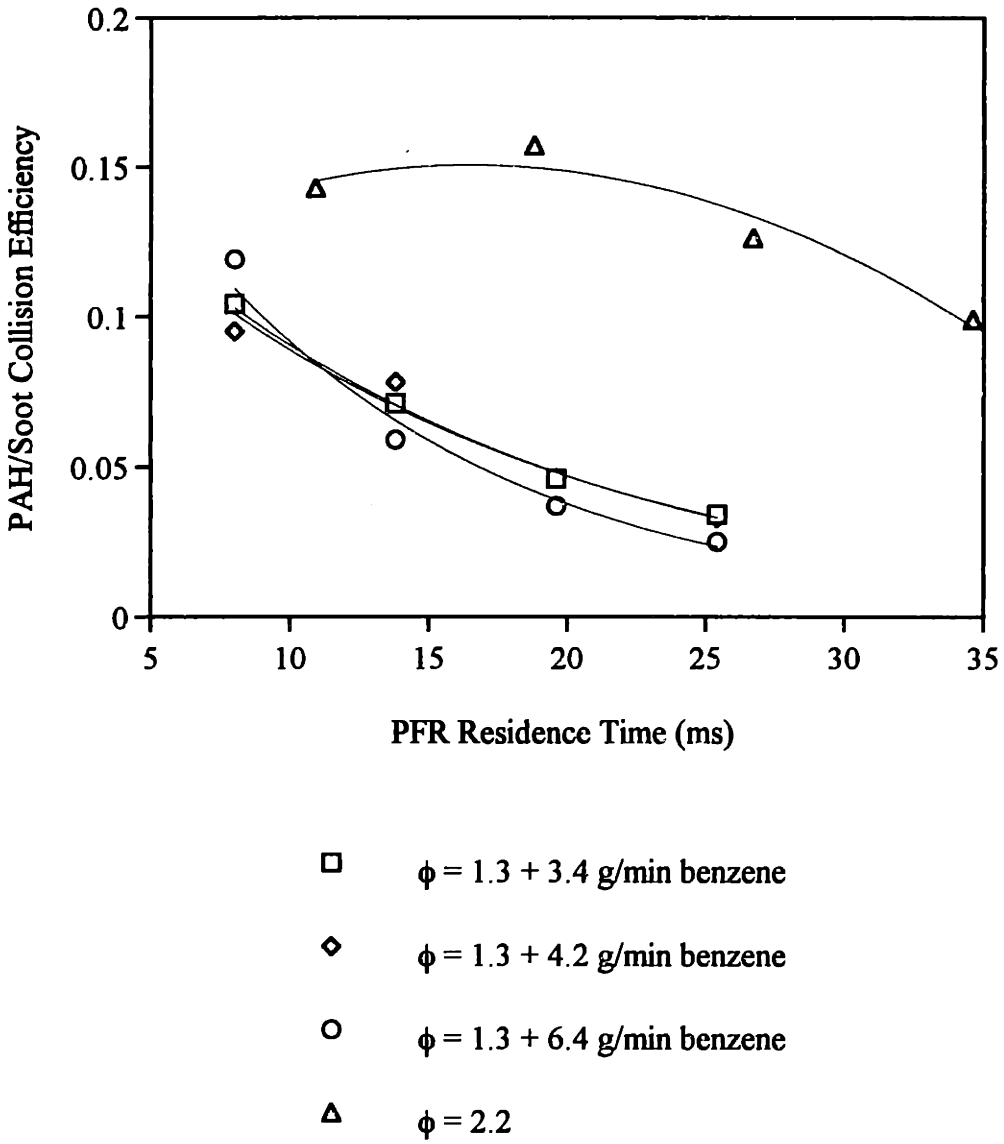

Figure 4.10 Apparent PAH/Soot Collision Efficiencies for 1580K Cases

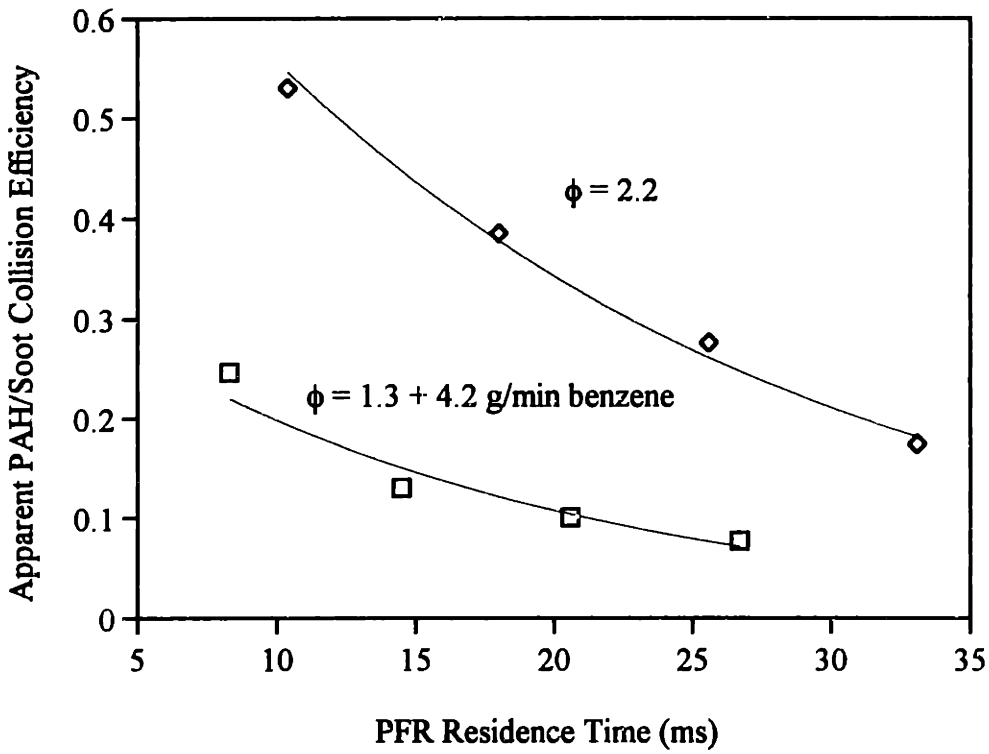

Figure 4.11 Apparent PAH/Soot Collision Efficiencies for 1650K Cases

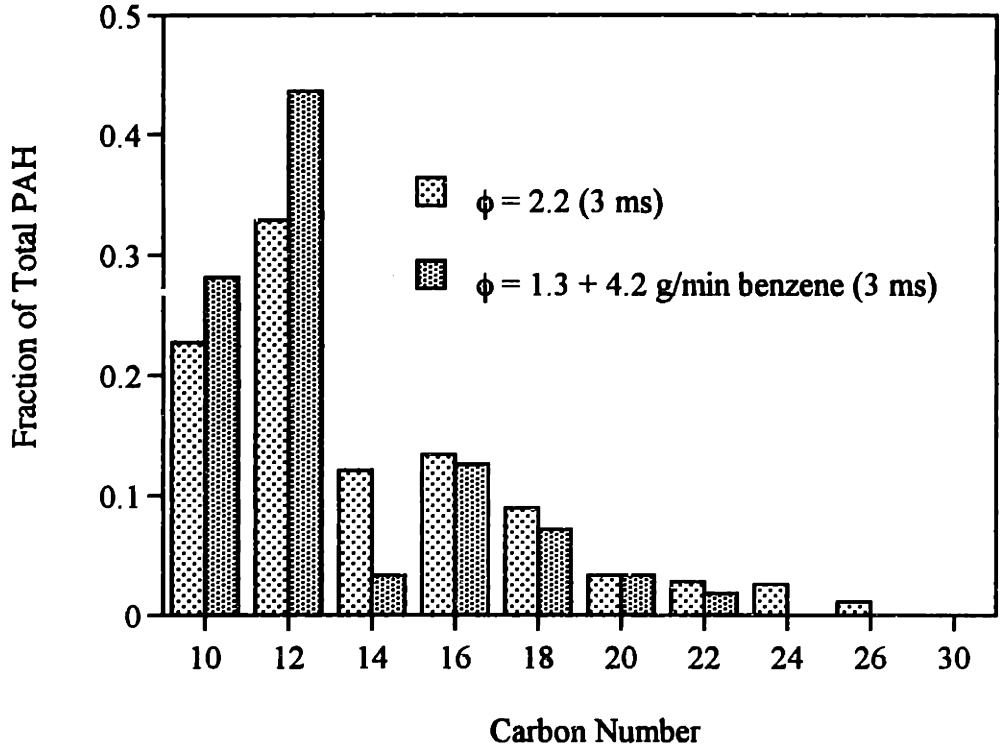

Figure 4.12 PAH Profiles for 1650K Cases at Lowest Residence Time

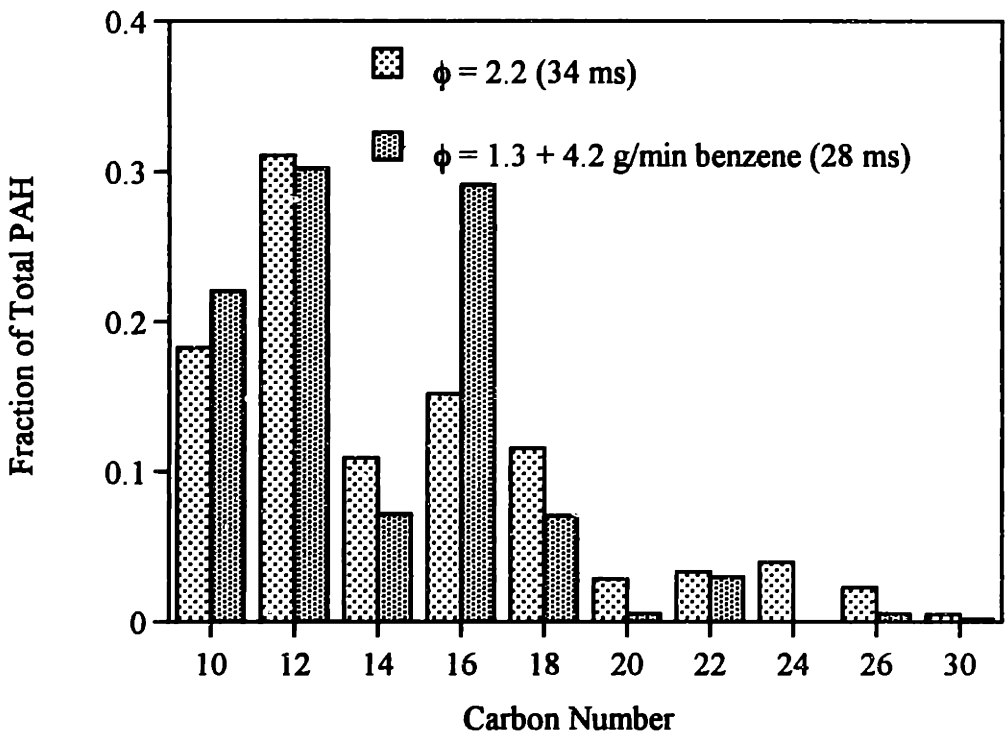

Figure 4.13 PAH Profiles for 1650K Cases at Highest Residence Time

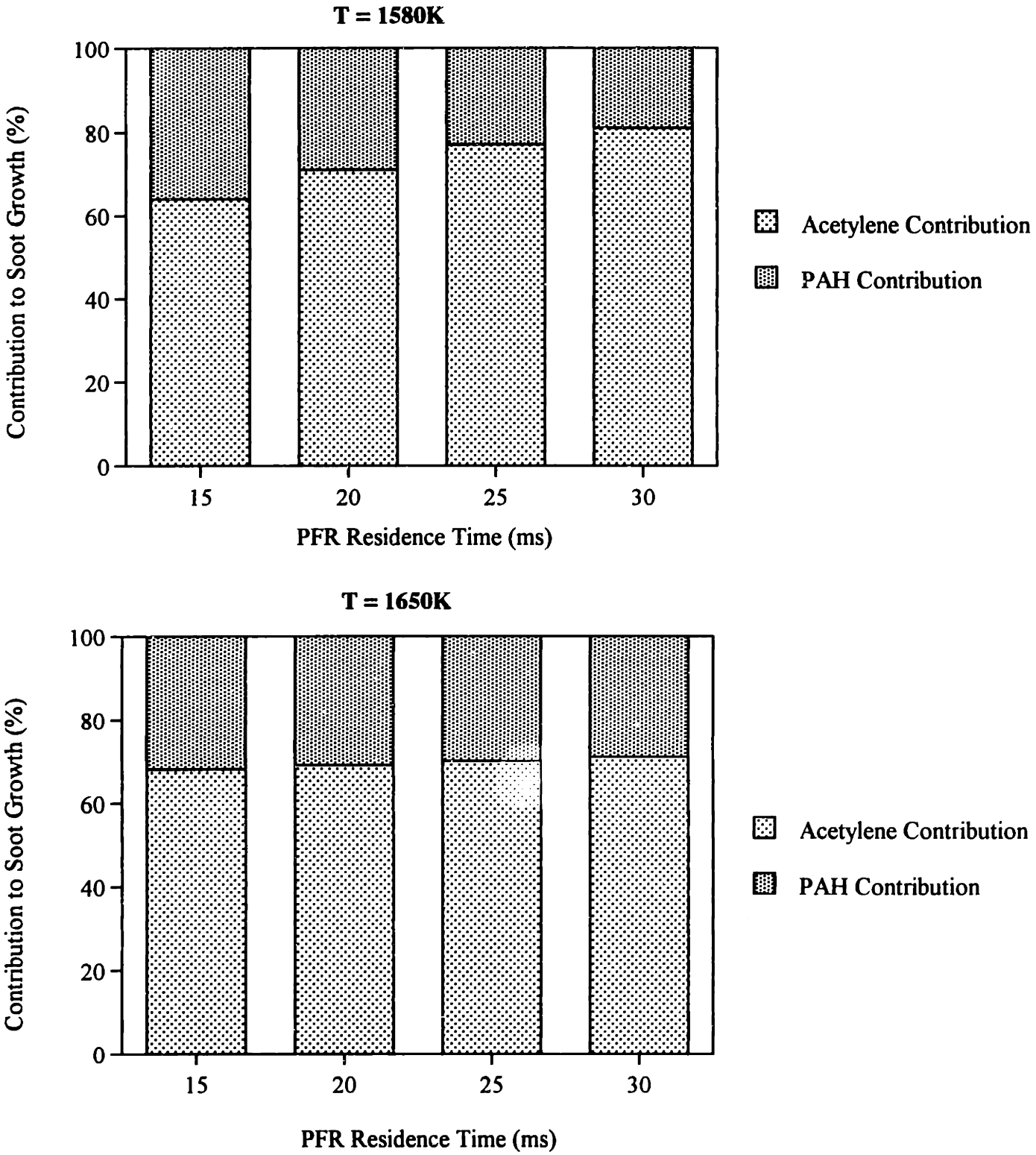

Figure 4.14 Relative Contributions of Acetylene and PAH to Soot Growth for the Acetylene Rich Cases ($\phi = 2.2$)

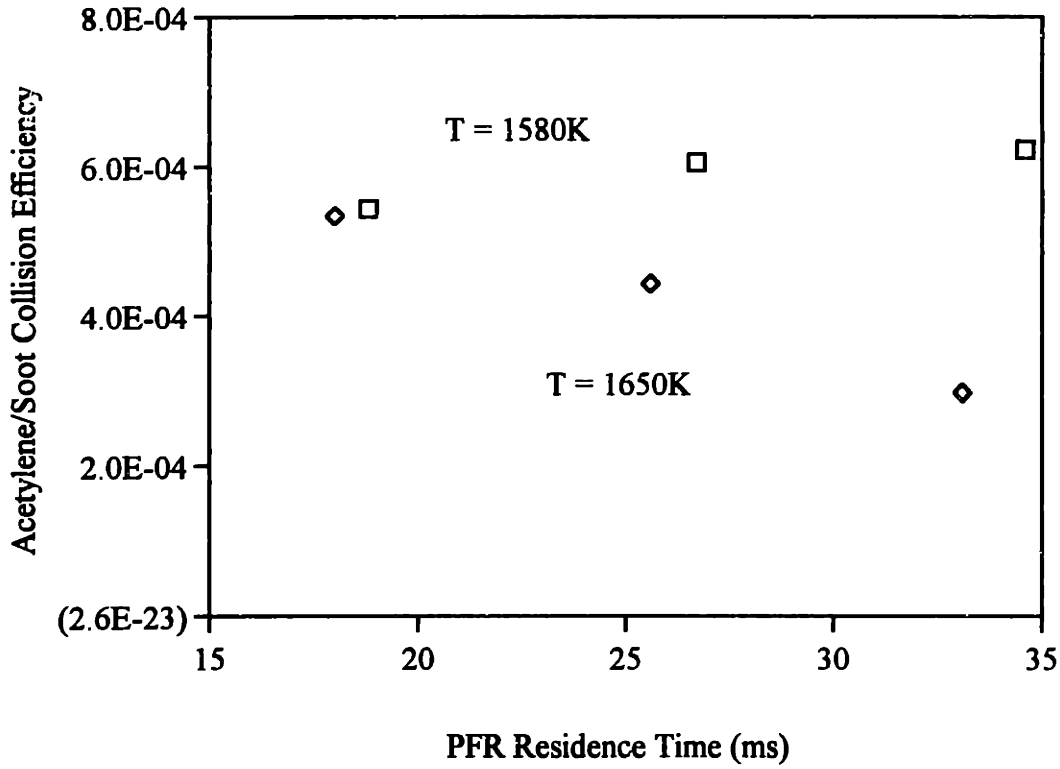

Figure 4.15 Acetylene/Soot Collision Efficiencies for Acetylene Rich Cases

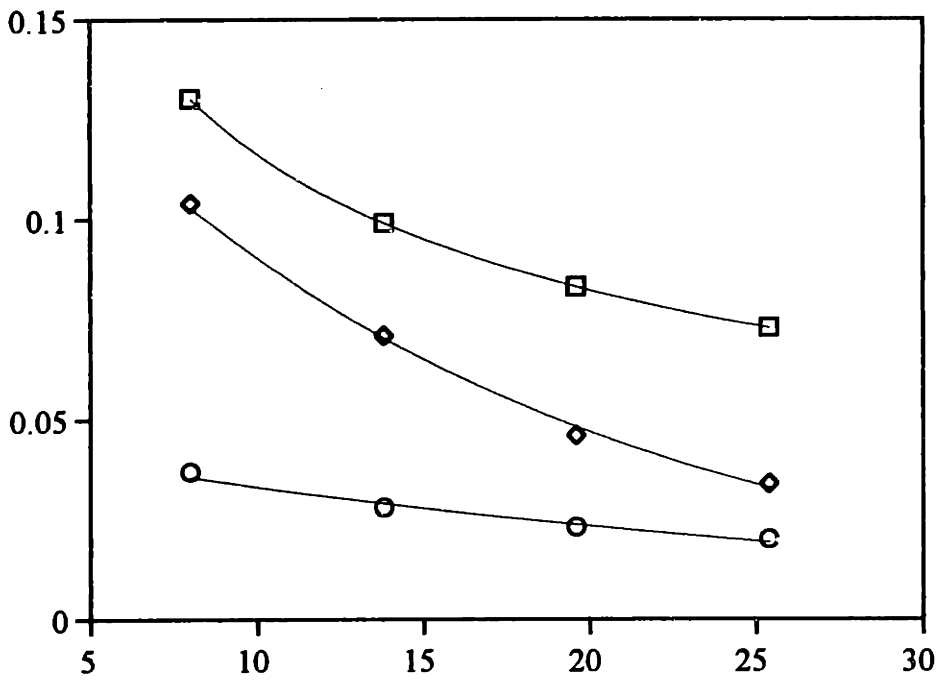

Figure 4.16 PAH/Soot Collision Efficiencies vs [Total PAH Radical]/[Total PAH] and H/H_2 Ratios

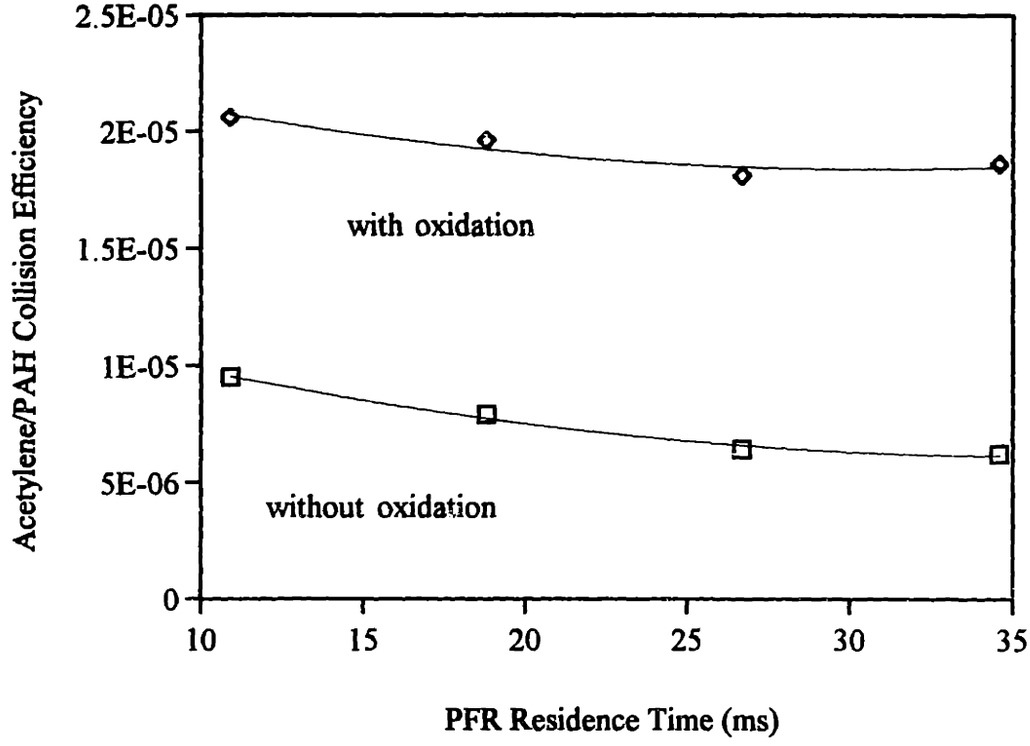

Figure 4.17 Acetylene/PAH Collision Efficiency for 1580K Acetylene Rich Case

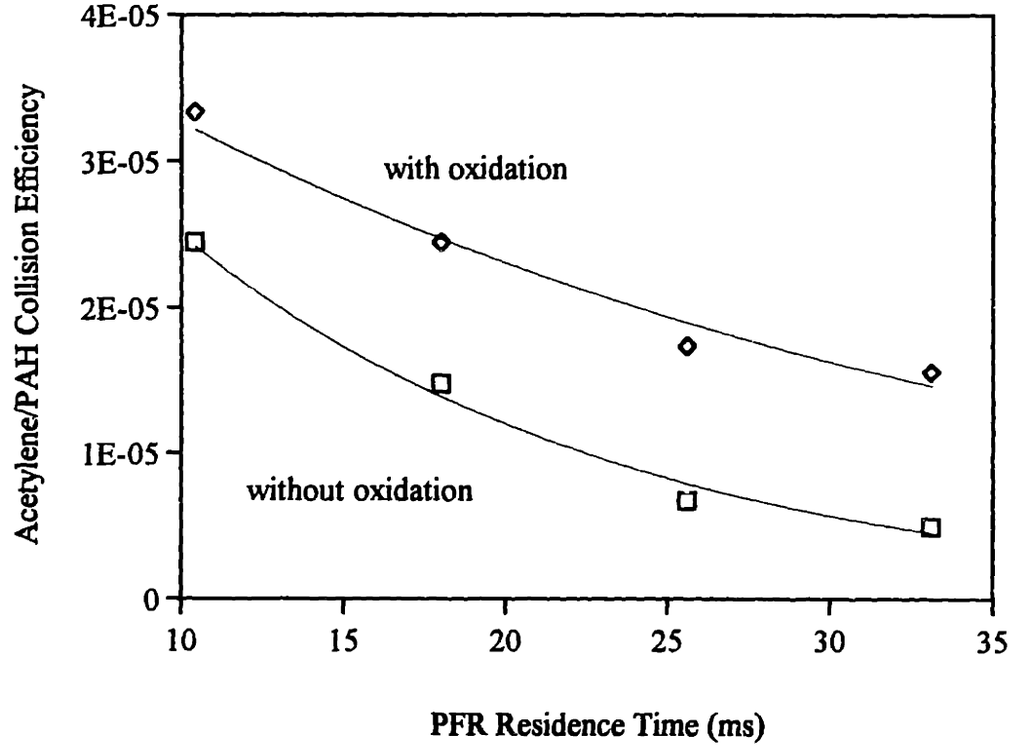

Figure 4.18 Acetylene/PAH Collision Efficiency for 1650 K Acetylene Rich Case

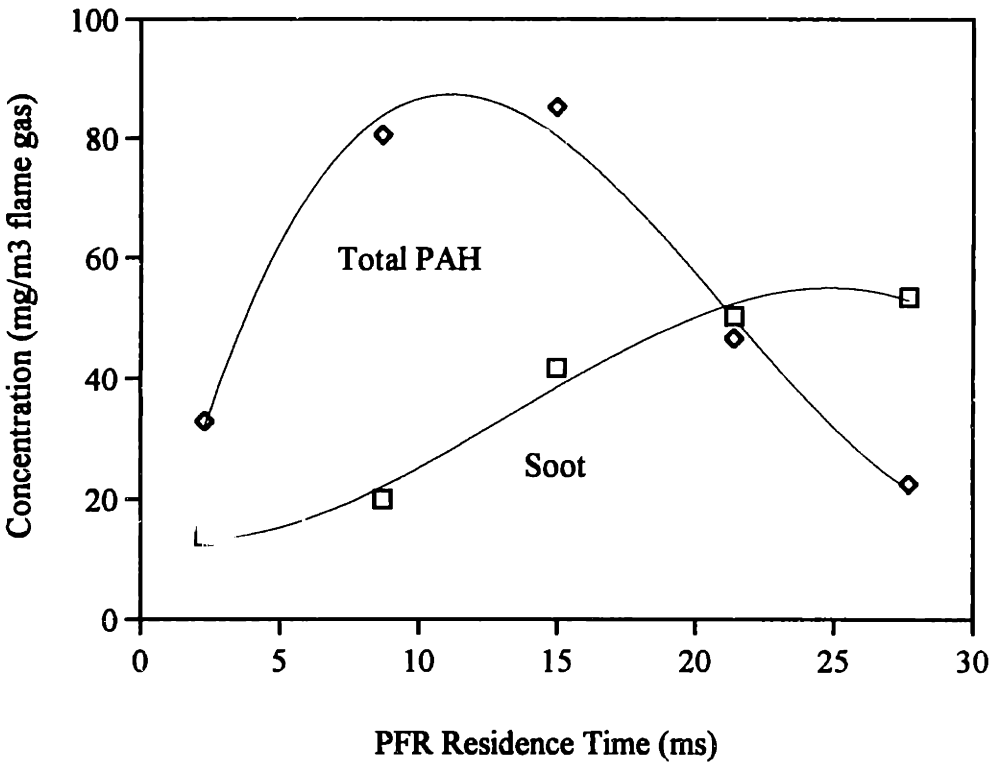

Figure 4.19 Soot and Total PAH Concentrations for 1580K $\phi = 1.6$ + benzene Case

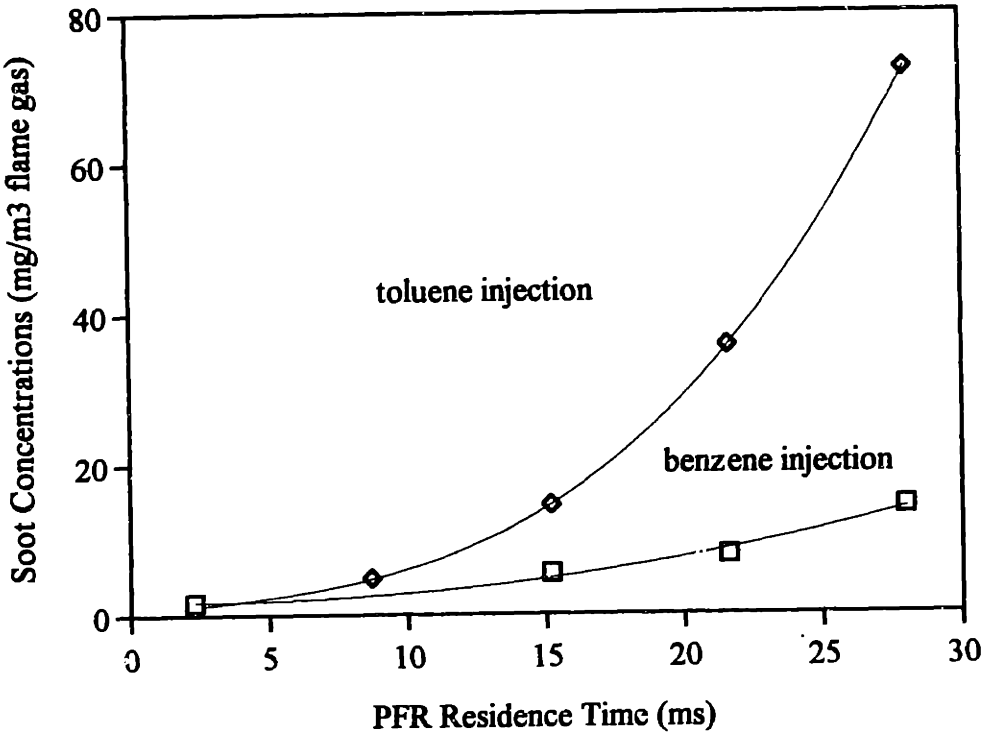

Figure 4.20 Soot Concentrations for 1540K Toluene & Benzene Injection Cases

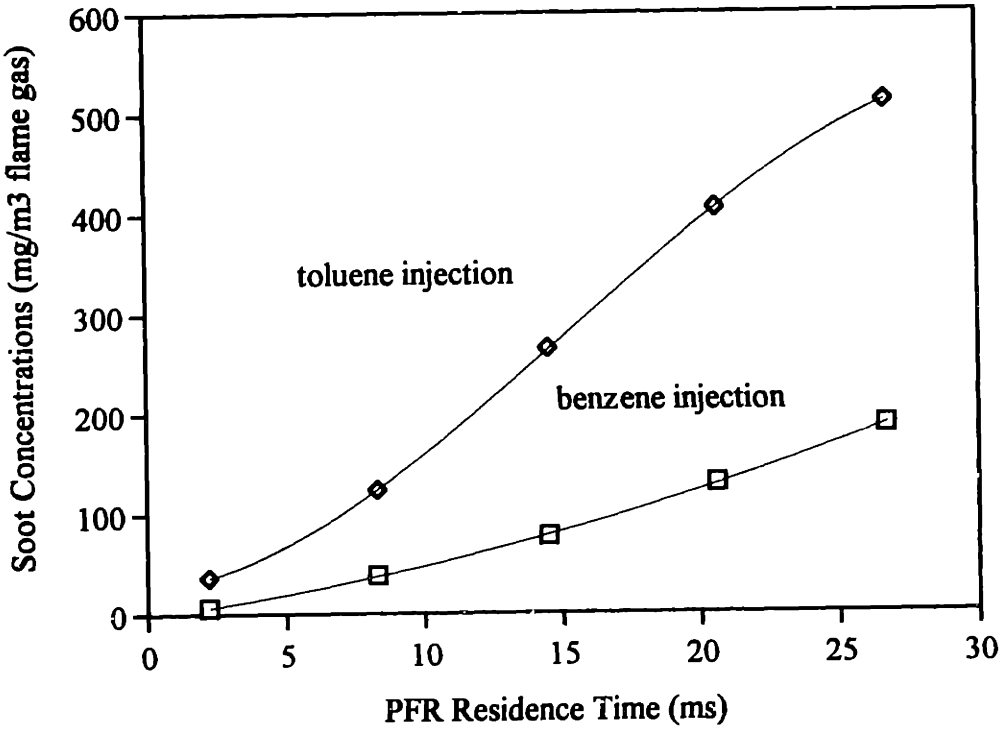

Figure 4.21 Soot Concentrations for 1670K Toluene & Benzene Injection Cases

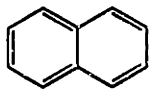

naphthalene
128 amu

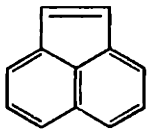

acenaphthylene
152 amu

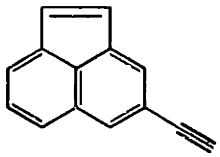

ethynyl acenaphthylene
176 amu

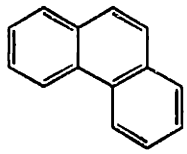

phenanthrene
178 amu

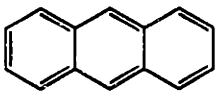

anthracene
178 amu

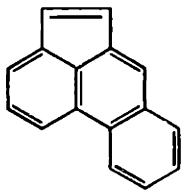

acephenanthrylene
202 amu

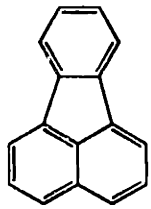

fluoranthene
202 amu

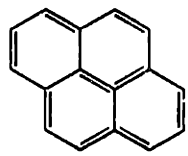

pyrene
202 amu

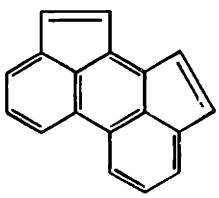

CPAP
226 amu

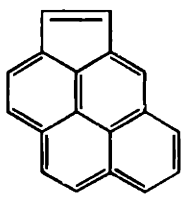

cyclopenta[c,d]pyrene
226 amu

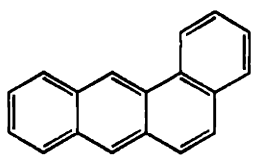

benz[a]anthracene
228 amu

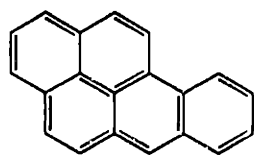

benzo[a]pyrene
252 amu

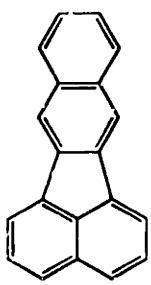

benzo[k]fluoranthene
252 amu

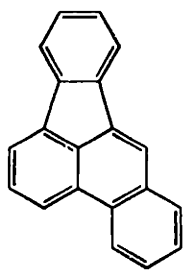

benzo[b]fluoranthene
252 amu

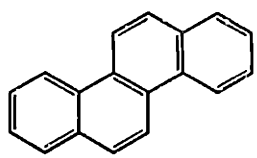

chrysene
228 amu

Figure 4.22a
PAH Species Identified by HPLC

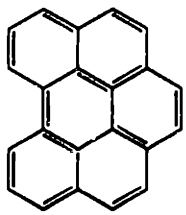

benzo[ghi]perylene
276 amu

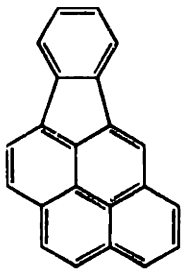

indeno[1,2,3-cd]pyrene
276 amu

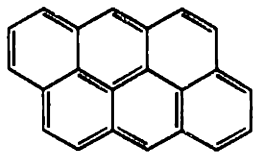

anthanthrene
276 amu

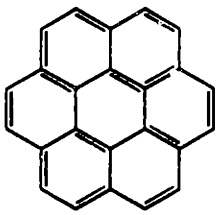

coronene
300 amu

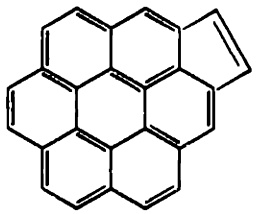

cyclopenta[c,d]coronene
324 amu

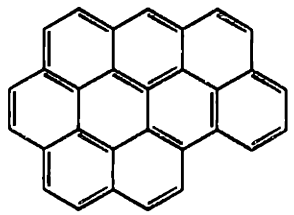

naphtho[8,1,2-abc]coronene
374 amu

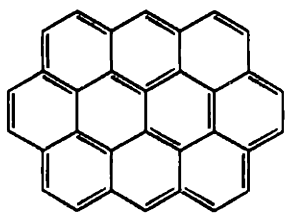

ovalene
398 amu

Figure 4.22b PAH Species detected by HPLC-UV

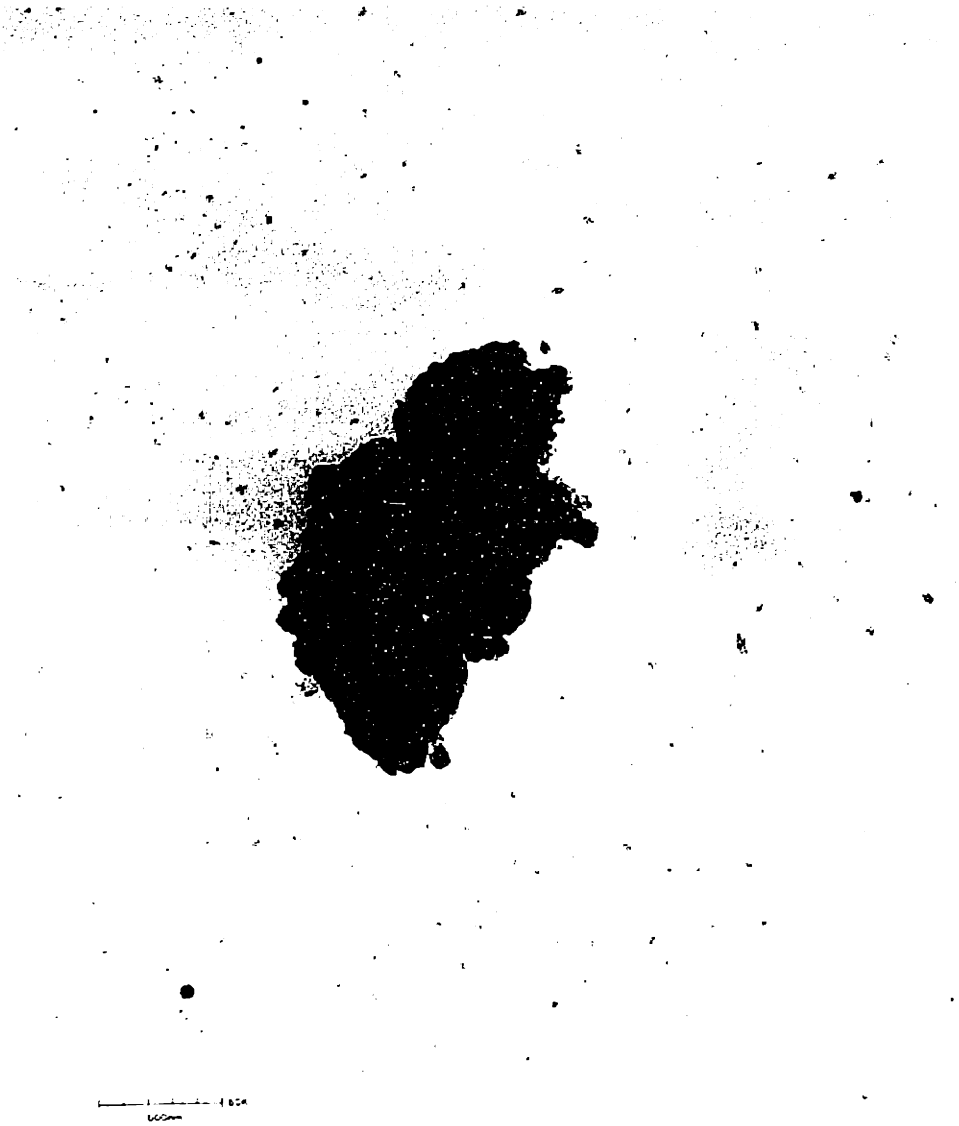

Figure 4.23 Soot Agglomerate Collected from PFR
Sample 1
ϕ = 1.3 + 4.2 g/min benzene, T = 1580K

Figure 4.24 Soot Agglomerates Collected from PFR
Sample 2
ϕ = 1.3 + 4.2 g/min benzene, T = 1580K

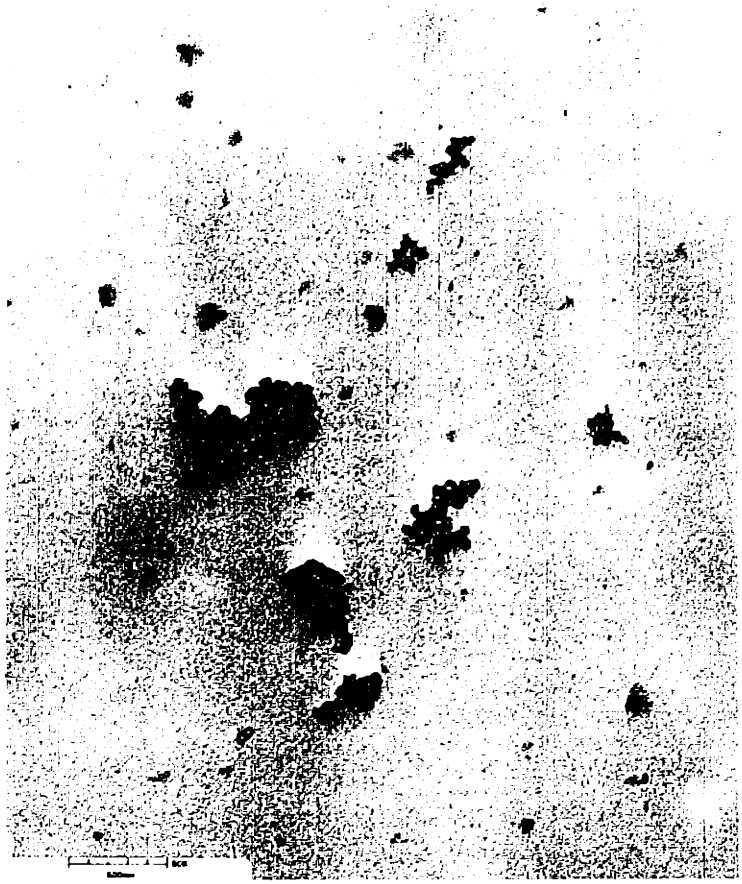

Figure 4.25 Soot Agglomerates from PFR Sample 3 (classic soot aggregate structure) ϕ = 1.3 + 4.2 g/min benzene, T = 1580K

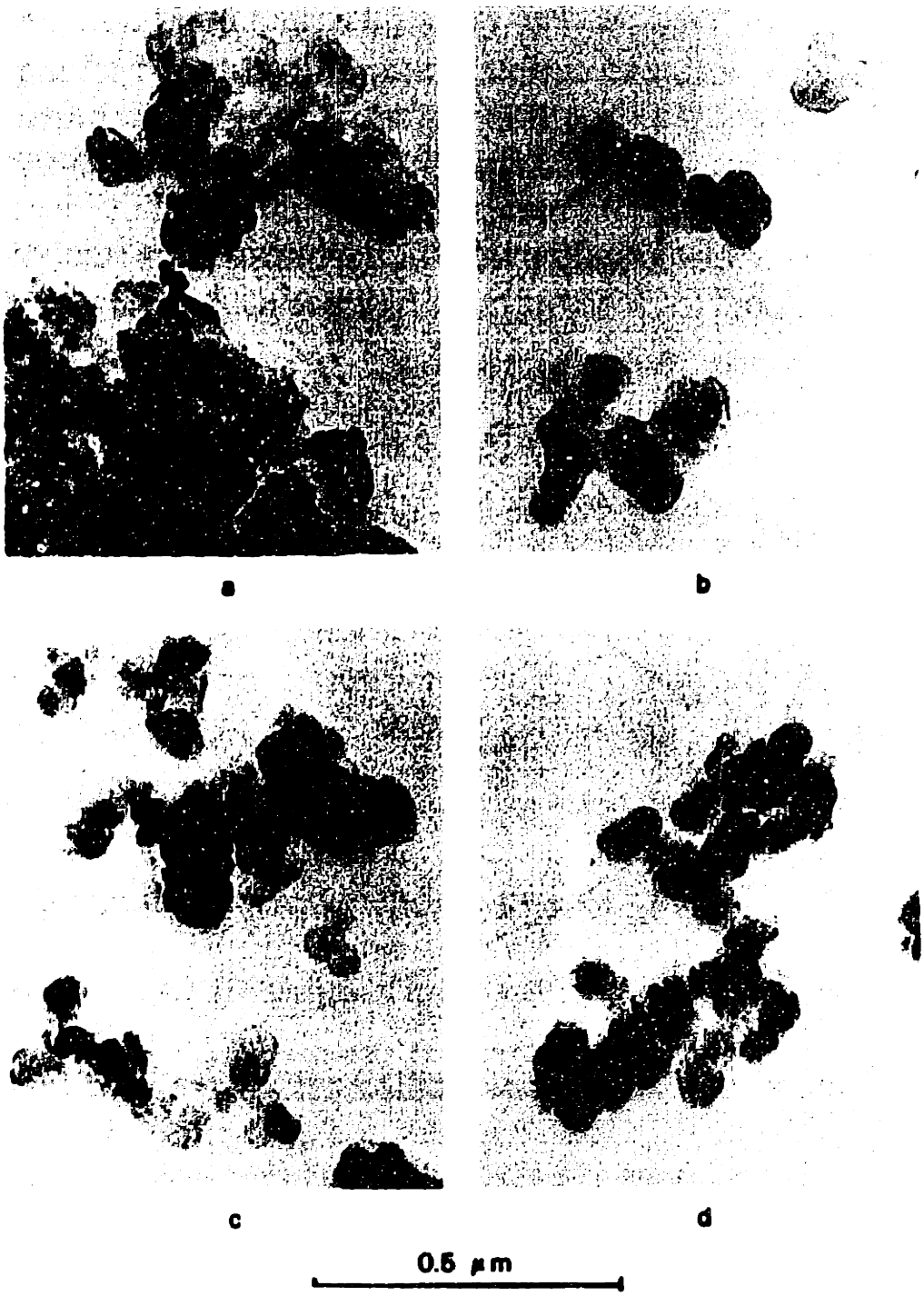

Figure 4.26 Carbonaceous Residue collected from 1383K Benzene Pyrolysis Experiment (a) 30ms (b) 50ms (c) 70ms (d) 100ms [Prado & Lahaye 1981]

Figure 4.27 Soot Agglomerate collected from 1 atm premixed ethylene/air flame, $\phi = 2.0$ [Jander 1997]

Chapter 5. The Effect of Fluegas Recirculation (FGR) on Soot and PAH Formation

This chapter outlines the strategy, methodology, and results of a study in which various diluents were injected into the JSR to simulate external flue gas recirculation (FGR). The goal was to meet objective number 3 of section 1.2 i.e. to determine the effects of diluent *type* and dilution *rate* on soot and PAH formation in the PFR.

5.1 Experimental Strategy

Previous experimental investigations into the effect of FGR on soot/PAH formation in flames have all involved the addition of diluents of some kind. The intention was to simulate fluegas (N_2, CO_2, H_2O) by introducing these species into the particular flame feed streams. However in these studies, no measures were taken to counteract the thermal effects of the respective diluents. This made it difficult to separate the dilution, thermal, and chemical effects of the diluents. Since the JS/PFR lends itself to a study in which the key parameters are varied independently, it was decided to use this apparatus to study the effects of the "fluegas diluents" on soot and PAH formation in the PFR. In addition to being a well-characterized, mono-dimensional, isothermal reactor, there is the option of preheating the ethylene/air/diluent feed stream. This extra degree of freedom allows us to compensate for the thermal effect of any diluent. In this way, the net effect of a given diluent at a given dilution rate on PAH/soot formation may be determined for a particular temperature and fuel equivalence ratio. In order to take advantage of the soot surface growth experiments which had already been carried out (described in Chapter 4), it was decided to produce soot and PAH in the PFR at a ϕ of 2.2 and at JSR temperatures of 1600K and 1670K (PFR temperatures of 1580K and 1650K respectively). The experimental parameters appear in Table 5.1.

Table 5.1 Experimental Parameters for FGR Tests

ϕ	PFR Temperature	Feed Temperature	N_2 Dilution Rate	CO_2 Dilution Rate
2.2	1580K	20°C	13.5%	0
2.2	1580K	180°C	21%	0
2.2	1580K	170°C	5.5%	8%
2.2	1650K	130°C	13.5%	0
2.2	1650K	210°C	5.5%	8%

Dilution rates expressed as percentages of total feed

5.2 Dilution with Nitrogen

The baseline case of this investigation refers to the case where no feed preheat took place and where nitrogen dilution was used to maintain a given JSR temperature. For a JSR temperature of 1600K (PFR temperature ~ 1580K) and a fuel equivalence ratio (ϕ) of 2.2, the baseline nitrogen dilution rate was 13.5% (molar) of the total flow. This is the 1580K, acetylene-rich case described in Chapter 4. Upon heating the feed to 180°C, a nitrogen dilution rate of 21% was required to maintain the JSR temperature at 1600K. The soot concentrations for both the baseline case and this "extra N_2 dilution" case appear in Figure 5.1. These soot levels, determined by the customary gravimetric technique, illustrate the effect of the degree of dilution on soot formation. They reveal that increasing the nitrogen dilution rate from 13.5% to 21% resulted in a 30% drop in soot levels. The corresponding total PAH and total tar levels appear in figure 5.2. The total PAH data were obtained by summing the concentrations of the PAH species identified by HPLC-UV analysis. The list of identifiable PAH compounds ranges from naphthalene (128 amu) to ovalene (398 amu). "Total Tar" is defined as all methylene chloride (DCM) soluable material in the PAH samples. Although the drop in PAH and total tar levels appears to be more

modest than the soot reduction, the increased nitrogen dilution rate was nonetheless effective in reducing PAH formation. The acetylene concentrations for these two cases appear in figure 5.3. Due to its very active role in both PAH and soot formation, acetylene was used as the representative PAH/soot growth agent. As figure 5.3 indicates, the effect of increasing the N_2 dilution rate resulted in a drop in C_2H_2 levels of about 10%. Since the prime C_2H_2 source is unreacted C_2H_4, the expected effect of the nitrogen dilution would be a proportional drop in acetylene levels.

5.3 Dilution with Carbon Dioxide

The effect of CO_2 as a diluting species was compared with N_2 by substituting the 13.5% N_2 diluent stream with an 8% CO_2 + 5.5% N_2 stream and preheating the feed to compensate for the higher heat capacity of the carbon dioxide. The total diluent flowrate was kept at 13.5%. Again, the JSR temperature was set to 1600K (PFR temperature ~ 1580K) and the fuel equivalence ratio to 2.2. The soot measurements for these two experiments appear in Figure 5.4. This plot indicates that the soot reduction due to 8% CO_2 + 5.5% N_2 dilution was comparable to that of the 21% N_2 dilution case. This interesting result indicates that, under these conditions, carbon dioxide does not behave as an inert species but rather acts as a soot/PAH suppressor. To investigate the dependence of this effect on temperature, the baseline (13.5% N_2 dilution) and 8% CO_2 + 5.5% N_2 dilution experiments were repeated at 1670K (PFR temperature ~ 1650K). To attain this higher temperature without varying the diluent rate, additional preheat was applied to the feed stream. The baseline case is the 1650K, acetylene-rich case reported in Chapter 4. Figure 5.5 contains the soot concentrations for these two cases. It is evident from this plot that CO_2 dilution reduced soot formation at the higher temperature and that the reduction was higher than that of the 1580K case.

The question that arises is how exactly does CO_2 act as a soot inhibitor? This issue was examined by exploring the possibility of i) CO_2 acting as a significant soot oxidizer and ii) CO_2 reducing soot precursor levels. The idea of CO_2 being an important soot oxidizing agent (relative to O_2, OH, and O) was dismissed since experimental evidence suggests otherwise. In the study conducted by Neoh *et al.* [1981], it was shown that, in their methane flames, the act of varying the fuel equivalence ratio significantly altered the soot oxidation rate but maintained constant CO_2 levels. This result ruled out the idea of CO_2 acting as a soot oxidizer in our case, and pointed towards the possibility of CO_2 reducing soot *precursor* levels. Due to its active role in both PAH and soot formation, acetylene was used as the single representative soot precursor since the expectation was that any effect of CO_2 on acetylene levels would lead to noticeable variations in soot levels.

The measured acetylene concentrations for this case and the baseline cases appear in figure 5.7. As was observed in the 21% N_2 dilution case, acetylene levels were reduced by roughly 10%. Since the dilution rate and all other parameters bar the CO_2 concentration were equal for the two cases, the result suggests that CO_2 acted as a hydrocarbon oxidizer. To shed some light on how CO_2 oxidizes hydrocarbons, the JS/PFR was modeled by using the well-established technique of simulating the JSR as a perfectly stirred reactor (Chemkin PSR model) and the PFR as an ideal plugflow reactor (Senkin) [Kee *et al.* 1989]. Detailed descriptions of how Chemkin is applied to the JS/PFR appear in Marr [1993]. The predicted acetylene levels for the 13.5% N_2, 21% N_2, and 8% CO_2 + 5.5% N_2 cases (T = 1580K) appear in figure 5.6, while the results for the 13.5% N_2 and 8% CO_2 + 5.5% N_2 cases (T = 1650K) appear in figure 5.7. These results, which are consistent with the measured data, illustrate the effect of CO_2 on the prime soot/PAH precursor. The reaction by which CO_2 oxidizes hydrocarbons is believed to be reaction 5.1

$$CO_2 + H \Rightarrow CO + OH \qquad \text{(reaction 5.1)}$$

According to this reaction, a result of boosting the CO_2 levels by adding CO_2 to the feed would be a higher formation rate of OH radicals. OH has been identified as a significant hydrocarbon and soot oxidizing species, and as such could play an active role in reducing acetylene levels. This mechanism could also be considered a component of a global fuel reforming reaction such as reaction 5.2.

$$CH_n + CO_2 \Rightarrow 2CO + {}^{n}/_{2}\, H_2 \qquad \text{(reaction 5.2)}$$

To examine the influence of N_2 and CO_2 dilution on the formation of aromatics, a PAH mechanism was incorporated into the Chemkin model of the JS/PFR. Marr's GROW model [Marr 1993] was selected for this purpose. This mechanism comprises over 300 reactions and 115 species ranging from the fixed gases through the polycyclic aromatics to coronene. Although the model has shortcomings in accurately predicting PAH concentrations, it is capable of reproducing trends. Figure 5.8 contains the model predictions for a representative PAH, namely acenaphthylene, at a PFR temperature of 1580K. These results are consistent with the measured soot and PAH concentrations at 1580K. The 1650K predictions for acenaphthylene appear in Figure 5.9. They also show consistency with the soot data.

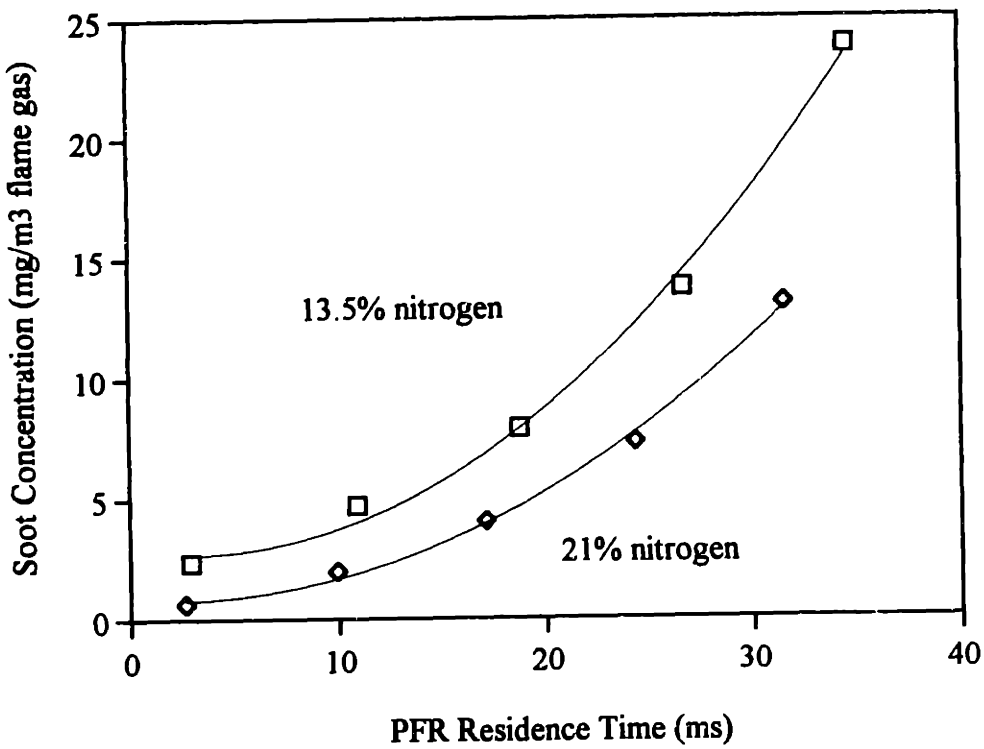

Figure 5.1
Soot Concentrations for Nitrogen Dilution Experiments
$\phi = 2.2$, T = 1580K

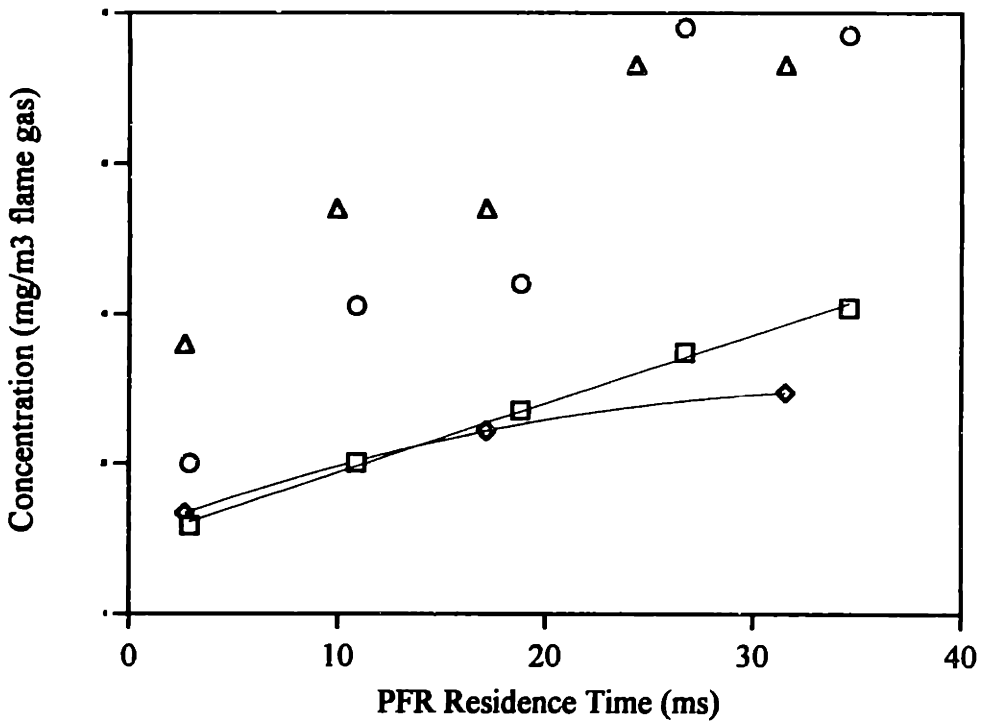

Figure 5.2
Total PAH and Total Tar Concentrations for Nitrogen Dilution Experiments $\phi = 2.2$, T = 1580K

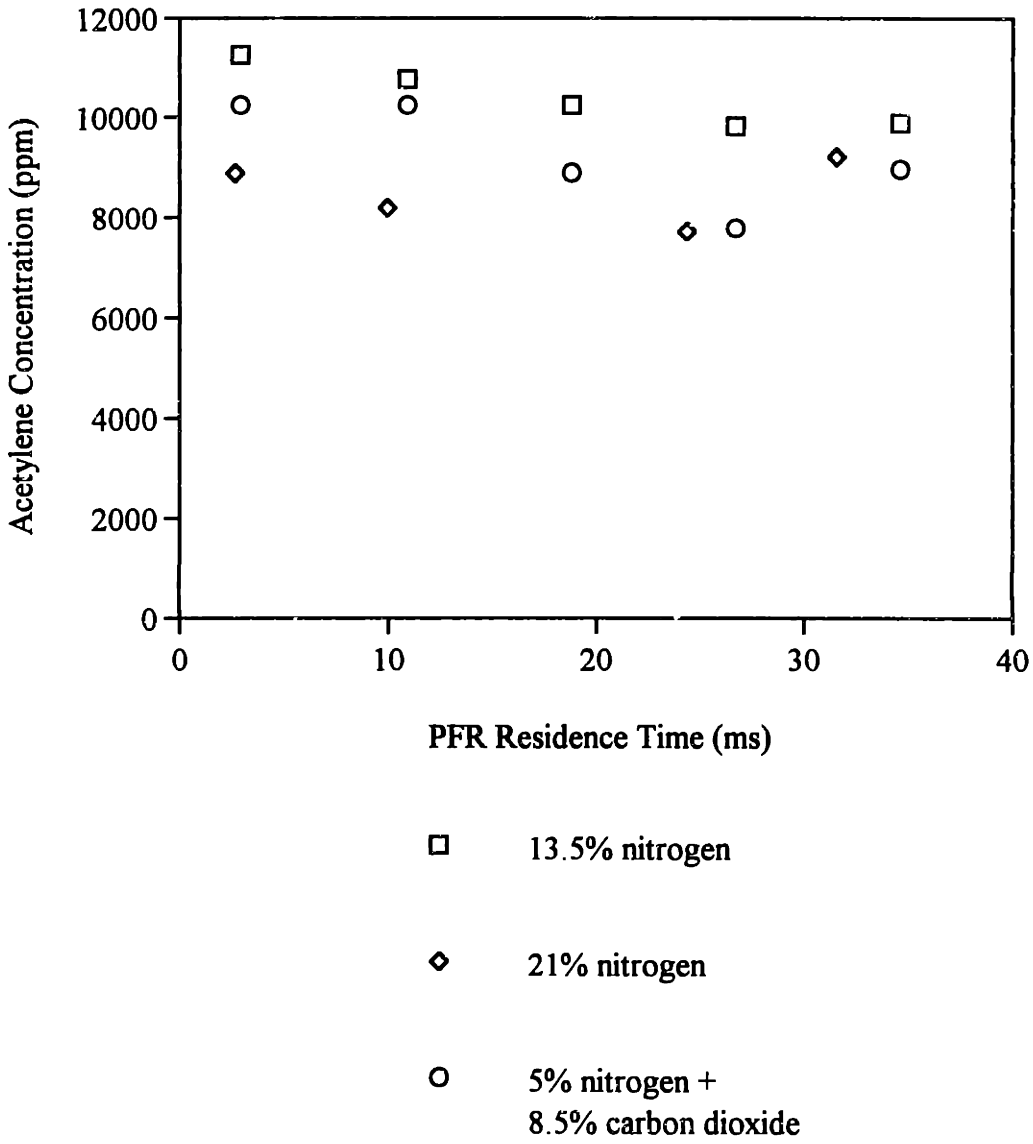

Figure 5.3 Acetylene Concentrations for 1580K Cases
$\phi = 2.2$

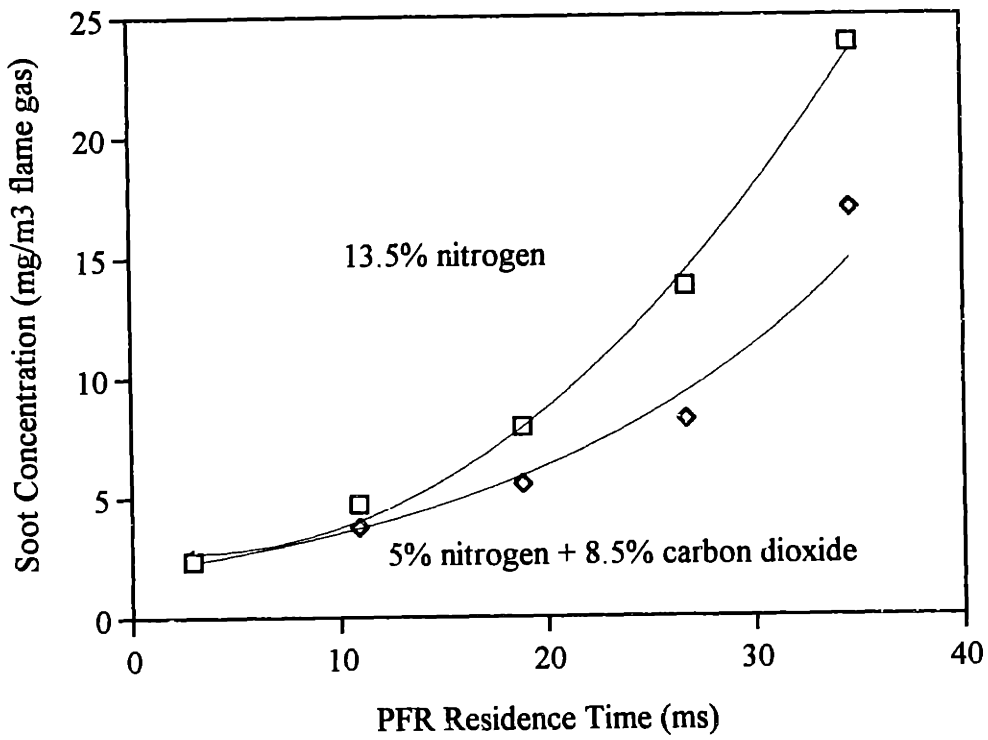

Figure 5.4 Soot Concentrations for 1580K Carbon Dioxide Dilution Case $\phi = 2.2$

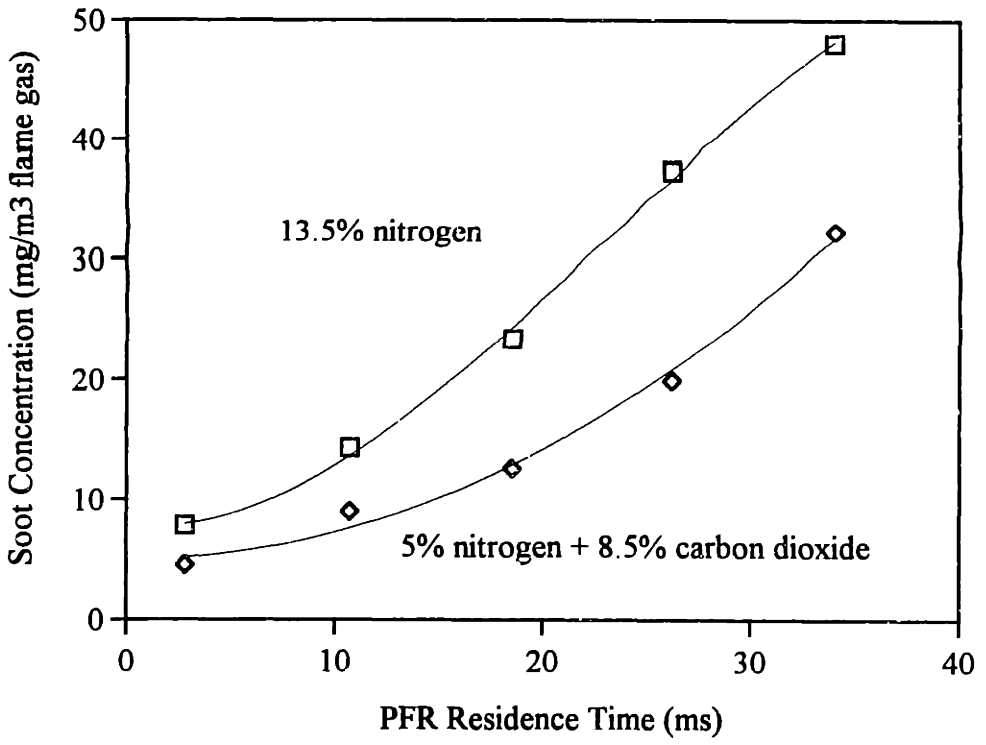

Figure 5.5 Soot Concentration for 1650K Carbon Dioxide Dilution Case
$\phi = 2.2$

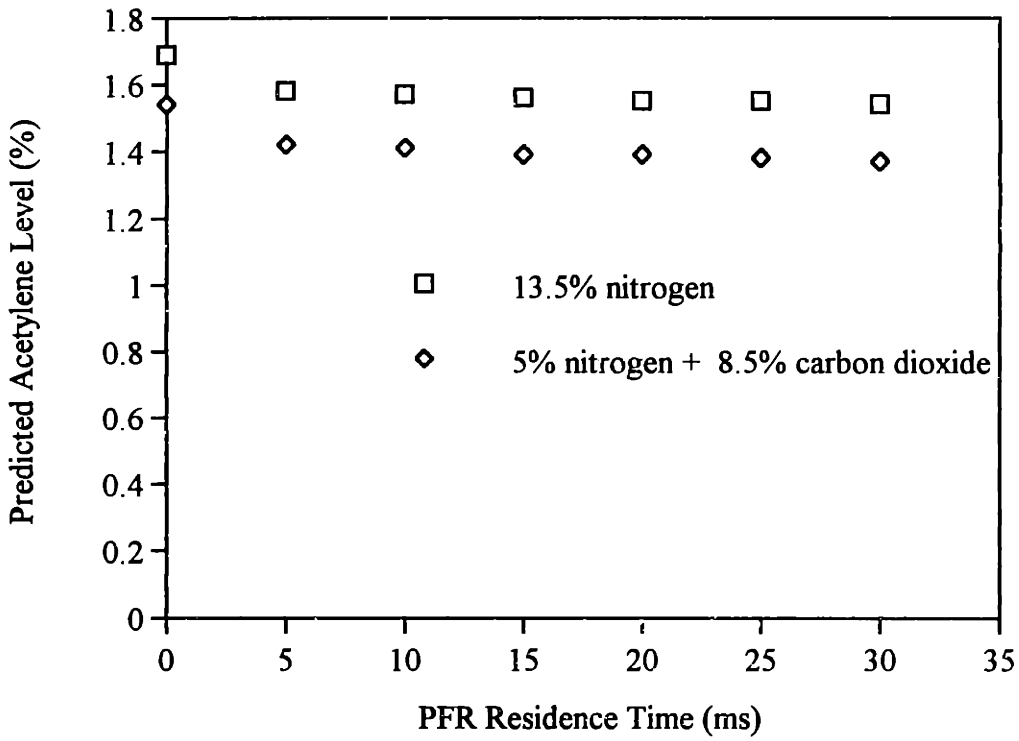

Figure 5.6 Predicted Acetylene Levels for 1580K Carbon Dioxide Dilution Case

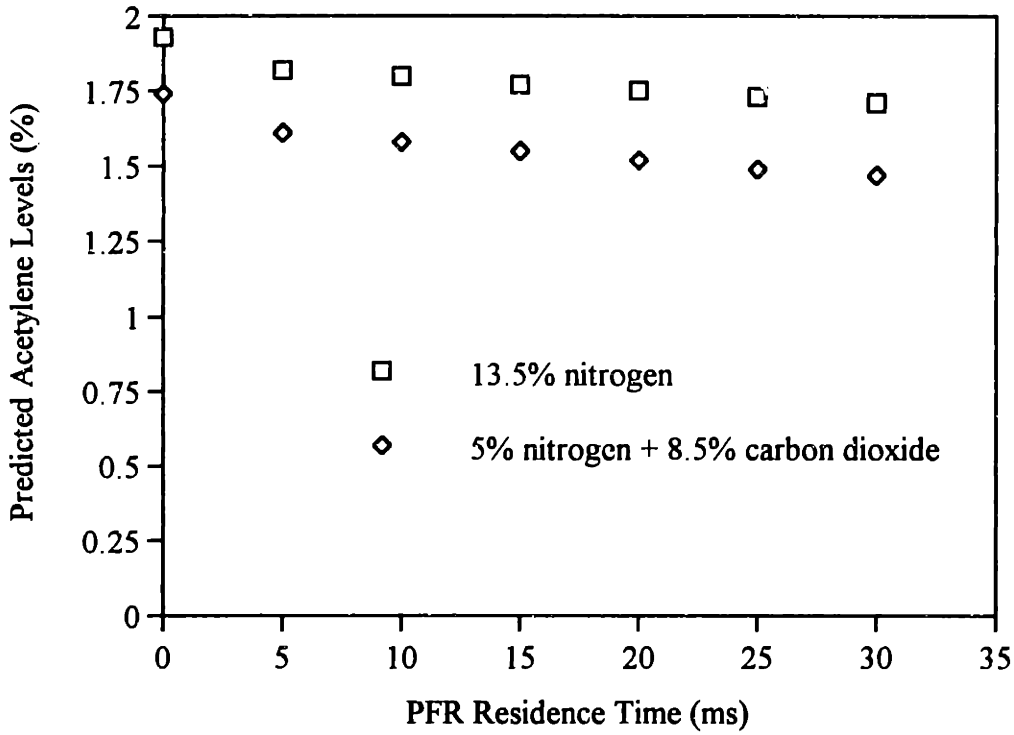

Figure 5.7 Predicted Acetylene Levels for 1650K Carbon Dioxide Dilution Case

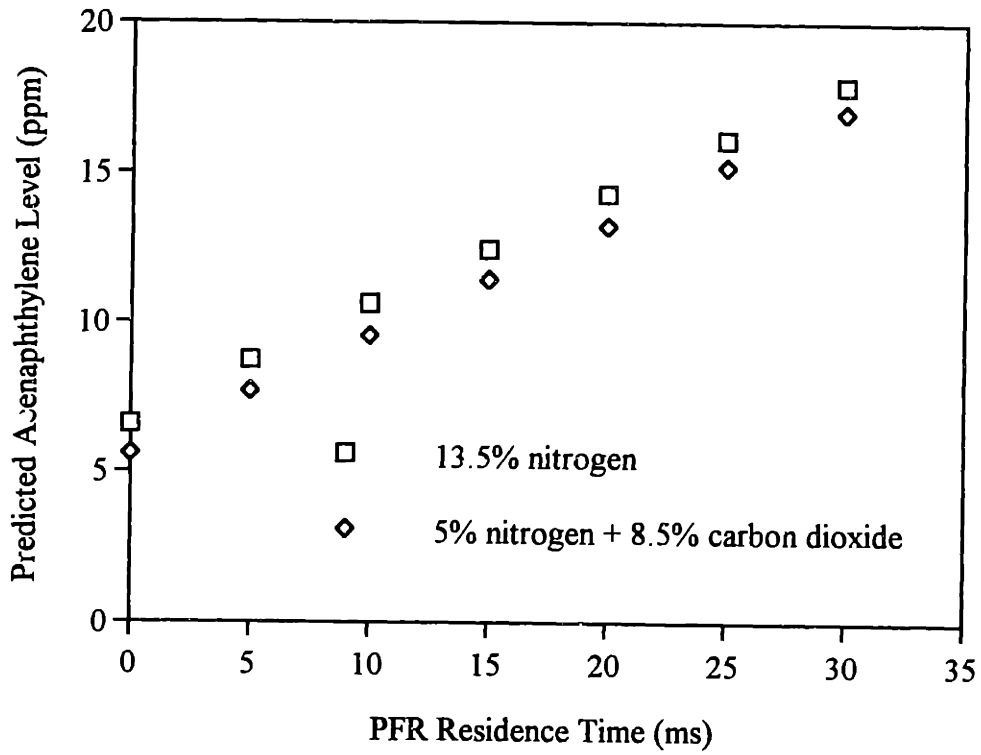

Figure 5.8 Predicted Acenaphthylene Levels for Carbon Dioxide Dilution Case
T = 1580K, $\phi = 2.2$

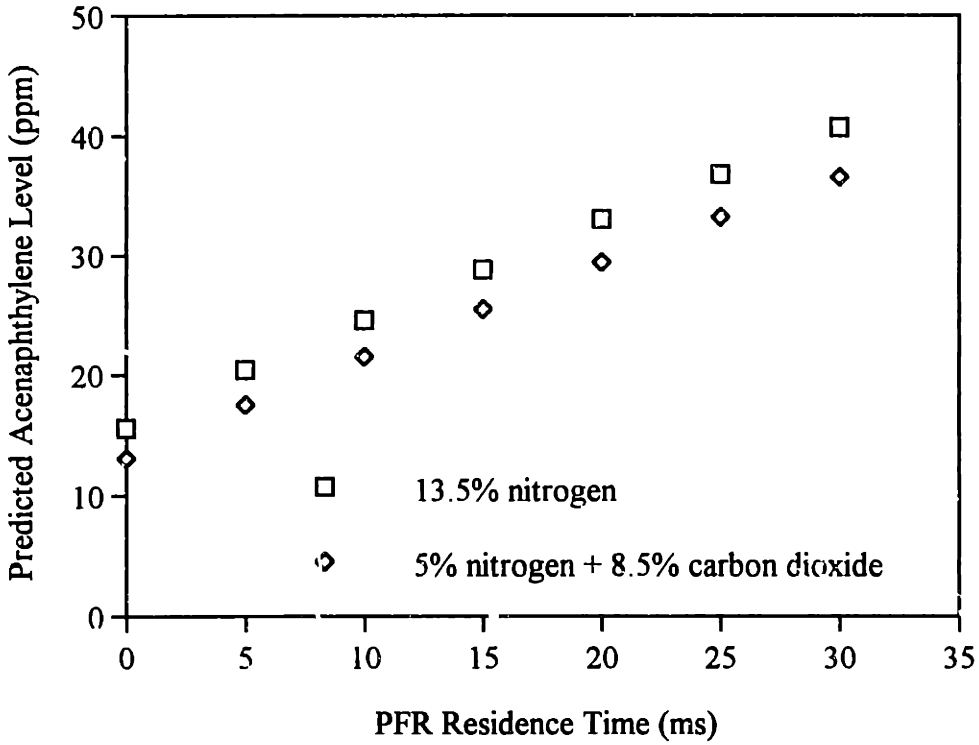

Figure 5.9 Predicted Acenaphthylene Levels for Carbon Dioxide Dilution Case
T = 1650K, ϕ = 2.2

Chapter 6. PAH Isomer Analysis

The material presented in this chapter is an extension of the PAH isomer work of Wornat [1988], Mulholland [1992], Mukherjee [1993], and Masonjones [1995]. Each of these studies focused on the formation of biaryl compounds in the pyrolysis of two ringed (naphthalene), three ringed (anthracene), and four ringed (pyrene) PAH. The work was motivated by the fact that aryl-aryl combination reactions play an important role in the PAH molecular weight growth process, which itself plays an important role in soot nucleation and in the formation of mutagenic PAH species. These particular issues are discussed in somewhat more detail in section 2.2.3.

The focus of this study is on the kinetic pathways which follow the cyclo-dehydrogenation of the biaryls in question. The pathways of most interest are those involving the internal rearrangement of the various biaryl condensation products. The underlying goal is to determine the most favorable isomerization pathways leading to mutagenic PAH compounds.

6.1 Previous Biaryl Results

The experimental work was carried out using a drop tube furnace (see Appendix D for a description). This apparatus allowed the researchers to study the pyrolysis of various PAH reactants under well-characterized, isothermal conditions. In a typical experimental series, samples were taken from the exit of the furnace (which had a residence time of roughly two seconds) and over a temperature range of 1100-1500K.

Sample analysis consisted of the identification and quantification of all the biaryl isomers and some of the condensation products produced in each pyrolysis run. Concentration data for the naphthyl-anthracene isomers may be found in Masonjones [1995], the bianthryl isomer data in Wornat [1988], and the bipyrene isomer data in Mukherjee [1993].

In their analysis of the biaryl isomer distributions, Mulholland *et al.* [1993] developed a methodology to qualitatively predict the relative abundance of each isomer. In this method, the expected abundance of each isomer was ranked according to two criteria : i) statistical factors i.e. the number of possible aryl-aryl combination reactions leading to the formation of each isomer and ii) steric hindrance effects i.e. the number of "bays", "coves", and "fjords" in each isomer. These terms are defined in Figure 6.1.

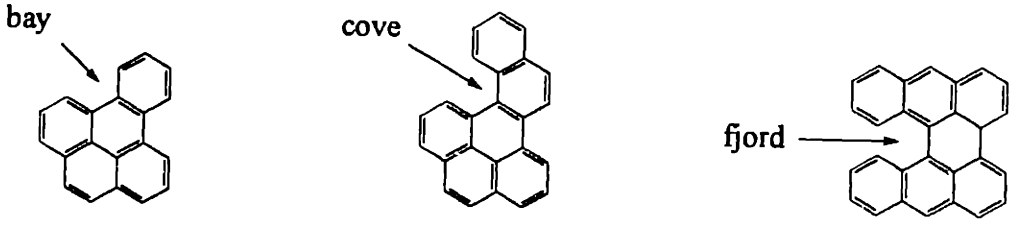

Figure 6.1

This figure indicates that steric hindrance effects are increasingly significant in bay, cove, and fjord containing molecules. Steric hindrance effects were examined more rigorously by carrying out MOPAC [Coolidge & Stewart 1990] simulations on all relevant biaryl compounds. It was found that a reliable measure of steric hindrance is the angle between the planes of the two aryl units, when the biaryl is in its most stable configuration. Angles approaching 90° are indicative of significant steric repulsion between opposite hydrogens, while small angles indicate

minor repulsive forces. This angle is well correlated with the steric hindrance factor determined by using the fjord/cove/bay technique.

Thus, according to this methodology, the biaryl isomer distributions for a particular pyrolysis run may be estimated by i) ranking them according to their statistical factors and ii) ranking those with equal statistical factors by their steric hindrance factors. These results are summarized in Table 6.1.

Table 6.1 Relative Distributions of Biaryl Isomers

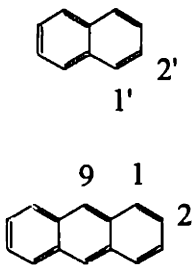

Naphthyl-Anthracenes

Biaryl	Combinations	Steric Factor	Ranking	Relative Yield ‡
2,2'	16	bay-bay	1	1.0
1,2'	16	bay-cove	2	0.46
2,1'	16	bay-cove	2	0.29
1,1'	16	cove-cove	4	0.09
9,2' §	8	cove-cove	5	0.17
9,1'	8	cove-fjord	6	0.05

‡ Naphthalene-Anthracene pyrolysis at 1350K

§ co-eluted with benzo[a]pyrene

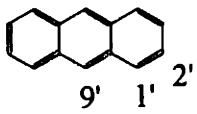

Bianthryls

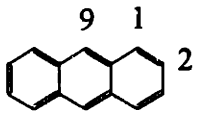

Biaryl	Combinations	Steric Factor	Ranking	Relative Yield ‡
1,2'	16	bay-cove	1	1.0
2,2'	8	bay-bay	2	1.0
2,9'	8	bay-cove	3	0.24
1,1'	8	cove-cove	4	0.29
1,9'	8	cove-fjord	5	0.25
9,9'	2	fjord-fjord	6	0.07

‡ Anthracene Pyrolysis at 1350K

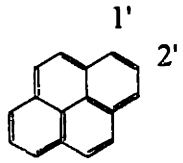

Bipyrenes

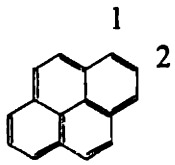

Biaryl	Combinations	Steric Factor	Ranking	Relative Yield ‡
1,5'	16	bay-fjord	1	1.0
1,2'	8	bay-cove	2	0.74
2,5'	8	bay-cove	2	0.70
5,5'	8	cove-cove	4	0.58
1,1'	8	cove-cove	4	0.48
2,2'	2	bay-bay	6	0.35

‡ Pyrene pyrolysis at 1300K

In all three cases, there is qualitative agreement between the measured isomer yields and their rankings as determined by the aforementioned methodology. Mulholland *et al.* [1993] proposed that the formation of the various biaryl isomers is controlled by thermodynamics. This is based on the observation that the relative yields of the isomers match their yields predicted by thermodynamics. However, Masonjones *et al.* [1995] asserted that the process is kinetically controlled and pointed out that the correct ranking provided by the thermodynamic model is likely due to the dominant change in the heat of formation term in the free energy calculation. They stated that this term is strongly affected by steric factors, which would also be a major

consideration in a kinetic model since, in that case, they would influence the enthalpy change to the transition state.

6.2 Molecular Mechanics (MM3) Simulations

The MM3 (1992) molecular mechanics program [Allinger *et al.* 1989] is designed to i) determine optimal structures for organic molecules and ii) use the structural information to calculate relevant thermodynamic data. It is essentially a sophisticated "ball and spring" model [Pope 1997]. Since it is more powerful than programs which employ Benson's group additivity method (e.g. THERM), and more versatile than semi-empirical methods such as MOPAC, it is particularly useful for studying large polycyclic aromatic isomers.

In the MM3 input files, estimated molecular structures are specified by listing the cartesian coordinates of the constituent atoms, the atom types, bond types, and connectivities. In the case of conjugated systems, the program carries out VESCF calculations on the pi-system, and from the calculation obtains bond orders, which are then used to determine stretching and torsion constants. If there is no conjugated system, the stretching and torsion constants are not functions of bond order, and that part of the program is bypassed. If a planar input structure is specified, the program will assume that the output structure is also planar. Optimal structures are determined by executing an energy minimization calculation. The scheme used in MM3 is the block diagonal Newton-Raphson method, although in certain cases the full Newton-Raphson method is preferred. On occasion, the program will arrive at a local energy minimum instead of the global minimum, and as a result will generate incorrect thermodynamic data. This problem may occur in cases where a planar structure is specified and the true structure is non-planar. When this happens, one or more of the calculated vibrational frequencies will be imaginary (due to a negative Eigenvalue in the Hessian matrix). The problem is overcome by making the convergence criteria increasingly strict and/or specifying a non-planar input structure. The

program generates an output containing the optimal molecular structure (in cartesian coordinates), standard heats of formation, entropies, and specific heat capacities over a specified temperature range. Appendix G contains sample input and output files.

6.3 Proposed Pathways

The process whereby two and three ringed PAH are converted to peri-condensed six and seven ringed compounds in a pyrolytic environment is comprised of three steps i) biaryl formation ii) cyclodehydrogenation (condensation) of the biaryls and iii) isomerization of the condensation products. The former two steps are fairly well understood since it is relatively easy to determine the precursors of the various biaryls and cyclodehydrogenation products. In the third step, however, there is still a great deal of uncertainty as to precisely which mechanisms are at play in the rearrangement of the condensation products. The proposed isomerization pathways which appear in the following section are all based on the Scott-Roelofs and the Stone-Wales mechanisms. This by no means excludes other mechanisms from playing a role in the process, but rather outlines the most likely pathways based on energy barrier factors.

6.3.1 Biaryl Condensation (Cyclodehydrogenation) Reactions

The converson of biaryl compounds into condensation products occurs via a pathway such as reaction 6.1. The example used here is the conversion of naphthyl-anthracene to dibenzo[a,k]fluoranthene.

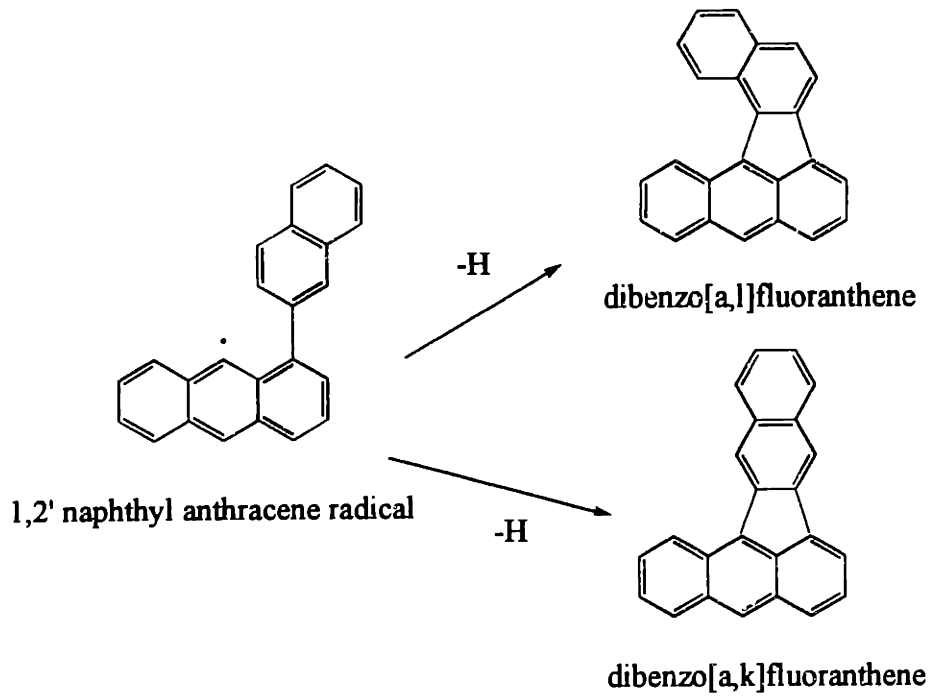

(reaction 6.1)

According to this mechanism, a hydrogen is abstracted from one of several sites adjacent to the aryl-aryl bond. The newly created radical site then serves as a platform for the formation of a second aryl-aryl bond, thus completing the condensation process. The net effect is the formation of an internal five membered ring with the loss of two hydrogen atoms. In this process, a non-planar structure with an internal rotor is converted to a rigid molecule.

As this reaction indicates, a single biaryl may undergo two parallel condensations to form two different isomers. This is a result of the fact that once the initial hydrogen is abstracted from a condensible site, the biaryl has two sites to choose from to complete the condensation process. The relative abundance of each of the two isomers would depend on the relative probability of the appropriate biaryl precursor being in the required configuration. Since the optimum orientation of a biaryl is largely governed by steric factors [Mulholland *et al.* 1993, Masonjones

et al. 1995], it stands to reason that the fluoranthene which condenses from the more stable biaryl configuration will be more abundant than the isomer condensing from the less stable configuration. This is simply because the biaryl will spend more time in the more stable position. To gauge the relative stabilities of the isomers in question, and to obtain estimates of the energy barriers involved in the reactions, heats of formation were calculated for all molecules. Although heats of formation are not as useful as activation energies, they do provide an indication as to which pathways are more favorable. The results of the molecular mechanics MM3 simulations for the naphthyl-anthracene and bianthryl condensation products appear in Table 6.2.

Table 6.2 Heats of Formation of Naphthyl-Anthracene and Bianthryl Cyclodehydrogenation Products

Bianthryl Products	Heat of Formation‡	Configuration
Benzo[a]naphtho[2,3-j]fluoranthene	129.1 kcal/mole	planar
Benzo[a]naphtho[2,3-k]fluoranthene	125.4 kcal/mole	planar
Benzo[a]naphtho[2,3-l]fluoranthene	132.5 kcal/mole	non-planar
Naphthyl-Anthracene Products	**Heat of Formation‡**	**Configuration**
Dibenzo[a,j]fluoranthene	110.0 kcal/mole	planar
Dibenzo[a,k]fluoranthene	106.7 kcal/mole	planar
Dibenzo[a,l]fluoranthene	113.6 kcal/mole	non-planar
Naphtho[2,3-j]fluoranthene	108.1 kcal/mole	planar
Naphtho[2,3-k]fluoranthene	104.6 kcal/mole	planar

‡ Standard Heat of Formation (as calculated by MM3)

Based on this information, a methodology was developed to estimate the relative concentrations of the biaryl condensation products. This is an extension of the biaryl method outlined by Mulholland *et al.* [1993]. However, in this case, three factors rather than two were considered. They are i) relative concentrations of biaryl precursors ii) steric hindrance effects and iii) statistical factors.

This was applied to the bianthryl case in the following manner :

Precursor Concentrations For the 1350K anthracene pyrolysis run [Wornat *et al.* 1992], the relative concentrations of the four bianthryls (see Figure 6.4) are [2,1'] ~ 10, [2,9'] ~ 2, [1,1'] ~ 2, and [1,9'] ~ 2. These are in arbitrary units.

Steric Factors The 2,1' bianthryl may condense to form either benzo[a]naphtho[2,3-k] fluoranthene or benzo[a]naphtho[2,3-l]fluoranthene. MM3 simulations have indicated that the latter compound has a relatively high heat of formation and and has a non-planar structure due to steric interactions between opposing hydrogens (see Table 6.2). Because of this, the 2,1' bianthryl should preferentially condense into the "k" isomer. As an initial approximation, it could be assumed that 90% of the 2,1' condensation reactions lead to the formation of the "k" isomer and 10% to the "l" isomer. The other branched cyclodehydrogenation pair is the condensation of the 2,9' bianthryl to form either the "j" or the "k" fluoranthene. Benzo[a]naphtho[2,3-j]fluoranthene and benzo[a]naphtho[2,3-k]fluoranthene appear to have similar heats of formation and are both planar. Therefore, the 2,9' bianthryl is expected to have no strong preference for either of the two pathways. As a first order approximation, 50% of the condensations could be assumed to lead to formation of the "j" isomer and 50% to the "k" isomer.

Statistical Factors For each bianthryl condensation, the reaction may take place after a hydrogen is abstracted from one of *two* possible sites. The one exception is the 1,1' bianthryl, which can form benzo[a]naphtho[2,3-j]fluoranthene after hydrogen abstraction from *four* possible sites. This is due to the symmetry of the molecule. This condensation can then be assigned a statistical factor of 2, while the rest of the condensation reactions are assigned a factor of 1.

With this information, the relative yields of the three condensation products (fluoranthenes) may be estimated as follows :

(fluoranthene concentration) ~ $\sum$ {(precursor concentration) x (steric factor) x (statistical factor)}

[BaN23kF] ~ [2,1'] x 0.9 x 1 + [2,9'] x 0.5 x 1 = 10

[BaN23jF] ~ [2,9'] x 0.5 x 1 + [1,1'] x 2 = 5

[BaN23lF] ~ [2,1'] x 0.1 x 1 + [1,9'] x 1 = 3

The measured yields of [BaN23kF]:[BaN23jF]:[BaN23lF] were found to be in the ratio of 10:9:1, which is consistent with the ranking methodology.

The methodology was also applied to the 1350K naphthalene/anthracene pyrolysis run [Masonjones *et al.* 1995]. In this case, the relative yields of the condensation products are estimated to be DBakF ~ 10, N23jF ~ 4, N23kF ~ 3, DBajF ~ 2, and DBalF ~ 2, in arbitrary units. Although DBakF, N23jF, and N23kF were positively identified in the sample [Plummer-Turano 1997], no quantitative information was available for a comparison.

6.3.2 Scott-Roelofs Rearrangements

As was described in chapter 2, a polycylic aromatic containing both five and six membered rings may undergo a four-centered reaction in which one carbon-carbon bond and one carbon-hydrogen bond are severed to form new carbon-carbon and carbon-hydrogen bonds [Scott & Roelofs 1987]. Essentially, a five membered ring changes place with an adjacent six membered ring. The simplest example is the interconversion of fluoranthene, acephenanthrylene, and aceanthrylene (see reaction 6.5).

In the case of the pyrolysis of two and three ringed aromatics, this type of isomerization plays an important role in the conversion of "primary fluoranthenes" (cyclodehydrogenation products) into "secondary fluoranthenes". A relevant example is reaction 6.2, where dibenzo[b,k]fluoranthene rearranges to form naphtho[2,3-b]fluoranthene. Since dibenzo [b,k]fluoranthene is a condensation product of 1,2' naphthyl phenanthrene, it is classified as a primary fluoranthene while naphtho[2,3-b]fluoranthene is a secondary fluoranthene. Because of the relative ease with which this isomerization reaction proceeds, the two isomers should be in equilibrium within the residence time of the drop tube furnace.

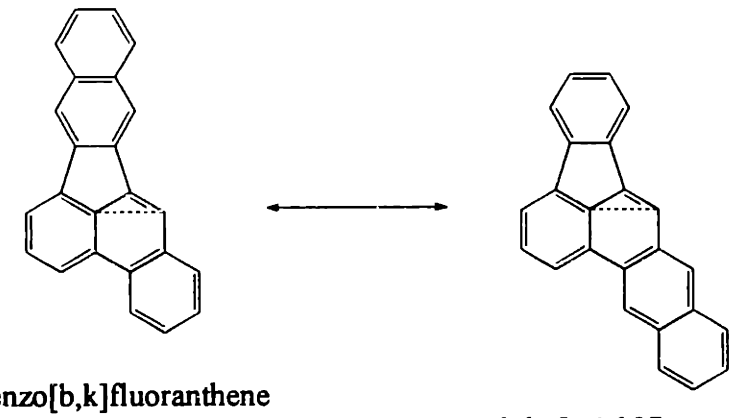

dibenzo[b,k]fluoranthene

naphtho[2,3-b]fluoranthene (reaction 6.2)

This specific isomerization is supported by experimental evidence as these compounds have both been positively identified in naphthalene/phenanthrene as well as naphthalene/anthracene pyrolysis samples [Plummer-Turano 1997]. Since naphtho[2,3-b] fluoranthene is clearly not a biaryl condensation product, it was probably formed via this Scott-Roelofs rearrangement. The calculated equilibrium ratio of dibenzo[b,k]fluoranthene to naphtho[2,3-b]fluoranthene is 2:1 at 1350K, which is within qualitative agreement with the data. Secondary fluoranthenes have been determined for all the condensation products of the naphthyl-phenanthrenes, naphthyl-anthracenes, bianthryls, biphenanthryls, and anthryl-phenanthrenes. These compounds appear in Figures 6.2-6.6. As the figures indicate, all the primary fluoranthenes, with the exception of the naphthofluoranthenes, have one secondary fluoranthene isomer.

An interesting finding is the fact that substantial levels of dibenzo[b,k]fluoranthene were detected in the naphthalene/anthracene pyrolysis samples. Based on structure alone, it would seem that this compound was formed by the pyrolysis of naphthalene and phenanthrene (rather then naphthalene and anthracene) as no naphthyl-anthracene condensation product has a benzo ring in the "b" position. There are two explanations for the this result : i) significant conversion of anthracene into phenanthrene occurred and the phenanthrene then combined with naphthalene

and ii) dibenzo[a,k]fluoranthene was converted into dibenzo[b,k]fluoranthene. The Scott-Roelofs rearrangement has been used to explain the conversion of azulene into naphthalene [Brouwer & Troe 1988]. A similar isomerization may also convert anthracene into phenanthrene (reaction 6.3) and dibenzo[a,k]fluoranthene into dibenzo[b,k]fluoranthene (reaction 6.4).

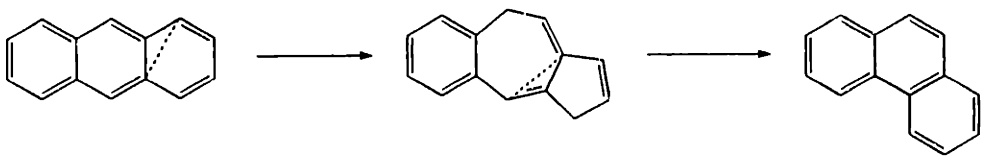

anthracene benzazulene phenanthrene

(reaction 6.3)

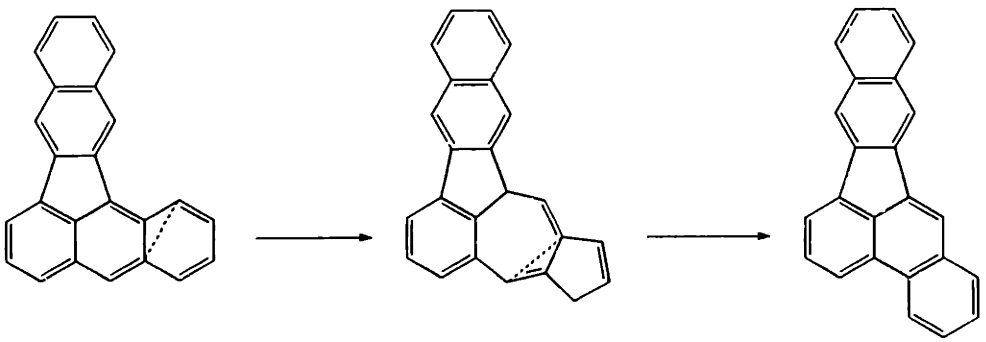

dibenzo[a,k]fluoranthene dibenzo[b,k]fluoranthene

(reaction 6.4)

According to MM3 simulation results, the difference in heat of formation between anthracene and the benzazulene intermediate is 30 kcal/mole. The corresponding ΔH_f difference between dibenzo[a,k]fluoranthene and the "[a,k] - [b,k]" intermediate is 19 kcal/mole. This would support the idea that reaction 6.4 is more favorable than reaction 6.3. Another piece of evidence is the fact that the measured levels of phenanthrene in the naphthalene-anthracene pyrolysis runs were only around 1% of the anthracene levels [Masonjones 1996], even though

phenanthrene is more thermodynamically stable than anthracene. This suggests that, for this pyrolysis run, conditions did not favor the formation of dibenzo[b,k]fluoranthene from naphthalene and phenanthrene. Therefore, in this case, the most likely source of the dibenzo[b,k]fluoranthene appears to be dibenzo[a,k]fluoranthene, which was converted by reaction 6.4.

6.3.3 Stone-Wales Rearrangements

This class of isomerization is based on a four-centered reaction in which two carbon-carbon bonds are severed to form two new carbon-carbon bonds, as is described in section 2.3. It is particular important to this study because it plays an important role in the hypothesized reaction sequence which converts fluoranthene to pyrene [Howard *et al.* 1995, Pope 1997]. As reaction 6.5 indicates, the conversion comprises three Scott-Roelofs followed by one Stone-Wales rearrangement.

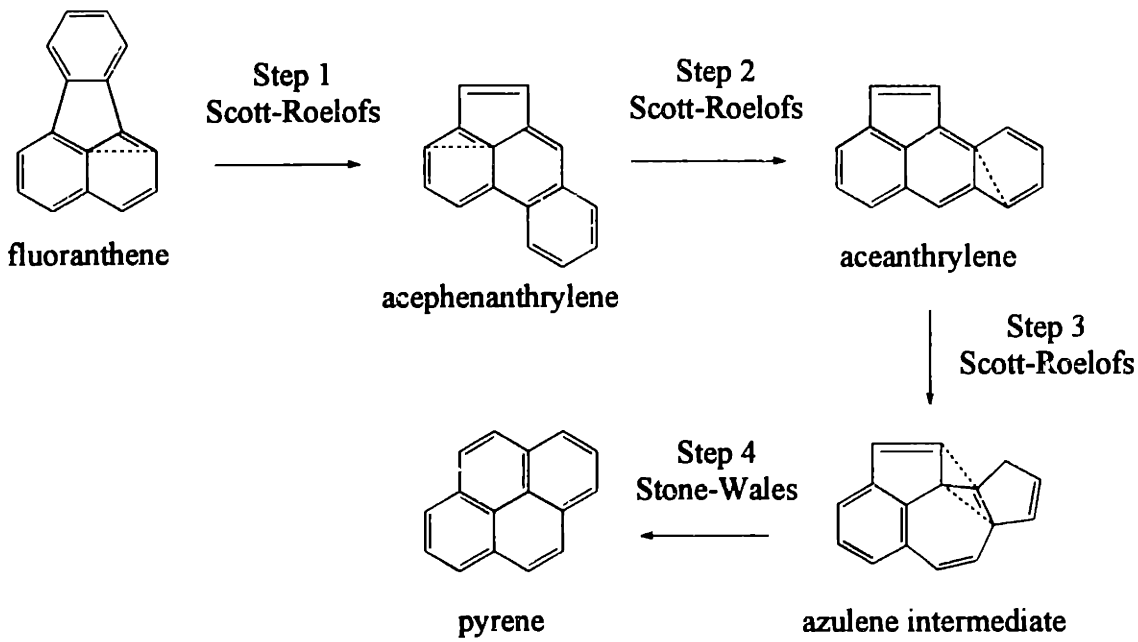

(reaction 6.5)

For comparison, two alternative (but less probable) fluoranthene-to-pyrene mechanisms are presented (reactions 6.6a & 6.6b)

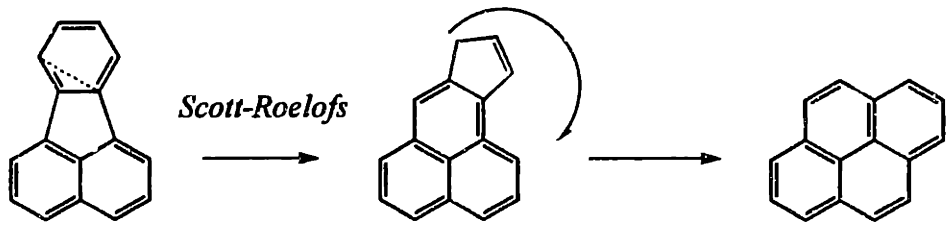

(reaction 6.6a)

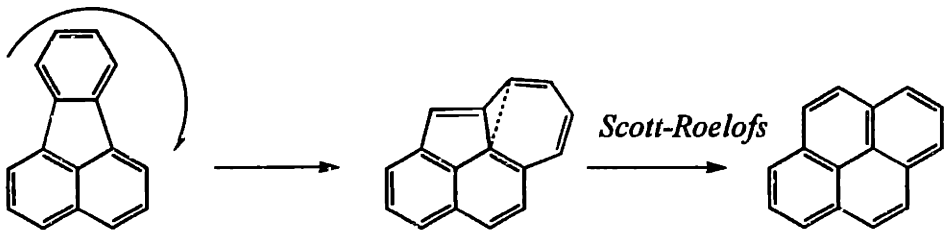

(reaction 6.6b)

In reaction 6.5, steps one and two have relatively low energy barriers, as is evident in Howard *et al.* [1995]. The transformation in step three, however, requires relatively high amounts of energy to form the seven membered ring, while step four requires the breaking of two carbon-carbon bonds. Howard *et al.* [1995] found that fluoranthene and pyrene were far from their equilibrium concentrations when they were produced in the original PFR at 1620K, and this was seen again in our JS/PFR experiments (section 4.4.1). This was ascribed to the large number of steps and high energy barriers of this pathway (relative to a simple Scott-Roelofs transformation).

It is evident that step 3 is similar to the first step of reaction 6.4. However, these two transformations put the five membered rings in different positions. Therefore, it would seem that a fluoranthene with a benzo group in the "a" position may undergo a Scott-Roelofs reaction to form two different azulene-like compounds. One compound may undergo reverse reactions to

yield either the benzo[a]fluoranthene or benzo[b]fluoranthene, while the other compound either undergoes the reverse reaction or goes through a Stone-Wales rearrangement to yield a pyrene. Heats of formation for key Stone-Wales azulene intermediates derived from naphthalene-anthracene and anthracene pyrolysis appear in Table 6.3

Table 6.3 Heats of Formation of Stone-Wales Intermediates

Precursor of Intermediate	Heat of Formation‡	Configuration
Dibenzo[a,j]fluoranthene	132.6 kcal/mole	non-planar
Dibenzo[a,k]fluoranthene	129.0 kcal/mole	non-planar
Dibenzo[a,l]fluoranthene	133.6 kcal/mole	non-planar
Dibenzo[b,j]fluoranthene	135.1 kcal/mole	non-planar
Benzo[a]naphtho[2,3-j]fluoranthene	151.5 kcal/mole	non-planar
Benzo[a]naphtho[2,3-k]fluoranthene	148.0 kcal/mole	non-planar
Benzo[a]naphtho[2,3-l]fluoranthene	152.5 kcal/mole	non-planar

‡ Standard Heat of Formation (as calculated by MM3)

These heats of formation values are all 22-24 kcal/mole higher than those of their precursors (see Table 6.2). The small variation in these differences indicates that the energy barriers associated with each transformation are similar, regardless of the isomer involved. Also revealed by the MM3 simulations is the fact that all intermediates are non-planar. This is obviously a result of the seven membered ring forcing the structure out of plane.

The heats of formation for all pyrene products of the Stone-Wales rearrangements proved to be lower than those of their fluoranthene precursors. This is indicative of the relative stability of the condensed pyrene structure. These results appear in Table 6.4.

Table 6.4 Heats of Formation of Stone Wales Pyrene Products

Compound	Heat of Formation‡	Configuration
Naphtho[2,3-e]pyrene	90.0 kcal/mole	planar
Naphtho[2,1-e]pyrene	94.8 kcal/mole	non-planar
Naphtho[2,3-a]pyrene	94.3 kcal/mole	planar
Dibenzo[a,l]pyrene	96.6 kcal/mole	non-planar
Dibenzo[a,e]pyrene	90.5 kcal/mole	planar
Anthraceno[2,3-e]pyrene	109.7 kcal/mole	planar
Benzo[a]naphtho[2,3-i]pyrene	110.1 kcal/mole	planar
Phenanthreno[2,3-a]pyrene	107.6 kcal/mole	planar

‡ Standard Heat of Formation (as calculated by MM3)

These results indicate that once the Stone-Wales intermediate is formed, thermodynamic factors favor the transformation to a pyrene over the transformation back to the fluoranthene precursor. However, these values do not reveal anything about the activation energy associated with severing the two carbon-carbon bonds in the Stone-Wales reaction. Nevertheless, pyrene species have been identified both in the naphthalene-anthracene pyrolysis samples [Plummer-Turano 1997] and the anthracene pyrolysis samples [Wornat *et al.* 1992]. These are cases where pyrenes could only have been formed via the isomerization of fluoranthenes.

The MM3 results have also revealed those pyrene compounds that are non-planar due to steric effects. Two examples are dibenzo[a,l]pyrene and naphtho[2,1-e]pyrene. Since they both contain "coves", the steric repulsion between opposing hydrogens is sufficient to force the structures out of plane. This non-planarity has also been seen in smaller, cove containing molecules such as benzo[c]phenanthrene [Herbstein & Schmidt 1954].

For the 1350K naphthalene-anthracene pyrolysis case, only one pyrene was positively identified in the sample, namely naphtho[2,1-a]pyrene [Plummer-Turano 1997]. According to Figures 6.2 and 6.3, the only Scott-Roelofs & Stone-Wales pathways leading to this compound is the rearrangement of either dibenzo[b,j]fluoranthene or naphtho[2,1-j]fluoranthene. Neither of these two compounds was identified in the same sample, but this was due to a lack of the appropriate standards rather than the absence of peaks. These compounds are both cyclodehydrogenation products of naphthalene-phenanthrene pyrolysis, rather than naphthalene-anthracene pyrolysis. However, the presence of dibenzo[b,k]fluoranthene in the sample implies that these two may also be present. If that is the case, then the dibenzo[b,j]fluoranthene was most likely formed via the rearrangement of dibenzo[a,j]fluoranthene (as was discussed in section 6.3.2), while the naphtho[2,1-j]fluoranthene may have been formed from naphtho[2,3-j] fluoranthene.

The results of the pathway analyses are all contained in Figures 6.2-6.6. These figures show the steps by which the MW 304 and 354 biaryls are converted to primary fluoranthenes, and how these are then converted to secondary fluoranthenes and pyrenes. The cases of naphthalene/anthracene, naphthalene/phenanthrene, anthracene, phenanthrene, and anthracene /phenanthrene pyrolysis were examined.

6.4 Pathways Leading to the Formation of Mutagenic PAH

Appendix F contains a brief summary of the carcinogenic potentials of certain PAH detected in the PFR as well as certain isomers relevant to this study. From literature sources [Durant *et al.* 1996], [Busby *et al.* 1995], it would appear that some of the more mutagenic MW 302 isomers are dibenzo[a,l]pyrene, dibenzo[a,e]pyrene, dibenzo[a,i]pyrene, dibenzo[a,h]pyrene, naphtho[2,1-a]pyrene, dibenzo[a,k] fluoranthene, and dibenzo[b,k]fluoranthene. Due to the high

uncertainties and variations of the various bioassay techniques used to measure mutagenic potentials of PAH, it is difficult to rank these compounds on a quantitative basis. Nevertheless, it may be said that all these species pose a health hazard, and that the most mutagenic isomer seems to be dibenzo[a,l]pyrene [Ralston *et al.* 1993].

Using the results represented in figures 6.2-6.4, the most probable pathways which convert two and three ringed PAH into these isomers were identified.

Dibenzo[a,l]pyrene is formed from the rearrangement of dibenzo[a,l]fluoranthene, which in turn is formed from the condensation of either 9,1' naphthyl-anthracene or 1,2' naphthyl-anthracene. Due to the significant steric repulsions expected in dibenzo[a,l]fluoranthene and dibenzo[a,l] pyrene itself, the rate of formation of this compound is expected to be relatively low.

Dibenzo[a,e]pyrene is formed from the rearrangement of dibenzo[a,k]fluoranthene, which in turn is formed from the condensation of either 9,2' naphthyl-anthracene or 1,2' naphthyl-anthracene. Steric factors are not expected to hinder the formation of this molecule.

Dibenzo[a,i]pyrene is formed from the rearrangement of naphtho[2,3-b]fluoranthene, which is the secondary fluoranthene counterpart of dibenzo[b,k]fluoranthene. The latter compound is formed from the condensation of either 9,2' naphthyl-phenanthrene or 1,2' naphthyl-phenanthrene. Steric factors are not expected to hinder the formation of this molecule.

Dibenzo[a,h]pyrene is formed from the rearrangement of naphtho[1,2-b]fluoranthene, which is the secondary fluoranthene counterpart of dibenzo[b,j]fluoranthene. The latter compound is formed from the condensation of either 9,2' naphthyl-phenanthrene or 1,1' naphthyl-phenanthrene. Due to the cove contained in naphtho[1,2-b]fluoranthene, steric factors are expected to hinder the formation of dibenzo[a,h]pyrene.

Naphtho[2,1-a]pyrene is formed from the rearrangement of either dibenzo[b,j]fluoranthene or naphtho[1,2-j]fluoranthene. The former compound is formed from the condensation of either 9,2' naphthyl-phenanthrene or 1,1' naphthyl-phenanthrene while the latter is formed from the condensation of 2,1' naphthyl-phenanthrene. Steric factors are not expected to hinder the formation of this molecule.

Dibenzo[a,k]fluoranthene is formed from the condensation of either 9,2' naphthyl-anthracene or 1,2' naphthyl-anthracene. Steric factors are not expected to hinder the formation of this molecule.

Dibenzo[b,k]fluoranthene is formed from the condensation of either 9,2' naphthyl-phenanthrene or 1,2' naphthyl-phenanthrene. Steric factors are not expected to hinder the formation of this molecule.

Nomenclature for Figures 6.2-6.6

Prefixes
B = benzo
DB = dibenzo
TB = tribenzo
N = naphtho
A = anthraceno
P = phenanthreno

Suffixes
F = fluoranthene
P = pyrene

sites on fluoranthene molecule

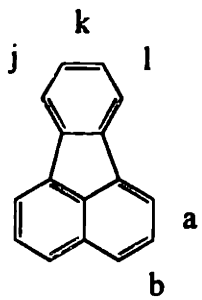

sites on pyrene molecule

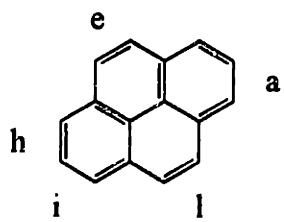

sites on naphthyl molecule

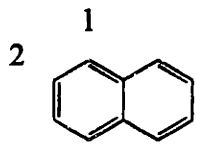

sites on anthryl molecule

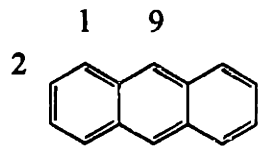

sites on phenanthryl molecule

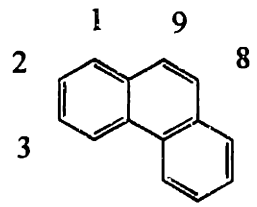

less favored pathway

more favored pathway

Figure 6.2 Naphthalene-Anthracene Pyrolysis Pathways

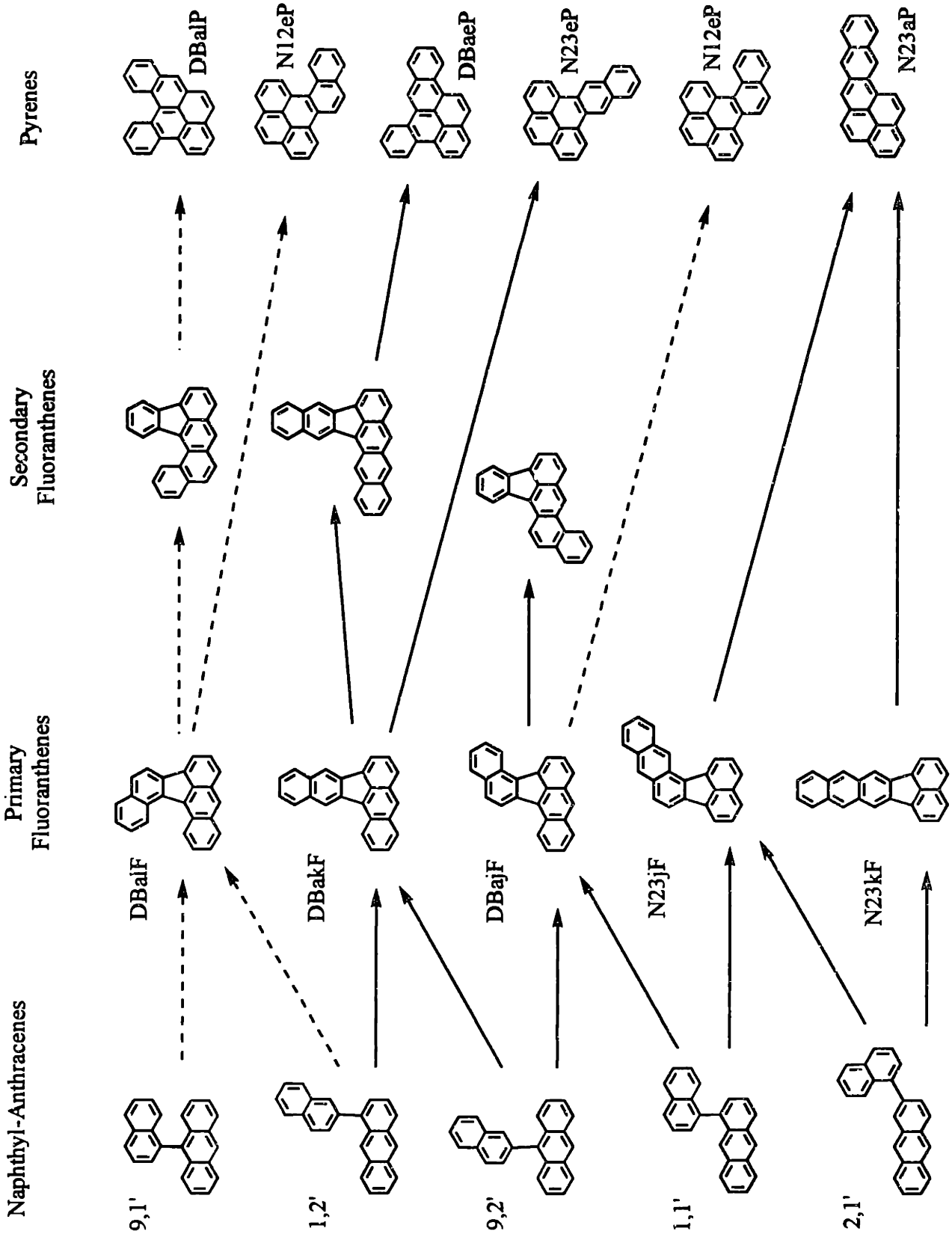

Figure 6.3 Naphthalene-Phenanthrene Pyrolysis Pathways

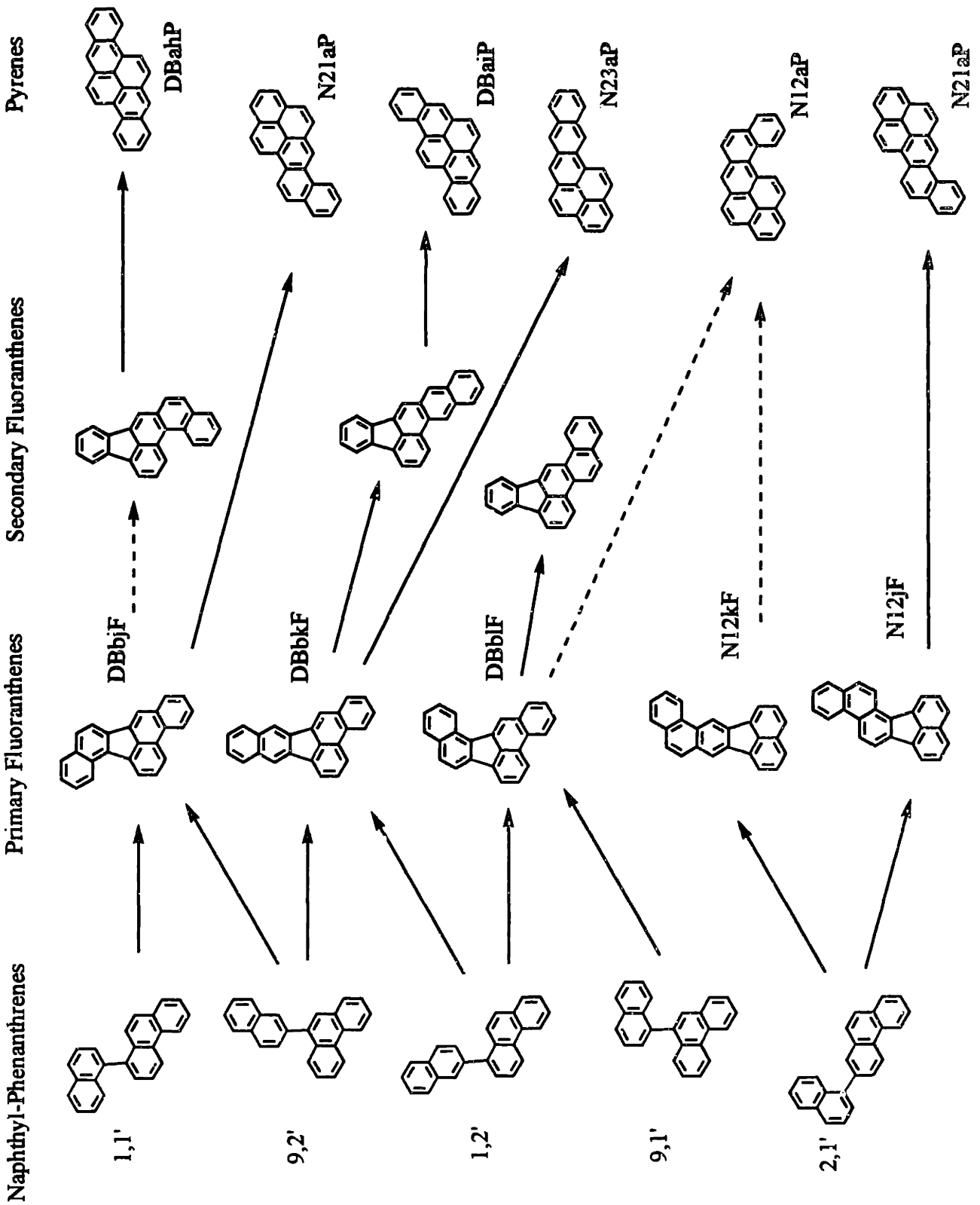

Figure 6.4 Anthracene Pyrolysis Pathways

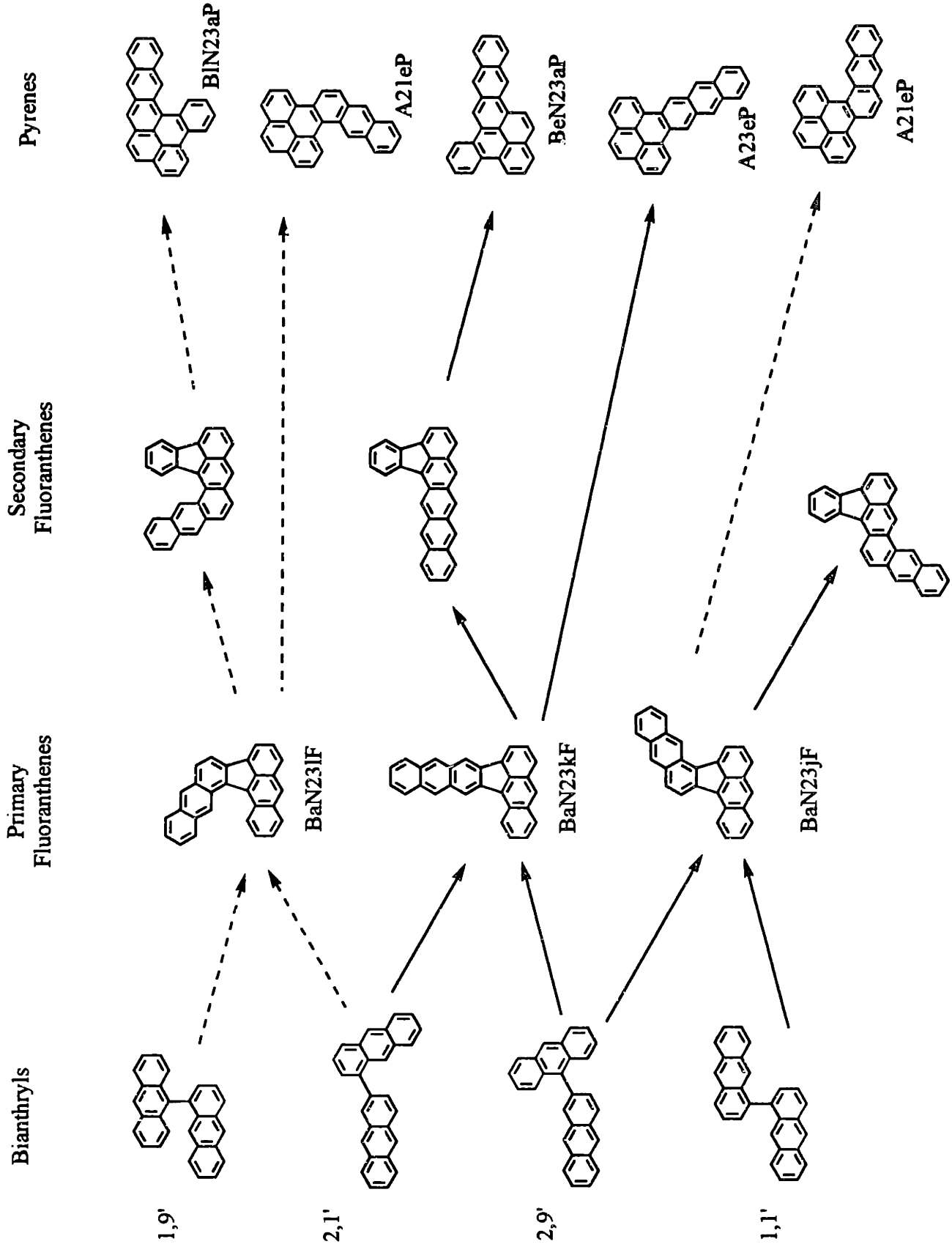

Figure 6.5a Condensation of Biphenanthryls

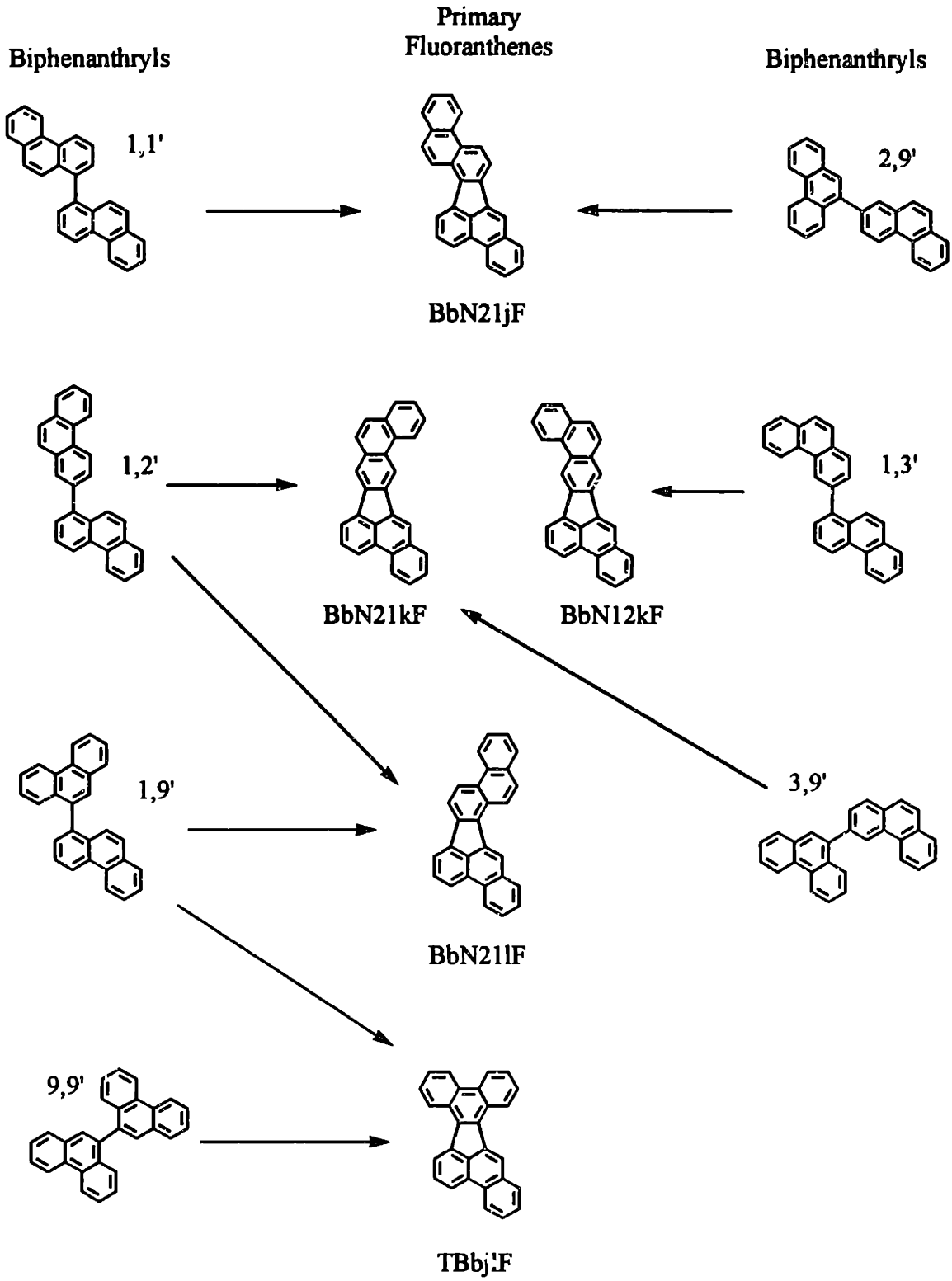

Figure 6.5b Biphenanthryl Isomerization Pathways

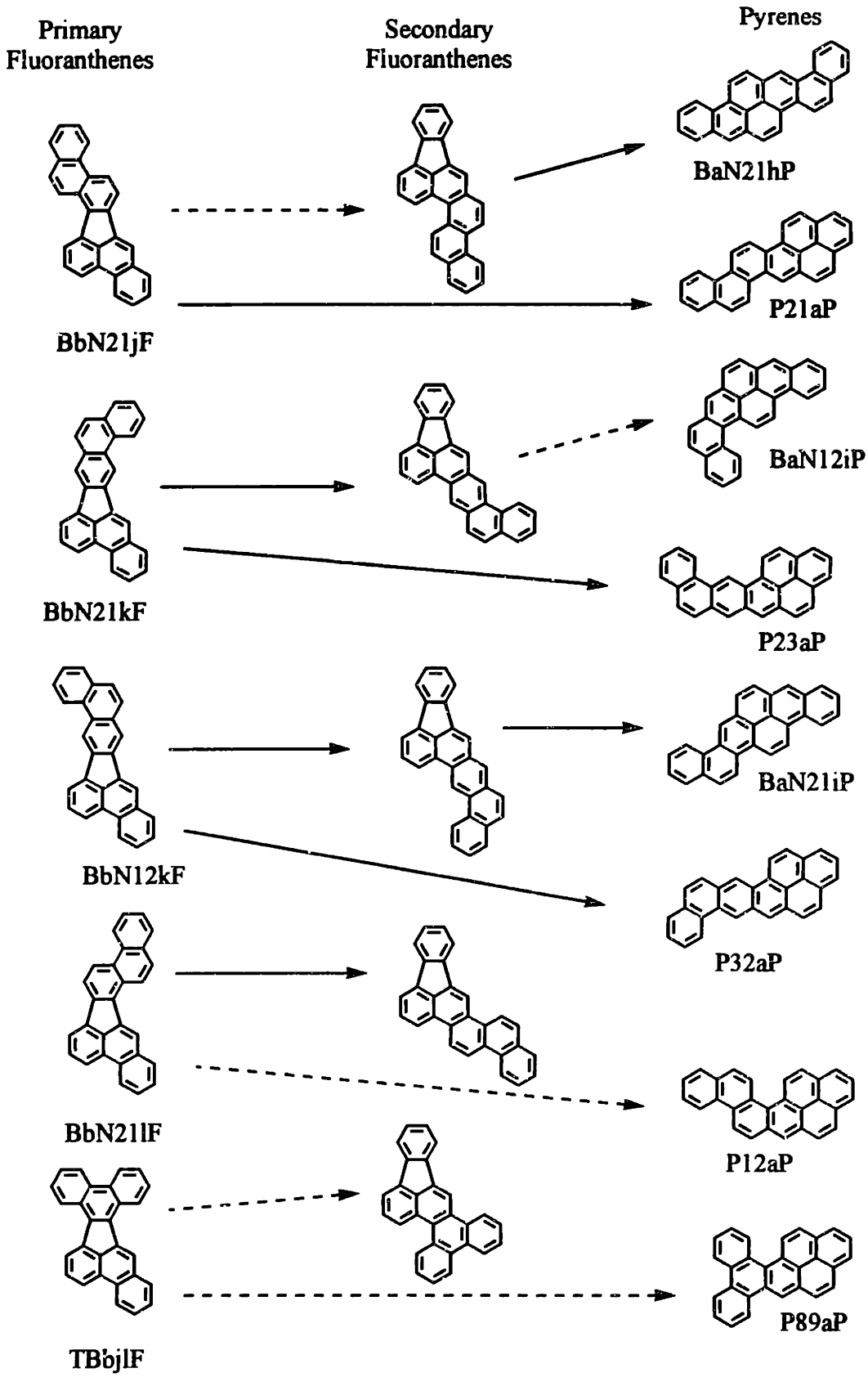

Figure 6.6a Condensation of Phenanthryl-Anthracenes

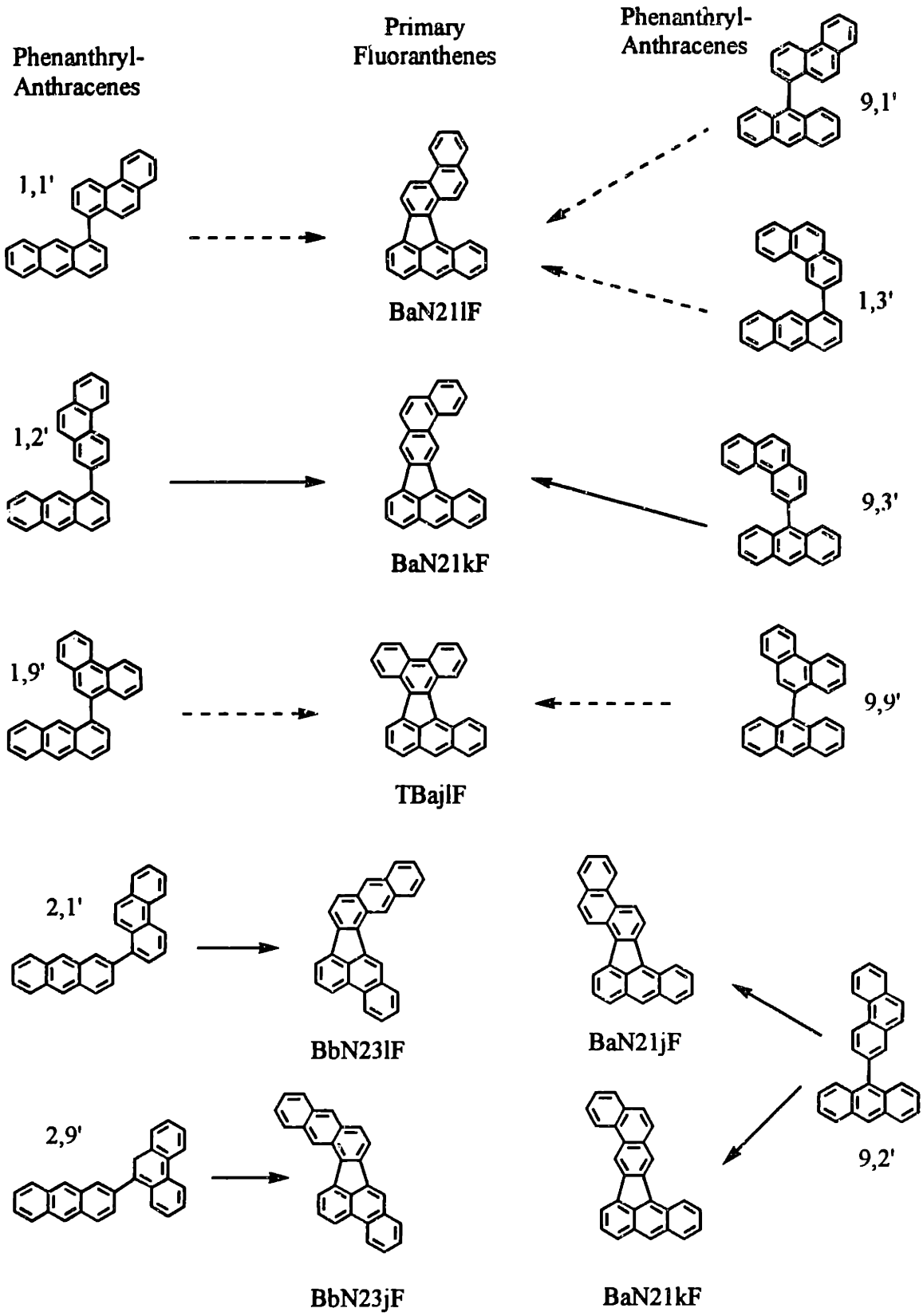

Figure 6.6b Isomerization of Phenanthryl-Anthracenes

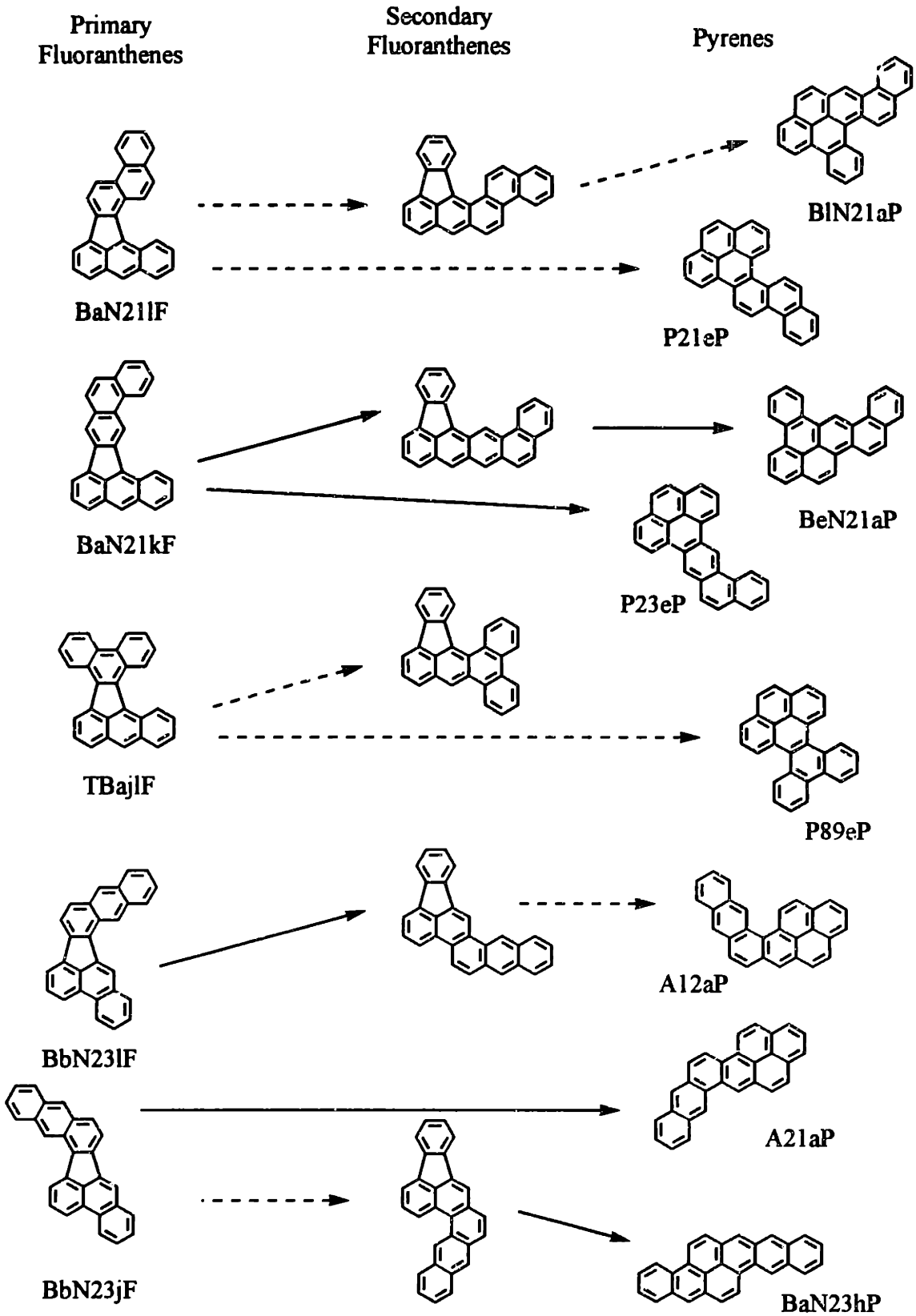

Chapter 7. Conclusions

7.1 Concluding Remarks

The final conclusions reached in the soot surface growth, flue gas recirculation, and PAH isomer studies appear as follows :

1. For the case of benzene injection into a baseline ϕ of 1.3, soot growth was dominated by PAH addition. At 1580K, collision efficiencies for soot/PAH interactions were found to fall from 0.11 to 0.03 with increasing residence time, while at 1650K they fell from 0.24 to 0.08. The higher values for the 1650K case were attributed to the higher radical levels expected at the higher temperature.

2. For the $\phi = 2.2$ non injection case, 65-75% of the observed soot growth was attributed to acetylene addition. Soot/acetylene collision efficiencies declined from $5x10^{-4}$ to $3x10^{-4}$ with increasing residence time The PAH/acetylene collision efficiencies were found to range from $1x10^{-5}$ to $3x10^{-5}$.

3. The trend of a declining soot/PAH collision efficiency with residence time may be attributed to changes in the gas phase environment, specifically a declining H/H_2 ratio.

4. For a ϕ of 2.2 and a temperature of 1580K, the effect of increasing the nitrogen dilution rate from 13.5% to 21% resulted in a 30% drop in soot levels and a 20% drop in PAH levels. This was attributed to the dilution of acetylene.

5. For a ϕ of 2.2 and a temperature of 1580K, replacing the 13.5% nitrogen dilution stream with a 5% nitrogen + 8.5% carbon dioxide stream led to a 30% decline in soot levels at 1580K and a 45% decline at 1650K. This was attributed to the reaction of carbon dioxide with H atoms to produce OH, which then enhanced the oxidation of hydrocarbons such as acetylene.

6. The relative distributions of condensation products resulting from the cyclodehydrogenation of M.W. 304 and 354 biaryls may be estimated by considering i) the relative concentrations of their precursors ii) steric factors and ii) statistical factors. Steric factors are especially significant for fluoranthenes with benzo rings in both the "a" and "l" positions since these compounds are non-planar.

7. Biaryl condensation products (primary fluoranthenes) may undergo Scott-Roelofs rearrangements to form secondary fluoranthenes. The relative concentrations are close to their equilibrium values. There is evidence to suggest that fluoranthenes with benzo groups in the "a" position may undergo Scott-Roelofs rearrangements which shift the groups to the "b" position.

8. Assuming the dominance of the Scott-Roelofs and Stone-Wales rearrangements, the pathways leading from M.W. 304 (naphthyl-anthracene) and M.W. 354 (bianthryl, biphenanthryl, phenanthryl-anthracene) biaryls through their condensation products to pyrene structures have been identified. Less favorable pathways are those involving "a,l fluoranthenes" and pyrenes containing "coves".

7.2 Recommendations for Future Activities

It is recommended that detailed soot particle size information be obtained for the acetylene lean and rich cases for two or more temperatures, and at different residence times. Since our TEM results have indicated that the soot particles produced in the PFR are likely to be tar droplets, the recommended approach is one involving the use of a laser. The obvious advantage in using this technique is that it allows one to infer size information from the particles/droplets *in-situ*, regardless of whether they are soot particles or viscous tar droplets. Average particle sizes may then be determined either by i) measuring both scattering and extinction coefficients or by ii) measuring scattering coefficients and collecting soot samples for gravimetric analysis.

A thorough TEM analysis of PFR soot samples collected at lower temperatures will also yield useful information. If the soot particles actually are viscous droplets in the PFR, it will be of interest to use a high resolution TEM instrument to examine their morphology. The results may provide further insights into the soot nucleation process.

Concerning the effect of flue gas recirculation on soot and PAH formation, it will be of value to extend the experimental parameters and look at wider temperature ranges and higher fuel equivalence ratios. It will also be interesting to use the same experimental approach to examine the effectiveness of *water* as a soot/PAH suppressor, since H_2O is the one "flue gas diluent" not considered in the present study.

Regarding the PAH isomerization study, it will be useful to analyze existing naphthalene/anthracene, naphthalene/phenanthrene, and anthracene pyrolysis samples for the MW 302 and 352 species not yet identified. If all the stable species involved in the proposed

pathways may be analyzed for, these same pathways may be experimentally verified. To accomplish this, appropriate standards will need to be procured. Better quantification of the currently detectable isomers is also recommended.

Appendix A Experimental Parameters

Table A.1 Soot Surface Growth Experiments

All flowrates in liters/sec (at 293K, 1 atm)

Experimental Case	Air	C_2H_4	N_2	C_6H_6	Second. N_2
T_{PFR} = 1580K					
ϕ = 1.3 + 3.4 g/min C_6H_6	3.86	0.354	2.96	0.0175	0.025
ϕ = 1.3 + 4.2 g/min C_6H_6	3.86	0.354	2.96	0.0215	0.025
ϕ = 1.3 + 6.4 g/min C_6H_6	3.86	0.354	2.96	0.0328	0.025
ϕ = 1.6 + 4.2 g/min C_6H_6	3.86	0.428	2.11	0.0215	0.025
ϕ = 2.2	3.86	0.599	0.69	-	0.042
T_{PFR} = 1650K				-	
ϕ = 1.3 + 4.2 g/min C_6H_6	3.42	0.314	2.65	0.0215	0.025
ϕ = 2.2	3.86	0.599	0.69	-	0.042

Table A.2 Fluegas Recirculation Experiments

All flowrates in liters/sec (at 293K, 1 atm)

T_{PFR}	T_{FEED}	Air	C_2H_4	N_2	CO_2
1580K‡	20°C	3.86	0.599	0.69	0
1580K	180°C	3.86	0.599	1.07	0
1580K	170°C	3.86	0.599	0.28	0.41
1650K‡	130°C	3.86	0.599	0.69	0
1650K	210°C	3.86	0.599	0.28	0.41

‡ These experiments also appear in Table A.1

Table A.3 Benzene/Toluene Experiments

All flowrates in liters/sec (at 293K, 1 atm)

T_{PFR}	T_{FEED}	Air	C_2H_4	N_2	Additive	Second. N_2
1520	20°C	3.42	0.314	2.92	0.0215 (Ben.)	0.025
1520	20°C	3.42	0.314	2.92	0.0182 (Tol.)	0.025
1650‡	140°C	3.42	0.314	2.65	0.0215 (Ben.)	0.025
1650	140°C	3.42	0.314	2.65	0.0182 (Tol.)	0.025

‡ This experiment also appears in Table A.1

Appendix B Experimental Data

Table B.1 Light Hydrocarbon and Fixed Gas Data

T = 1580K					
baseline phi = 1.3			**all in ppm**		
benzene = 3.4 g/min					
Residence Time (ms)	2.1	8	13.8	19.6	25.4
methane	31.98	43.52	50.97	45.92	64.68
ethylene	5.39	5.94	6.08	4.98	6.59
acetylene	266.89	401.54	461.65	406.35	557.83
benzene = 4.2 g/min					
Residence Time (ms)	2.1	8	13.8	19.6	25.4
methane	29.57	22.51	37.99	40.63	48.09
ethylene	18.59	3.13	7.21	7.09	8.32
acetylene	339.02	225.29	406.35	432.80	562.64
benzene = 6.4 g/min					
Residence Time (ms)	2.1	8	13.8	19.6	25.4
methane	42.32	49.29	66.12	76.70	100.75
ethylene	5.29	5.58	7.02	8.22	20.13
acetylene	264.49	353.45	413.56	483.29	553.02
T = 1580K					
baseline phi = 1.6					
benzene = 4.2 g/min					
Residence Time (ms)	2.3	8.7	15	21.4	27.7
methane	627.55	627.55	735.75	454.44	740.56
ethylene	30.54	31.74	34.86	31.26	35.59
acetylene	4231.79	4376.05	4760.76	3462.37	4856.94

T = 1580K					
baseline phi = 2.2			**all in ppm**		
dilution = 13.5% nitrogen					
Residence Time (ms)	2.9	10.9	18.8	26.7	34.6
methane	4628	4644	4578	4444	4516
ethylene	174	140	133	127	130
acetylene	11254	10762	10244	9822	9890
carbon monoxide	125436	130732	133002	126540	125098
carbon dioxide	30536	32530	33626	32244	32420
dilution = 21% nitrogen					
Residence Time (ms)	2.7	9.9	17.2	24.4	31.6
methane	3928	3636	2564	3474	4504
ethylene	149	100	67	92	116
acetylene	8888	8196	5991	7708	9210
carbon monoxide	103994	96692	74498	94976	112214
carbon dioxide	24874	23694	18514	23666	28388
dilution = 5.5% nitrogen plus 8% carbon dioxide					
Residence Time (ms)	2.9	10.9	18.8	26.7	34.6
methane	3806	4872	4656	4052	4846
ethylene	154	127	110	95	113
acetylene	10250	10252	8896	7774	8962
carbon monoxide	142320	146174	141624	124602	139316
carbon dioxide	66844	67515	64774	57010	64352

T = 1650K					
baseline phi = 1.3			**all in ppm**		
benzene = 4.2 g/min					
Residence Time (ms)	2.9	10.9	18.8	26.7	34.6
methane	83	122	167	181	213
ethylene	4		6		7
acetylene	341	507	696	788	821
carbon monoxide	28950	25507	27846	26394	26201
carbon dioxide	29476	26835	29804		28164
baseline phi = 2.2					
dilution = 13.5% nitrogen					
Residence Time (ms)	2.7	9.9	17.2	24.4	31.6
methane	5613	5435	5146	3642	5209
ethylene	208	190	171		172
acetylene	13844	12685	11723	6157	11524
carbon monoxide	121611	121396	104608	83161	98825
carbon dioxide	38831	31855	29213	29267	27077
baseline phi = 2.2					
dilution = 5.5% nitrogen					
plus 8% carbon dioxide					
Residence Time (ms)	2.9	10.9	18.8	26.7	34.6
methane	5042	5051	5017	5133	5304
ethylene	95	155	148	146	151
acetylene	13233	12196	11459	11047	11179
carbon monoxide	133320	135505	132078	150018	129709
carbon dioxide	59529	59135	61007	68313	57317

Table B.2 Monocyclic Aromatic Hydrocarbon Data

T = 1580K **baseline phi = 1.3** **benzene = 3.4 g/min**	all in mg/m3 flame gas				
Residence Time (ms)	**2.1**	**8**	**13.8**	**19.6**	**25.4**
benzene	294.89	424.64	448.23	426.12	493.94
toluene	1.15	1.21	0.94	1.04	1.28
phenyl acetylene	6.25	15.56	16.87	20.44	23.52
styrene	0.26	0.55	0.51	0.55	0.64
indene	5.09	5.76	5.91	5.07	5.48
phenyl-1,3-butadiene	0.79	1.72	1.84	2.15	2.24
baseline phi = 1.3 **benzene = 4.2 g/min**					
benzene	508.69	557.34	580.93	498.36	570.61
toluene	1.64	1.04	1.72	1.10	1.40
phenyl acetylene	9.83	17.39	23.33	21.98	27.19
styrene	0.26	0.55	0.51	0.55	0.64
indene	3.67	6.20	5.59	5.87	5.85
phenyl-1,3-butadiene	1.00	1.76	2.10	2.62	2.92

T = 1580K **baseline phi = 1.3** **benzene = 6.4 g/min**	all in mg/m3 flame gas				
Residence Time (ms)	**2.1**	**8**	**13.8**	**19.6**	**25.4**
benzene	799.15	923.01	887.62	989.36	1085.20
toluene	1.68	2.16	2.47	2.90	3.83
phenyl acetylene	15.44	30.27	38.18	45.70	56.49
styrene	0.59	1.06	1.23	1.32	1.49
indene	8.41	10.67	10.96	11.76	12.33
phenyl-1,3-butadiene	2.23	3.79	4.48	4.53	4.66
baseline phi = 1.6 **benzene = 4.2 g/min**					
benzene	2005.25	1562.92	1390.41	816.85	819.80
toluene	5.83	4.94	4.38	2.96	3.04
phenyl acetylene	82.14	97.18	94.67	63.63	64.79
styrene	1.70	1.68	1.51	1.04	1.04
indene	15.41	14.48	12.04	7.46	7.00
phenyl-1,3-butadiene	0.71	1.50	1.43	0.53	0.19

Table B.3 Polycyclic Aromatic Hydrocarbon Data

T = 1580K **baseline phi = 1.3** **benzene = 3.4 g/min**	all in mg/m3 flame gas				
Residence Time (ms)	**2.1**	**8**	**13.8**	**19.6**	**25.4**
naphthalene	5.78	12.00	15.90	20.59	25.65
acenaphthylene	9.45	18.07	23.10	28.16	35.05
ethynyl acenaphthylenes	0.00	0.18	0.69	1.00	1.19
phenanthrene	0.33	1.09	1.83	2.41	3.32
anthracene	0.04	0.06	0.07	0.07	0.09
acephenanthrylene	0.22	0.63	0.98	1.37	1.74
fluoranthene	0.57	1.60	2.54	3.68	5.00
pyrene	0.19	0.52	0.77	1.27	1.65
CPAP	0.45	1.26	2.20	2.94	2.45
cyclopenta[cd]pyrene	0.84	0.72	2.10	5.30	4.31
dicyclopenta pyrenes	0.00				
benzo[a]anthracene	0.00				
chrysene	0.16	0.54	0.99	0.80	1.36
cyclopenta[cd]fluoranthene	0.56	0.18	0.61	0.68	1.07
benzo[ghi]fluoranthene	0.00	1.44	2.20	2.74	2.43

T = 1580K **baseline phi = 1.3** **benzene = 4.2 g/min**	all in mg/m3 flame gas				
Residence Time (ms)	**2.1**	**8**	**13.8**	**19.6**	**25.4**
naphthalene	8.11	14.37	20.40	28.31	40.89
acenaphthylene	12.87	20.49	26.92	37.64	50.86
ethynyl acenaphthylenes	0.21	0.56	0.82	1.37	1.88
phenanthrene	0.56	1.18	1.74	2.90	4.04
anthracene	0.48	0.74	0.76	1.06	1.35
acephenanthrylene	0.28	0.59	0.84	1.41	2.12
fluoranthene	0.77	1.62	2.36	4.01	6.19
pyrene	0.20	0.50	0.79	1.44	2.39
CPAP	0.90	1.82	2.47	3.82	5.34
cyclopenta[cd]pyrene	1.57	3.51	5.38	9.61	14.70
dicyclopenta pyrenes					
benzo[a]anthracene					
chrysene	0.22	0.30	0.38	0.69	0.90
cyclopenta[cd]fluoranthene	0.19	0.65	0.98	1.68	2.33
benzo[ghi]fluoranthene	1.14	1.86	2.32	3.56	4.96

T = 1580K **baseline phi = 1.3** **benzene = 6.4 g/min**	all in mg/m3 flame gas				
Residence Time (ms)	**2.1**	**8**	**13.8**	**19.6**	**25.4**
naphthalene	9.92	21.44	32.42	41.38	52.51
acenaphthylene	17.33	35.05	53.16	62.35	93.67
ethynyl acenaphthylenes	0.28	1.01	2.04	2.42	3.28
phenanthrene	1.07	3.10	6.06	8.08	14.77
anthracene	0.09	0.31	0.76	1.01	1.98
acephenanthrylene	0.43	1.31	2.54	3.38	5.65
fluoranthene	1.09	3.46	6.49	8.94	15.35
pyrene	0.20	0.65	1.36	1.82	3.12
CPAP	1.21	3.36	5.72	7.39	12.22
cyclopenta[cd]pyrene	2.76	8.25	14.06	17.00	22.00
dicyclopenta pyrenes	0.00				
benzo[a]anthracene	0.00				
chrysene	0.69	1.69	2.75	3.71	6.58
cyclopenta[cd]fluoranthene	0.26	1.44	2.00	2.56	3.88
benzo[ghi]fluoranthene	1.84	4.96	8.37	10.08	14.53

T = 1580K **baseline phi = 1.6** **benzene = 4.2 g/min**	all in mg/m3 flame gas				
Residence Time (ms)	**2.1**	**8**	**13.8**	**19.6**	**25.4**
naphthalene	11.06	35.57	23.59	12.75	5.69
acenaphthylene	14.34	22.67	27.90	14.83	6.81
ethynyl acenaphthylenes	0.41	1.33	2.30	1.19	0.51
phenanthrene	1.17	2.98	3.53	1.74	0.74
anthracene	0.57	1.21	1.14	0.54	0.22
acephenanthrylene	0.17	0.87	1.15	0.73	0.28
fluoranthene	0.45	2.18	2.78	1.70	0.75
pyrene	0.29	1.67	1.88	1.20	0.55
CPAP	0.55	0.59	2.21	1.35	0.56
cyclopenta[cd]pyrene	0.55	4.00	9.70	6.28	2.94
dicyclopenta pyrenes					
benzo[a]anthracene					
chrysene	0.04	0.00	0.26	0.15	0.07
cyclopenta[cd]fluoranthene	0.00	0.00	0.46	0.40	0.17
benzo[ghi]fluoranthene	0.49	1.53	2.82	1.47	0.69

T = 1580K **baseline phi = 2.2** **dilution rate = 13.5% (nitrogen)**	all in mg/m3 flame gas				
Residence Time (ms)	**2.9**	**10.9**	**18.8**	**26.7**	**34.6**
naphthalene	2.20	2.80	3.62	7.27	7.38
acenaphthylene	2.98	4.67	4.02	6.76	8.56
acenaphthene	0.17	0.17	0.00	0.27	0.00
fluorene	0.00	0.00	0.00	0.00	0.00
phenanthrene	0.37	0.78	0.58	0.79	1.06
anthracene	0.07	0.15	0.06	0.09	0.19
cyclopenta[def]phenanthrene	0.22	0.45	0.31	0.48	0.67
acephenanthrylene	0.24	0.55	0.37	0.57	0.84
fluoranthene	0.40	0.95	0.67	1.03	1.55
pyrene	0.64	1.59	1.15	1.78	2.49
CPAP	0.11	0.24	0.21	0.33	0.41
cyclopenta[cd]pyrene	1.09	2.81	2.08	3.36	4.89
chrysene	0.00	0.00	0.00	0.00	0.00
dicyclopenta pyrenes	0.41	1.01	1.53	2.13	2.89
benzo[e]pyrene	0.09	0.19	0.26	0.27	0.34
benzo[b]fluoranthene	0.09	0.00	0.00	0.00	0.31
benzo[a]pyrene	0.12	0.20	0.26	0.52	0.41
benzo[ghi]perylene	0.22	0.40	0.38	0.91	1.10
indeno[1,2,3-cd]pyrene	0.13	0.28	0.29	0.46	0.53
anthanthrene	0.10	0.20	0.24	0.37	0.46
coronene	0.10	0.26	0.35	0.52	0.60
cyclopenta[bc]coronene	0.10	0.27	0.35	0.57	0.84
naphtho[8,1,2-abc]coronene	0.06	0.11	0.18	0.29	0.34
ovalene	0.05	0.08	0.14	0.19	0.17

T = 1580K **baseline phi = 2.2** **dilution rate = 21% (nitrogen)**		all in mg/m3 flame gas	
Residence Time (ms)	**2.6**	**17.1**	**31.6**
naphthalene	3.07	5.74	4.57
acenaphthylene	2.93	5.19	7.04
acenaphthene	0.50	0.60	0.28
fluorene	0.00	0.00	0.00
phenanthrene	0.54	0.73	0.95
anthracene	0.07	0.08	0.12
cyclopenta[def]phenanthrene	0.24	0.35	0.53
acephenanthrylene	0.20	0.38	0.69
fluoranthene	0.30	0.68	1.25
pyrene	0.45	1.07	1.86
CPAP	0.11	0.24	0.36
cyclopenta[cd]pyrene	0.69	2.04	4.02
chrysene	0.00	0.00	0.00
dicyclopenta pyrenes	0.51	0.90	2.80
benzo[e]pyrene	0.00	0.22	0.30
benzo[b]fluoranthene	0.00	0.00	0.30
benzo[a]pyrene	0.14	0.24	0.38
benzo[ghi]perylene	0.13	0.66	0.88
indeno[1,2,3-cd]pyrene	0.15	0.25	0.41
anthanthrene	0.10	0.21	0.42
coronene	0.10	0.28	0.48
cyclopenta[bc]coronene	0.09	0.28	0.62
napntho[8,1,2-abc]coronene	0.00	0.15	0.24
ovalene	0.00	0.11	0.15

T = 1650K **baseline phi = 1.3** **benzene = 4.2 g/min**	all in mg/m3 flame gas				
Residence Time (ms)	**2.2**	**8.3**	**14.5**	**20.6**	**26.7**
naphthalene	9.79	11.60	14.34	18.51	23.73
acenaphthylene	15.06	20.05	31.61	26.26	32.52
ethynyl acenaphthylenes	0.00	3.10	4.11	3.81	0.00
phenanthrene	1.15	2.31	3.73	3.54	3.87
anthracene	0.00	0.00	0.00	3.62	3.83
acephenanthrylene	1.36	2.02	0.00	8.05	9.32
fluoranthene	2.09	4.92	10.40	6.24	8.71
pyrene	0.88	3.44	5.06	5.65	13.25
CPAP	0.57	1.07	1.70	0.00	0.00
cyclopenta[cd]pyrene	1.31	3.13	5.14	6.50	7.11
dicyclopenta pyrenes	0.79	0.00	0.00	0.00	0.00
benzo[a]anthracene	0.39	0.54	0.64	0.55	0.51
chrysene	0.20	0.30	0.00	0.33	0.00
benzo[b]fluoranthene	0.17	0.00	0.00	0.92	0.00
benzo[k]fluoranthene	0.08	0.00	0.00	0.54	0.00
benzo[a]pyrene	0.13	0.33	0.49	0.64	0.61
benzo[ghi]perylene	0.27	0.00	0.00	0.45	0.50
indeno[1,2,3-cd]pyrene	0.24	0.85	1.63	1.97	2.03
anthanthrene	0.12	0.00	0.29	0.62	0.70
MW 300 isomers	0.00	0.31	0.77	0.84	0.00
coronene	0.00	0.13	0.00	0.23	0.00
cyclopenta[bc]coronene	0.00	0.00	0.09	0.44	0.59
naphtho[8,1,2-abc]coronene	0.00	0.00	0.05	0.17	0.19

T = 1650K **baseline phi = 2.2** **dilution = 13.5% nitrogen**	all in mg/m3 flame gas				
Residence Time (ms)	**2.8**	**10.4**	**18**	**25.5**	**33.1**
naphthalene	1.98	2.03	2.18	1.63	2.57
acenaphthylene	2.87	2.88	4.24	2.64	4.38
ethynyl acenaphthylenes	0.49	0.57	0.60	0.23	0.75
phenanthrene	0.28	0.26	0.37	0.22	0.36
anthracene	0.28	0.26	0.36	0.25	0.42
acephenanthrylene	0.22	0.25	0.32	0.26	0.40
fluoranthene	0.36	0.38	0.52	0.37	0.66
pyrene	0.58	0.62	0.92	0.61	1.07
CPAP	0.05	0.05	0.00	0.00	0.00
cyclopenta[cd]pyrene	0.73	0.85	1.35	0.76	1.63
dicyclopenta pyrenes	0.29	0.34	0.57	0.38	0.40
benzo[a]pyrene	0.00	0.12	0.00	0.00	0.00
benzo[ghi]perylene	0.19	0.22	0.36	0.53	0.47
anthanthrene	0.05	0.08	0.14	0.00	0.00
MW 300 isomers	0.13	0.19	0.37	0.22	0.35
coronene	0.09	0.13	0.24	0.11	0.21
cyclopenta[bc]coronene	0.10	0.13	0.32	0.16	0.32
naphtho[8,1,2-abc]coronene	0.00	0.00	0.05	0.04	0.07

Table B.4 Soot Data

T = 1580K					
baseline phi = 1.3	**all in mg/m3 (flame gas)**				
benzene = 3.4 g/min					
Residence Time (ms)	2.1	8	13.8	19.6	25.4
Soot Concentration	**0.8**	**2.2**	**3.5**	**5.3**	**7.5**
baseline phi = 1.3					
benzene = 4.2 g/min					
Residence Time (ms)	2.1	8	13.8	19.6	25.4
Soot Concentration	**2**	**2.6**	**4.8**	**9.8**	**14.8**
baseline phi = 1.3					
benzene = 6.4 g/min					
Residence Time (ms)	2.1	8	13.8	19.6	25.4
Soot Concentration	**1.1**	**3.1**	**10.5**	**27**	**39.5**
baseline phi = 1.6					
benzene = 4.2 g/min					
Residence Time (ms)	2.3	8.7	15	21.4	27.7
Soot Concentration	**13.8**	**19.9**	**41.7**	**50.4**	**53.5**
baseline phi = 2.2					
dilution = 13.5% nitrogen					
Residence Time (ms)	2.9	10.9	18.8	26.7	34.6
Soot Concentration	**2.4**	**4.7**	**7.9**	**13.8**	**23.8**
baseline phi = 2.2					
dilution = 21% nitrogen					
Residence Time (ms)	2.7	9.9	17.2	24.4	31.6
Soot Concentration	**0.7**	**2**	**4.1**	**7.3**	**13.1**
baseline phi = 2.2					
dilution = 5.5% nitrogen					
plus 8% carbon dioxide					
Residence Time (ms)	2.9	10.9	18.8	26.7	34.6
Soot Concentration	**2.5**	**3.7**	**5.5**	**8.2**	**17**

T = 1520K					
baseline phi = 1.3	**all in mg/m3 (flame gas)**				
benzene = 4.2 g/min					
Residence Time (ms)	2.3	8.7	15.2	21.6	28
Soot Concentration	**1.7**		**5.5**	**7.9**	**14.4**
T = 1520K					
baseline phi = 1.3					
toluene = 4.2 g/min					
Residence Time (ms)	2.3	8.7	15.2	21.6	28
Soot Concentration	**1.3**	**4.9**	**14.6**	**35.8**	**72.7**
T = 1650K					
baseline phi = 1.3					
benzene = 4.2 g/min					
Residence Time (ms)	2.2	8.3	14.5	20.6	26.7
Soot Concentration	**6.1**	**38.2**	**77.2**	**129.3**	**187.6**
T = 1650K					
baseline phi = 1.3					
toluene = 4.2 g/min					
Residence Time (ms)	2.2	8.3	14.5	20.6	26.7
Soot Concentration	**36.5**	**123.7**	**264.6**	**405.4**	**511.3**
T = 1650K					
baseline phi = 2.2					
dilution = 13.5% nitrogen					
Residence Time (ms)	2.8	10.4	18	25.6	33.1
Soot Concentration	**7.8**	**14.3**	**23.5**	**37.6**	**48.1**
T = 1650K					
baseline phi = 2.2					
dilution = 5.5% nitrogen					
plus 8% carbon dioxide					
Residence Time (ms)	2.8	10.4	18	25.6	33.1
Soot Concentration	**4.5**	**9**	**12.6**	**19.9**	**32.4**

Soot Size Data

Case of the soot sample collected from the 1580K, $\phi = 1.3 + 6.4$ g/min benzene experiment at a residence time of 19.6 ms.

Measured soot concentration = 27 mg/m^3.

Table B.5 Soot Primary Particles Observed in TEM Image

Size Range (nm)	Number of Particles
1-16	1
17-20	10
21-24	12
25-30	14
31-35	11
36+	9

mean particle diameter = 27.5 nm

root mean squared diameter = 28.8 nm

calculated number density = 1.3×10^{15} particles/m^3

Appendix C The Combustion Research Facility (CRF)

The "CRF Experiments" described in section 4.7 were all carried out in the Combustion Research Facility (Figure C.1). The facility was a 10m long tunnel furnace with a maximum thermal capacity of 3MW. The walls of the CRF were formed by interchangeable, separately water cooled sections that had either bare metal or refractory lining on the inside.

The CRF was equipped with a movable block multiannular variable swirl burner (MIT design), while a staged air supply could be positioned at a chosen location. The burner had a fuel gun plus a triannular air supply with an independently variable air flow rate and swirl number for each annulus. The natural gas was injected through a variety of nozzles to achieve the desired aerodynamic configuration. The first stage of the CRF consisted of 1.2x1.2m sections while the end sections (plugflow sections) had a diameter of 0.5m.

The secondary fuel used in the study was 99% pure toluene and benzene, purchased in 1 gallon containers. Prior to each experiment, the fuel was transferred to a closed (but not airtight) container. The fuel was pressurized with a variable speed gear-pump with teflon coated wetted parts. The fuel flow and pressure were measured with a rotameter and manometer respectively. The atomizing medium was nitrogen, which was administered at a constant flowrate and pressure. For a more detailed outline, see Thijssen [1993].

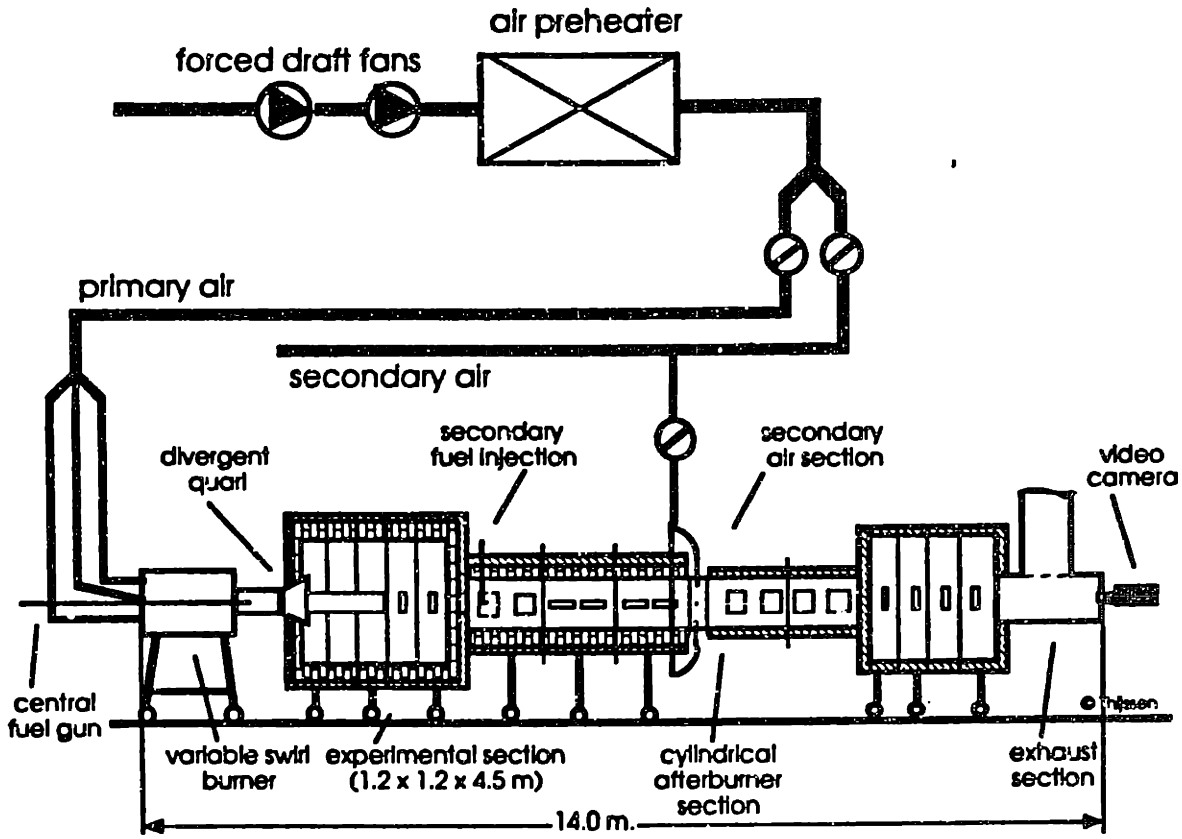

Figure C.1 The Combustion Research Facility

from Thijssen [1993]

Appendix D CRF Results

The set of experiments referred to in section 4.7 were carried out by firing the burner fuel lean ($\phi = 0.8$) with natural gas and injecting either benzene or toluene into the cylindrical plugflow section. The amount of secondary fuel injected ranged from 7.8% to 10% of the total heat input.

Total PAH levels were measured by *in-situ* by laser induced fluorescence (LIF). Soot concentrations were determined by measuring scattering signals as well as by collecting samples for gravimetric analysis.

The following plots (figures D.1-D.4) contain the soot and total tar data collected for the four experimental cases.

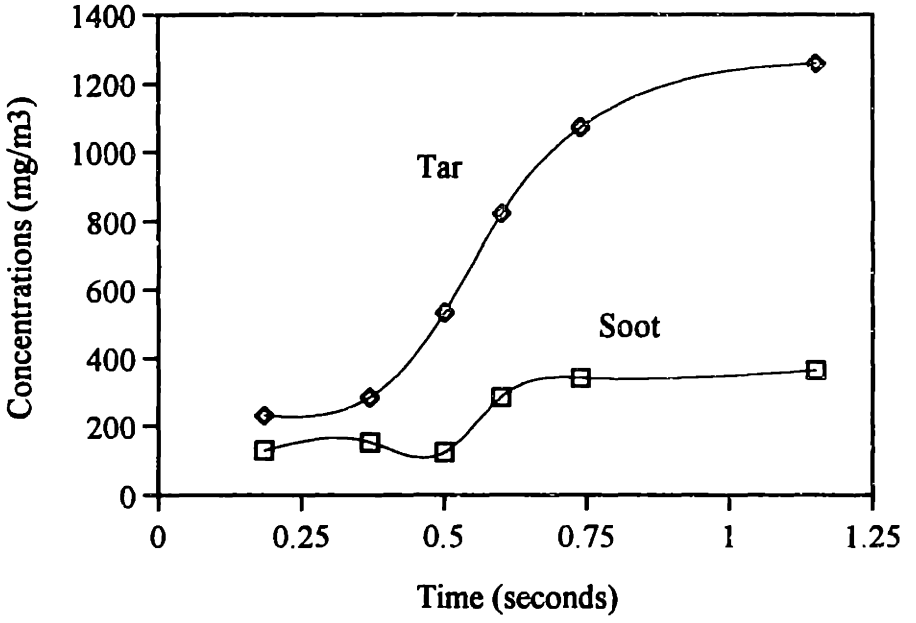

Figure D.1 Soot and Total Tar Concentrations in CRF with Benzene Injection at 1350K

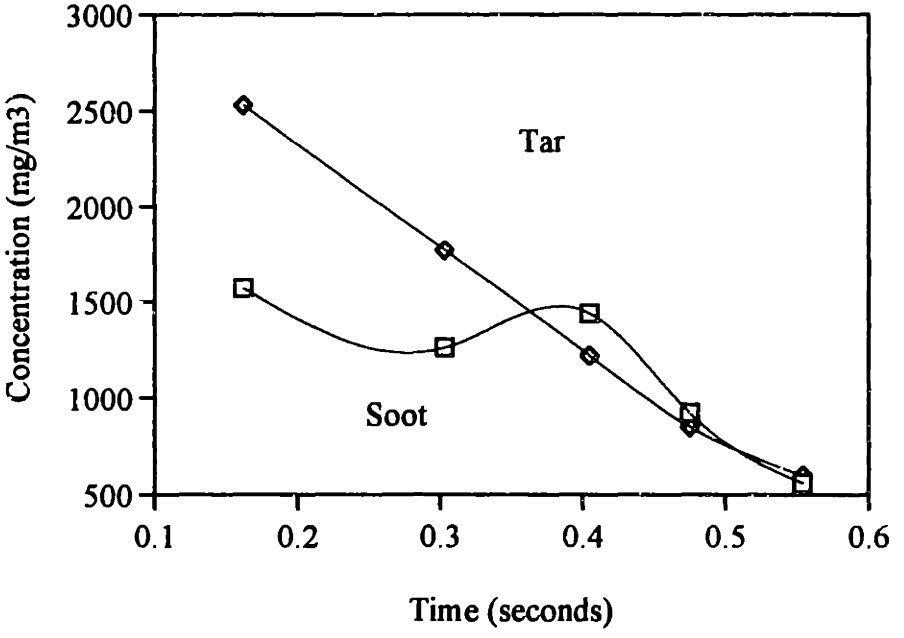

Figure D.2 Soot and Total Tar Concentrations in CRF with Toluene Injection at 1350K

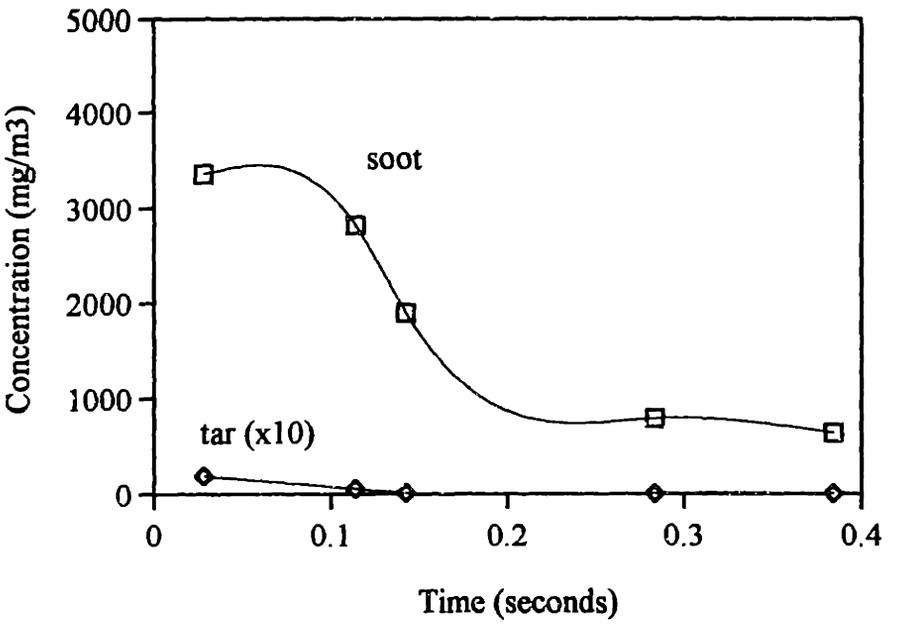

Figure D.3 Soot and Total Tar Concentrations in CRF with Benzene Injection at 1550K

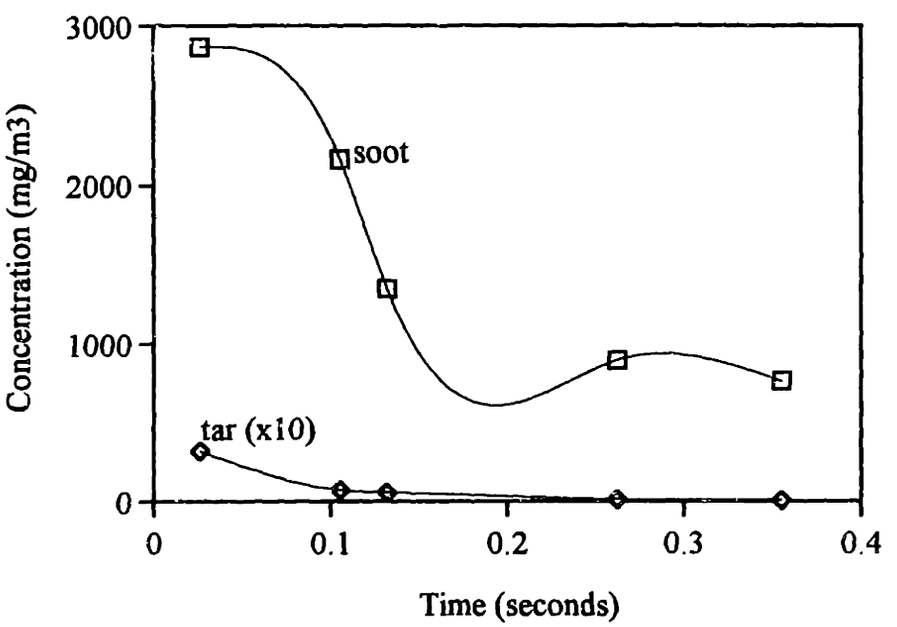

Figure D.4 Soot and Total Tar Concentrations in CRF with Toluene Injection at 1550K

Appendix E The Drop Tube Furnace

The experimental apparatus used in the pyrolysis studies of Masonjones [1995] and Wornat [1988] is a drop-tube furnace equipped with a solid particle feeder. The reactor is depicted in Figure E.1. For a detailed description, see Masonjones [1995].

As this figure indicates, the furnace is electrically heated and the temperature is controlled via a boron-graphite thermocouple. The reaction zone consists of the central 32cm of a 47mm diameter quartz probe. Solid fuel (e.g. naphthalene) is ground to produce particles 150-200 microns in size. The fuel is then fed to the furnace by a system which relies on nitrogen carrier gas to entrain the particles and carry them into the reaction zone.

Sample collection takes place by inserting a watercooled probe equipped with a quench gas inlet tube into the furnace, and drawing all of the product gas from the furnace with a vacuum pump. PAH and samples are deposited onto a preweighed filter.

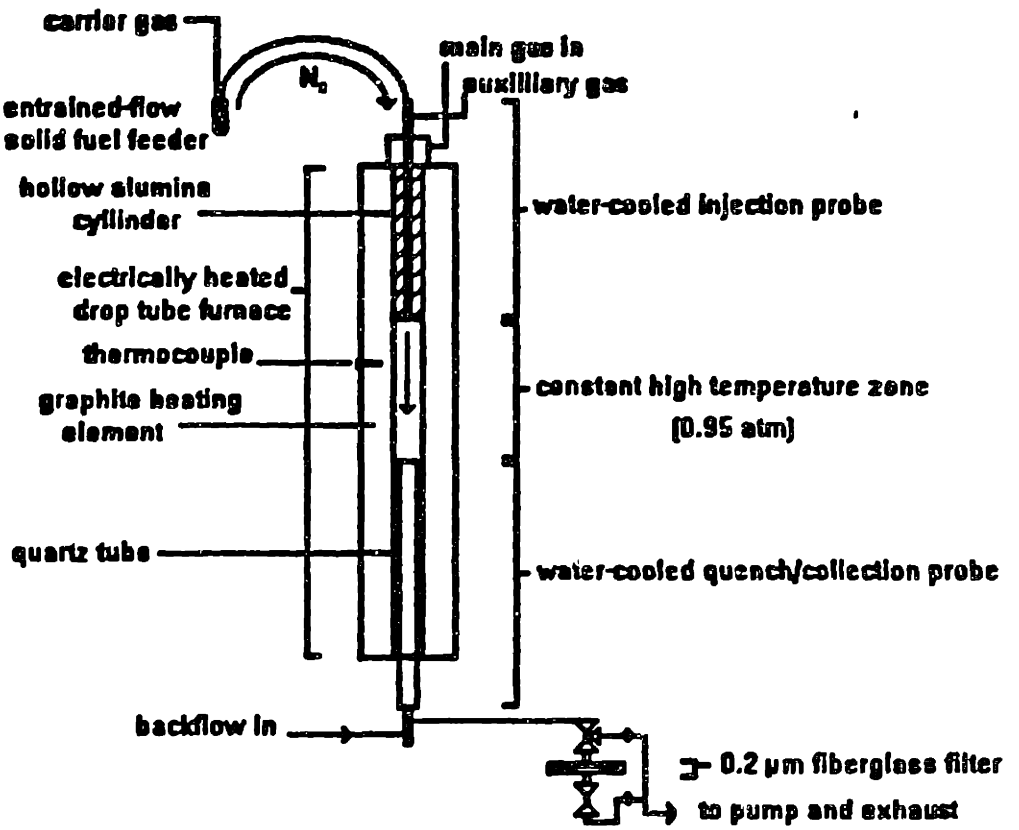

Figure E.1 The Drop Tube Furnace

from Masonjones [1995]

Appendix F Mutagenicities of PAH

The propensities of various PAH to induce cell mutations has been determined by carrying out either *in-vivo* or *in-vitro* bioassays. *In-vivo* testing, as the name implies, involves the use of experimental animals. However, the activity in animals is strongly dependent on variables such as species, strain, age, sex, site and mode of administration, and whether promoters are employed. This makes it difficult to compare literature results from different test systems. Due to the costs involved in *in-vivo* testing, various *in-vitro* bioassays have been developed to screen potential carcinogens. Since factors such as the concentration of metabolizing enzymes and the duration of the test strongly bias results, a battery of tests is commonly employed. A detailed review on *in-vitro* bioassay methods may be found in Weisburger & Williams [1984]. Historically there has been some difficulty in developing *in vitro* human cell lines that stably express oxidative enzymes necessary for the activation of promutagenic PAH. But recent modifications to a human B-lymphoblastoid cell line first described by Crespi & Thilly [1984] have led to the development of cell lines that stably express an array of cytochrome P450 enzymes e.g. Penman *et al.* [1994].

Recent research has led to the recognition that most carcinogens are metabolized to reactive intermediates which become covantly bound to proteins and nucleic acids. Binding of carcinogenic metabolites to nucleic acids, particularly DNA, is now generally accepted to be a critical event which leads ultimately to tumor induction. For most alternant PAH, it seems that the principle carcinogenic metabolites are the bay-region diol epoxides [Harvey 1991]. These metabolites are chemically reactive electrophiles that undergo relatively facile hydrolysis and react readily with nucleic acids, proteins, and other cellular molecules. This generalization is based on the results of DNA binding studies and from mutagenesis and carcinogenesis experiments. There are two views as to why bay region diol epoxides are so reactive. According to the "bay region theory", bay region diol epoxides are distinguished by their exceptional

chemical reactivity as predicted by molecular orbital theoretical calculations [Lehr *et al.* 1985], The alternate hypothesis is that they are not distinguished by their special reactivity but by their resistance to enzymatic detoxification. According to this concept, the bay region provides a pocket of protection that sterically interferes with the approach and proper orientation of epoxide hydrolase and other detoxifying enzymes [Harvey 1981].

Carcinogenic Potentials of Select PAH

The carcinogenic potentials of individual PAH detected in the PFR samples as well as the MW 302 species considered in the PAH isomer study appear below.

7,12-Dimethylbenz[a]anthracene (DMBA)

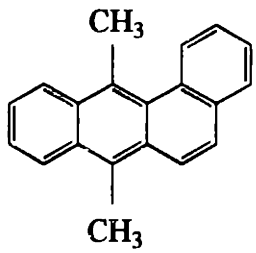

DMBA is one of the most potent carcinogenic PAH known, although it is questionable whether it is produced in combustion sources. Its potency has led to its wide use in experimental investigations of mouse skin and rat mammary gland tumorigenesis, and the DMBA-induced rat mammary developed by Huggins is the standard laboratory animal model in the study of breast cancer [Welsch 1985].

Benzo[a]pyrene

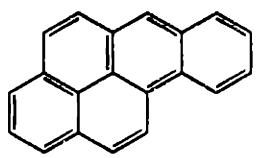

BaP was first isolated from coal tar and was subsequently identified as a widespread pollutant. It is a relatively potent carcinogen whose biological properties have been extensively documented

[IARC 1983]. It is mutagenic in bacterial and human cell bioassays [Busby *et al.* 1995], and is often used as a reference compound.

Dibenz[a,h]anthracene

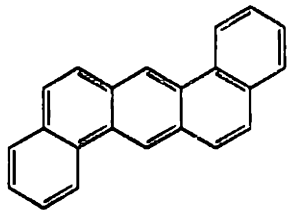

DBahA was the first synthetic PAH shown to be carcinogenic and its biological properties have been studied extensively. It is moderately active as a carcinogen and, according to bacterial bioassays, it is less mutagenic than benzo[a]pyrene [IARC 1983]. According to a series of human cell bioassays, its minimum mutagenic concentration is approximately three times that of benzo[a]pyrene [Durant *et al.* 1996].

Dibenzo[a,i]pyrene

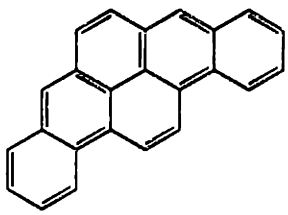

DBaiP exhibits exceptional potency in the induction of sarcomas in mice [Buu-Hoi 1964], and is a potent inducer of lung tumors in newborn mice [Chang *et al* 1982], but is less active than benzo[a]pyrene in the induction of skin tumors in mice. It is moderately less mutagenic than benzo[a]pyrene in *salmonella typhimurium* and substantially less mutagenic in human cells [Busby *et al.* 1995].

Dibenzo[a,l]pyrene

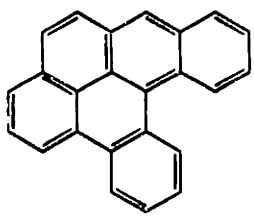

DBalP has been found to be many-fold more potent than benzo[a]pyrene as a rodent skin tumor inducer [Higginbotham *et al.* 1993] and more potent than DMBA in bacterial bioassays [Ralston et al. 1994]. According to Busby *et al.* [1995], it is 60% more potent than benzo[a]pyrene in *salmonella typhimurium* but 50-fold more potent in human cells. It is considered by many to be the most carcinogenic PAH.

Dibenzo[a,h]pyrene

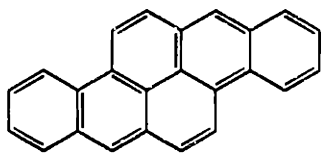

DBahP is tumorigenic on mouse skin at a lower level of activity than benzo[a]pyrene, but is a potent inducer of lung tumors in newborn mice [Chang *et al* 1982]. It displayed little or no mutagenic activity in *salmonella typhimurium* or human cells [Busby *et al.* 1995].

Dibenzo[a,e]pyrene

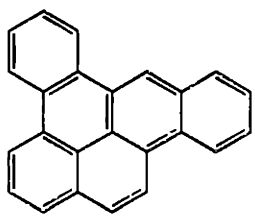

DBaeP exhibits strong sarcomagenic activity in mice [Buu-Hoi 1964] but is less active than benzo[a]pyrene in the induction of mouse skin tumors. However, it displays a comparable mutagenicity to benzo[a]pyrene in *salmonella typhimurium* and in human cells [Busby *et al.* 1995], [Durant *et al.* 1996].

Cyclopenta[c,d]pyrene

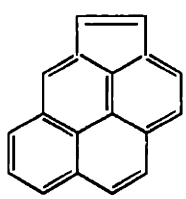

CPP has been shown to be more mutagenic than benzo[a]pyrene in bacterial mutation assays, but was considerably less active than benzo[a]pyrene in *in vitro* rodent assays. According to [Durant *et al.* 1996], its minimum mutagenic concentration in human cells is approximately seven times lower than that of benzo[a]pyrene.

Fluoranthene

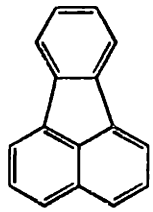

Fluoranthene is relatively potent mutagen, although it has shown no activity on mouse skin or on subcutaneous injection [Buu-Hoi 1964]. It is tumorigenic in a newborn mouse lung bioassay [Busby Jr. *et al.* 1984].

Indeno[c,d]pyrene

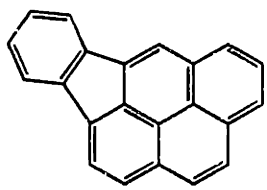

Indeno[c,d]pyrene is a complete carcinogen but exhibits an activity lower than that of benzo[a]pyrene e.g. according to Durant *et al.* [1996], its minimum mutagenic concentration in human cells is roughly three times that of BaP.

Appendix G : MM3(92) Sample Input and Output Files

Sample Input File
case of dibenzo[a,k]fluoranthene

```
 DBakFluoranthene                                                1  38 4  0 0
0 70.0
TTTTTTTTTTTTTTTTTTTTTTT                                          00 0 0 0 0 0
0 000 0
0  29       0.0000001        14     0          0     0     0     0     1
1     0
     1     2
     1     6
     1     7
     2     3
     2    10
     3     4
     3    12
     4     5
     5     6
     5    22
     7     8
     8     9
     9    10
    10    11
    11    12
    11    16
    12    13
    13    14
    14    15
    14    24
    15    16
    15    17
    17    18
    18    23
    23    24
     4    19
    19    20
    20    21
    21    22
6   15     7   16     8   17     9   18    10   19     3   20    11   21    12
22    19   25   22    26    6   27     7   28     8   29     9   30    16   31
17   32
    18    34    23    35    21    36    20    33    24    37    13    38
    2.28626    0.00000    0.00000 C  2(  1)
    0.90164    0.00000    0.00000 C  2(  2)
    0.10337    1.16906    0.00000 C  2(  3)
    0.72134    2.39506    0.00000 C  2(  4)
    2.15405    2.43664    0.00000 C  2(  5)
    2.92201    1.28078    0.00000 C  2(  6)
    2.92201   -1.28078    0.00000 C  2(  7)
    2.15406   -2.43664    0.00000 C  2(  8)
    0.72135   -2.39506    0.00000 C  2(  9)
    0.10337   -1.16906    0.00000 C  2( 10)
   -1.29226   -0.71007    0.00000 C  2( 11)
   -1.29226    0.71007    0.00000 C  2( 12)
```

-2.48508	1.42058	0.00000	C	2(13)
-3.69028	0.70067	0.00000	C	2(14)
-3.69028	-0.70067	0.00000	C	2(15)
-2.48508	-1.42058	0.00000	C	2(16)
-4.89548	-1.42058	0.00000	C	2(17)
-6.10068	-0.70067	0.00000	C	2(18)
0.10337	3.50718	0.00000	C	2(19)
0.72134	4.73318	0.00000	C	2(20)
2.15405	4.73318	0.00000	C	2(21)
2.92201	3.50718	0.00000	C	2(22)
-6.10068	0.70067	0.00000	C	2(23)
-4.89548	1.42059	0.00000	C	2(24)
-0.99866	4.05042	0.00000	H	5(25)
4.02261	4.05042	0.00000	H	5(26)
4.02261	1.35014	0.00000	H	5(27)
4.02261	-1.35014	0.00000	H	5(28)
2.65981	-3.41754	0.00000	H	5(29)
0.12986	-3.32474	0.00000	H	5(30)
-2.48534	-2.52261	0.00000	H	5(31)
-4.89548	-2.52261	0.00000	H	5(32)
0.17032	5.68756	0.00000	H	5(33)
-7.06010	-1.24569	0.00000	H	5(34)
-7.06010	1.24569	0.00000	H	5(35)
2.70506	5.68756	0.00000	H	5(36)
-4.89548	2.52261	0.00000	H	5(37)
-2.48534	2.52261	0.00000	H	5(38)

Excerpts from Sample Output File
case of dibenzo[a,k]fluoranthene

```
1       DBakFluoranthene

                CHEMICAL FORMULA :  C( 24)  H( 14)
                FORMULA WEIGHT   :   302.112
                                                                DATE 06-
Feb-97
                                                                TIME
18:02:12

           THE COORDINATES OF  38 ATOMS ARE READ IN.

      CONFORMATIONAL ENERGY, PART 1:  GEOMETRY AND STERIC ENERGY
                                      OF INITIAL CONFORMATION.


      CONNECTED ATOMS
            1-  2-
            1-  6-
            1-  7-
            2-  3-
            2- 10-
            3-  4-
            3- 12-
            4-  5-
            5-  6-
            5- 22-
            7-  8-
            8-  9-
            9- 10-
           10- 11-
           11- 12-
           11- 16-
           12- 13-
           13- 14-
           14- 15-
           14- 24-
           15- 16-
           15- 17-
           17- 18-
           18- 23-
           23- 24-
            4- 19-
           19- 20-
           20- 21-
           21- 22-

      ATTACHED ATOMS
           19- 25, 22- 26,  6- 27,  7- 28,  8- 29,  9- 30, 16- 31, 17-
32,
           18- 34, 23- 35, 21- 36, 20- 33, 24- 37, 13- 38,

      INITIAL ATOMIC COORDINATES
```

ATOM	X	Y	Z	TYPE	
C(1)	2.26626	0.00000	0.00000	(2)	PI-ATOM
C(2)	0.90164	0.00000	0.00000	(2)	PI-ATOM
C(3)	0.10337	1.16906	0.00000	(2)	PI-ATOM
C(4)	0.72134	2.39506	0.00000	(2)	PI-ATOM
C(5)	2.15405	2.43664	0.00000	(2)	PI-ATOM
C(6)	2.92201	1.28078	0.00000	(2)	PI-ATOM
C(7)	2.92201	-1.28078	0.00000	(2)	PI-ATOM
C(8)	2.15406	-2.43664	0.00000	(2)	PI-ATOM
C(9)	0.72135	-2.39506	0.00000	(2)	PI-ATOM
C(10)	0.10337	-1.16906	0.00000	(2)	PI-ATOM
C(11)	-1.29226	-0.71007	0.00000	(2)	PI-ATOM
C(12)	-1.29226	0.71007	0.00000	(2)	PI-ATOM
C(13)	-2.48508	1.42058	0.00000	(2)	PI-ATOM
C(14)	-3.69028	0.70067	0.00000	(2)	PI-ATOM
C(15)	-3.69028	-0.70067	0.00000	(2)	PI-ATOM
C(16)	-2.48508	-1.42058	0.00000	(2)	PI-ATOM
C(17)	-4.89548	-1.42058	0.00000	(2)	PI-ATOM
C(18)	-6.10068	-0.70067	0.00000	(2)	PI-ATOM
C(19)	0.10337	3.50718	0.00000	(2)	PI-ATOM
C(20)	0.72134	4.73318	0.00000	(2)	PI-ATOM
C(21)	2.15405	4.73318	0.00000	(2)	PI-ATOM
C(22)	2.92201	3.50718	0.00000	(2)	PI-ATOM
C(23)	-6.10068	0.70067	0.00000	(2)	PI-ATOM
C(24)	-4.89548	1.42058	0.00000	(2)	PI-ATOM
H(25)	-0.99866	4.05042	0.00000	(5)	
H(26)	4.02261	4.05042	0.00000	(5)	
H(27)	4.02261	1.35014	0.00000	(5)	
H(28)	4.02261	-1.35014	0.00000	(5)	
H(29)	2.65981	-3.41754	0.00000	(5)	
H(30)	0.12986	-3.32474	0.00000	(5)	
H(31)	-2.48534	-2.52261	0.00000	(5)	
H(32)	-4.89548	-2.52261	0.00000	(5)	
H(33)	0.17032	5.68756	0.00000	(5)	
H(34)	-7.06010	-1.24569	0.00000	(5)	
H(35)	-7.06010	1.24569	0.00000	(5)	
H(36)	2.70506	5.68756	0.00000	(5)	
H(37)	-4.89548	2.52261	0.00000	(5)	
H(38)	-2.48534	2.52261	0.00000	(5)	

THIS MOLECULE CONTAINS

1 5-MEMBERED RING(S)

PI-SYSTEM IS FOUND TO BE PLANAR

VESCF CALCULATION FOR PLANAR SYSTEM

ITER 1	VO= -11.219326(-7042.48KCAL)		
ITER 2	VO= -11.234626(-7052.09KCAL)	DIFF =	0.015300
ITER 3	VO= -11.238231(-7054.35KCAL)	DIFF =	0.003605
ITER 4	VO= -11.239817(-7055.35KCAL)	DIFF =	0.001586
ITER 5	VO= -11.240392(-7055.71KCAL)	DIFF =	0.000575
ITER 6	VO= -11.240687(-7055.89KCAL)	DIFF =	0.000296
ITER 7	VO= -11.240814(-7055.97KCAL)	DIFF =	0.000127
ITER 8	VO= -11.240889(-7056.02KCAL)	DIFF =	0.000074

```
              VESCF SEQUENCE REQUIRES   7.85 SECONDS.


          DIELECTRIC CONSTANT =  1.500


       INITIAL STERIC ENERGY IS     91.4428 KCAL.

                  COMPRESSION      29.4274
                  BENDING          63.8108
                  BEND-BEND         4.0834
                  STRETCH-BEND     -1.2457
                  VANDERWAALS
                    1,4 ENERGY     21.3856
                    OTHER          -3.2753

                  TORSIONAL       -30.6600
                  TORSION-STRETCH   0.0000
                  DIPOLE-DIPOLE     7.9166
                  CHARGE-DIPOLE     0.0000
                  CHARGE-CHARGE     0.0000


       DIPOLE MOMENT =          0.623 D


         PI-DIPOLE MOMENT    =  0.2079

         SIGMA-DIPOLE MOMENT =  0.5412

                      -------------------------------
                      PI-SYSTEM IS FOUND TO BE PLANAR
                      -------------------------------


       PLANAR
       ------
       F-MATRIX
        -0.20801 -0.14695 -0.01106  0.01077 -0.01104 -0.15212 -0.12659 -
0.01130
         0.01169 -0.01232  0.00008  0.00091  0.00012 -0.00036 -0.00020
0.00014
         0.00000  0.00005 -0.00024 -0.00710  0.00003  0.00890  0.00009 -
0.00003
        -0.20893 -0.15126 -0.01382  0.01005 -0.01301 -0.01329  0.01081 -
0.01480
        -0.12682 -0.00950 -0.01254  0.00799 -0.00200 -0.00329  0.00454 -
0.00097
         0.00136  0.00808 -0.00019 -0.00718 -0.00015  0.00077 -0.00163
        -0.20947 -0.15129 -0.01379  0.02589 -0.00563 -0.00036  0.01079 -
0.01348
        -0.01249 -0.10116 -0.00830  0.00092 -0.00087  0.00159 -0.00064
0.00012
        -0.01428  0.01331 -0.00083 -0.00875 -0.00008 -0.00005
        -0.21119 -0.12812 -0.01207  0.00044 -0.00500 -0.00096  0.00477
0.00333
        -0.00928  0.00592  0.00041 -0.00228 -0.00114  0.00023  0.00105 -
0.17164
        -0.01481  0.01458 -0.01094 -0.00025 -0.00138
        -0.21103 -0.15328  0.00528 -0.00051 -0.00509 -0.00014 -0.00048
```

```
                    (>= 5,< 20 /cm),
                  6 zero frequencies, and
                108 real frequencies.


 ================================================================================
=======
                      STATISTICAL THERMODYNAMICS ANALYSIS
 ================================================================================
=======

  Structure name    :  DBakFluoranthene
  Temperature       :   300.00 K
  Symmetry number   :   1
  Optical isomers   :   1
  Zero Point Energy :  184.059 Kcal/mol


                      ENERGY   ENTHALPY    ENTROPY  FREE ENERGY   HEAT
CAPACITY
                   (Kcal/mol) (Kcal/mol)     (eu)   (Kcal/mol)
(cal/mol/deg)
  Translational       0.894      1.490     43.025    -11.417
4.967
     Rotational       0.894      0.894     34.821     -9.552
2.980
    Vibrational     193.086%   193.086%    52.743    177.263%
66.808
      Potential      17.560#    17.560#     0.000     17.560#
0.000
         Mixing       0.000      0.000      0.000      0.000
0.000
          Total     212.435    213.031    130.589    173.854
74.756

  Enthalpy Function (H-Ho)/T     =   38.04 cal/mol/deg
  Free Energy Function -(G-Ho)/T =   92.55 cal/mol/deg

  % Includes zero point energy (ZPE).
  # Includes steric energy (SE).
    Internal rotation contributions are not considered

  This structure has   0 imaginary frequencies,
                       0 free internal rotation (fir) frequencies
                         (>= 0,< 5 /cm),
                       0 restricted internal rotation (rir) frequencies
                         (>= 5,< 20 /cm),
                       6 zero frequencies, and
                     108 real frequencies.


 ================================================================================
=======
                      STATISTICAL THERMODYNAMICS ANALYSIS
 ================================================================================
=======

  Structure name    :  DBakFluoranthene
  Temperature       :   400.00 K
  Symmetry number   :   1
```

HEAT OF FORMATION AND STRAIN ENERGY CALCULATIONS

(UNIT = KCAL/MOLE)
(# = TRIPLE BOND)

BOND ENTHALPY (BE) AND STRAINLESS BOND ENTHALPY (SBE) CONSTANTS AND SUMS

BOND OR STRUCTURE	NO	--- NORMAL ---		--STRAINLESS--	
C-H OLEFINIC	14	-4.590	-64.26	-3.460	-48.44
CYCLOPENTANE RINGS	1	-5.508	-5.51	0.000	0.00
2-2 DELOCALIZED	29	155.800	4518.20	153.873	4462.32
SEC-DELOCALIZED	14	-33.445	-468.23	-31.819	-445.47
TER-DELOCALIZED	10	-65.374	-653.74	-63.849	-638.49
		BE =	3326.46	SBE =	3329.92

PARTITION FUNCTION CONTRIBUTION (PFC)

CONFORMATIONAL POPULATION INCREMENT (POP)	0.00
TORSIONAL CONTRIBUTION (TOR)	0.00
TRANSLATION/ROTATION TERM (T/R)	2.40
PFC =	2.40

STERIC ENERGY (E)	17.56
SIGMA-STRETCHING (ECPI)	2.02
CORRECTED STERIC ENERGY (EC) = E-ECPI	15.55
ENERGY FROM PLANAR VESCF CALCULATION (ESCF)	-3237.72
HEAT OF FORMATION = EC + BE + PFC + ESCF	106.68
STRAINLESS HEAT OF FORMATION FOR SIGMA SYSTEM (HFS) HFS = SBE + T/R + ESCF - ECPI	92.58
INHERENT SIGMA STRAIN (SI) = E + BE - SBE	14.10
SIGMA STRAIN ENERGY (S) = POP + TOR + SI	14.10

(RESONANCE ENERGY IS NOT CALCULATED.)

END OF DBakFluoranthene

TOTAL CPU TIME IS 729.73 SECONDS.

THIS JOB COMPLETED AT 18:22:11

References

Alkemade, U., and Homann, K.H., *Zeit. für Phys. Chem.*, Volume 161, pp. 19-34, 1989

Allinger, N.L., Yuh, Y.H., and Lii, J.-H., "Molecular Mechanics : The MM3 Force Field for Hydrocarbons I, II, III", *J. Am. Chem. Soc.*, Volume 111, pp. 8551, 8566, 8576, 1989

Badger, G.M., Jolad, S.D., and Spotswood, T.M., *Australian Journal of Chemistry*, 1967

Bartok, W., and Kuriskin, R.J., *Comb. Sci. Tech.*, Volume 58, pp. 281-295, 1988

Baumgärtner, L., Hesse, D., Jander, H., and Wagner H.Gg., *20th Symposium (International) on Combustion*, The Combustion Institute, pp. 959-967, 1985

Bittner, J.D., *PhD Thesis*, Massachusetts Institute of Technology, 1981

Bittner, J.D., and Howard, J.B., *18th Symposium (International) on Combustion*, The Combustion Institute, pp. 1105-1116, 1981

Böhm, H., Hesse, D., Jander, H., Lüers, B., Pietscher, J., Wagner, H.Gg., and Weiss, M., *22nd Symposium (International) on Combustion*, The Combustion Institute, pp. 403-411, 1988

Bonne, U., Homann, K.H., and Wagner, H.Gg., *10th Symposium (International) on Combustion*, The Combustion Institute, p. 503, 1965

Brouwer L., and Troe J., "Thermal Isomerization of Azulene to Naphthalene in Shock Waves", *International Journal of Chemical Kinetics*, Volume 20, pp. 379-386, 1988

Brouwer, J., *PhD Thesis*, Massachusetts Institute of Technology, 1993

Busby, W.F. Jr., Goldman, M.E., Newberne, P.M., and Woogan, G.N., "Tumorigenicity of Fluoranthene in Newborn Mouse Lung Adenoma Bioassay", *Carcinogenesis*, Volume 5, pp. 1311-16, 1984

Busby, W.F. Jr., Smith, H., Crespi, C.L., and Penman, B.W., "Mutagenicity of benzo[a]pyrene and dibenzopyrenes in the Salmonella typhimurium TM677 and the MCL-5 human cell forward mutation assays", *Mutation Research*, Volume 342, pp. 9-16, 1995

Buu-Hoi, N.P., *Cancer Res.*, Volume 24, pp. 1511-1523, 1964

Cole, J.A., *M.S. Thesis*, Massachusetts Institute of Technology, 1982

Colket, M.B., *21st Symposium (International) on Combustion*, The Combustion Institute, pp. 851-864, 1986

Coolidge, M.B., and Stewart J.J.P., MOPAC Version 6.00, *Quantum Chemistry Program Exchange*, 1990

Cooper, P.W., Kamo, R., Marek, C.J., and Solbrig, C.W., "Recirculation and Fuel-Air Mixing as Related to Oil-Burner Design", API Publication1/23, *The American Petroleum Institute*, NY, May 1964

Crespi, C.L., and Thilly, W.G., "Assay for mutation in a human lymphoblastoid line, AHH-1, competent for xenobiotic metabolism", *Mutation Research*, Volume 128, pp. 221-230, 1984

D'Alessio, A., D'Anna, A., D'Orsi, A., Minutolo, P., Barbella, R., and Ciajolo, A., *24th Symposium (International) on Combustion*, The Combustion Institute, Pittsburgh, PA, pp. 973-980, 1992

Das L. M., Mathur R. "Exhaust gas recirculation for NOx control in a multicylinder hydrogen-supplemented S.I. engine, *International Journal of Hydrogen Energy*, Volume 18, Number 12, pp 1013-1018, 1993

Dockery, D. W., Schwartz, J., and Spengler, J.D., "Air Pollution and Daily Mortality: Association with Particulates and Acid Aerosols", *Environmental Research*, Volume 59, pp. 362-373, 1992

Durant, J.L., Busby, W.F. Jr., Lafleur, A.L., Penman, B.W., and Crespi, C.L., "Human cell mutagenicity of oxygenated, nitrated, and unsubstituted polycyclic aromatic hydrocarbons associated with urban aerosols", *Mutation Research*, Volume 371, pp. 123-157, 1996

Faraday, M., "Faraday's Chemical History of a Candle", Chicago Review Press, Chicago, IL, 1988

Fenimore, C.P., and Jones, G.W., *J. Phys. Chem.*, Volume 71(3), pp. 593-597, 1967

Frenklach, M., "Shock Tube Study of the Fuel Structure Effects on the Chemcial Kinetic Mechanisms Responsible for Soot Formation", *NASA Report CR-174661*, 1983

Frenklach, M., Clary, D.W., Gardiner, W.C., and Stein, S.E., *20th Symposium (International) on Combustion*, The Combustion Institute, Pittsburgh, PA, pp. 887-901, 1984

Frenklach, M., Clary, D.W., and Ramachandra, M.K., "Shock Tube Study of the Fuel Structure Effects on the Chemcial Kinetic Mechanisms Responsible for Soot Formation Part II", *NASA Report CR-174880*, 1985

Frenklach, M., Clary, D.W., Gardiner, W.C., and Stein., S.E., *21st Symposium (International) on Combustion*, The Combustion Institute, Pittsburgh, PA, pp. 1067-1076, 1986

Frenklach, M., *22nd Symposium (International) on Combustion*, The Combustion Institute, Pittsburgh, PA, pp. 1075-1082, 1988

Frenkiach, M., and Warnatz, J., *Comb. Sci. and Tech.*, Volume 74, pp. 283-296, 1990

Frenklach, M., and Wang H., *23rd Symposium (International) on Combustion*, The Combustion Institute, Pittsburgh, PA, pp. 1559-1566, 1991

Frenklach, M., *26th Symposium (International) on Combustion*, The Combustion Institute, Pittsburgh, PA, 1996

Garg A., "Specify Better Low-NOx Burners for Furnaces", *Chemical Engineering Progress*, Volume 90, Number 1, pp. 6, 1994

Gay, J.G., and Berne, B.J., *Journal of Colloidal and Interfacial Science*, Volume 109(1), pp. 90-100, 1985

Glassman, I., "Combustion", Academic Press, New York, 1987

Harris, S.J., and Weiner, A.M., *Comb. Sci. Tech.*, Volume 32, p. 267, 1983

Harris, S.J., and Weiner A.M., *Annu. Rev. Phys. Chem*, Volume 36, pp. 31-52, 1985

Harris, S.J., Weiner, A.M., and Blint, R.J., *Combustion and Flame*, Volume 72, pp. 91-109, 1988

Harris, S.J., and Weiner A.M., *22nd Symposium (International) on Combustion*, The Combustion Institute, p. 333, 1989

Harvey, R.G., *Acc. Chem. Res.*, Volume 14, pp. 218-226, 1981

Harvey, R.G., "Polycyclic Aromatic Hydrocarbons : Chemistry and Carcinogenicity", Cambridge University Press, 1991

Haynes, B.S., and Wagner, H.Gg., *Progress in Energy and Combustion Science*, Volume 7, pp. 229-273, 1980

Haynes, B.S., Jander, H., Mätzing, H., and Wagner, H.Gg., *19th Symposium (International) on Combustion*, The Combustion Institute, pp. 1379-1385, 1982

Herbstein, F.H, and Schmidt, G.M.J, *J. Chem. Soc.*, pp. 302-13, 1954

Higginbotham, S., Ramakrishna, N.V.S., Johansson, S.L., Rogan, E.G., and Cavalieri, E.L., *Carcinogenesis*, Volume 14, p. 875, 1993

Hoffmann, A.B., "Untersuchungen zum Einfluß polyzyklischer aromatischer Kohlenwasserstoffe (PAK) auf das Rußwachstum in einem Kolbenströmungsreaktor", *Diplom Thesis*, Universität Karlsruhe (TH), Karlsruhe Germany, 1996

Homann, K.H., and Wagner, H.Gg., *11th Symposium (International) on Combustion*, The Combustion Institute, p. 371, 1967

Hou, K.C., and Palmer, H.B., *Journal of Physical Chemistry*, Volume 69, Number 3, p. 863, 1965

Howard, J.B., *23rd Symposium (International) on Combustion*, The Combustion Institute, p. 1107, 1990

IARC, "Monograph on the Evaluation of the Carcinogenic Risk of the Chemical to Man: Certain Polycylic Aromatic Hydrocarbons and Heterocyclic Compounds", Volume 32, Lyon, France, International Agency for Research on Cancer, 1983

Jander, H., Personal communication, 1997

Katrinak, K.A., Anderson, J.R., and Buseck, P., *Environmental Science and Technology*, Volume 29, pp. 321-329, 199.

Kee, R.J., Rupley, F.M., and Miller, J.A., CHEMKIN II: *A Fortran Chemical Kinetics Package for the Analysis of Gas Phase Chemical Kinetics*, Sandia Report SAND89-8009, 1989

Kowalik, R.M., Ruth, L.A., and Blazowski, W.S., in *Particulate Carbon Formation in Combustion*, Siegla, D.C., and Smith, G.W. (eds), Plenum Publishing Corp., p. 285, 1981

Lafleur A.L., Monchamp, P.A., Plummer E.F., and Kruzel E.L., "Evaluation of Gravimetric Methods for Dissoluable Matter in Extracts of Environmental Samples", *Analytical Letters*, 19 (21 & 22), pp. 2103-2119, 1986

Lam, F.W., *PhD Thesis*, Massachusetts Institute of Technology, 1988

Lehr, R., Kumar, S., Levin, W., Wood, A.W., Chang, R.L., Conney, A., Yagi, H., Sayer, J.M., and Jerina, D.M., *Polycyclic Aromatic Hydrocarbons and Carcinogenesis*, Am. Chem. Soc. Monogr. 283, R.G. Harvey (ed), pp. 63-84, 1985

McKinnon, J.T., and Howard, J.B., *24th Symposium (International) on Combustion*, The Combustion Institute, p. 965, 1992

Macadam, S., Hoffmann, A.B., Beér, J.M., and Sarofim, A.F., *26th Symposium (International) on Combustion*, The Combustion Institute, p. 2295, 1996

Manegold, C.W.E., "Konstruktion eines Verdampfers und erste Messungen zur Rußbildung in heißen Rauchgasen mit und ohne Eindüsung von benzolbeladenen Stickstoffströmen", *Diplom Thesis*, Universität Karlsruhe (TH), Karlsruhe Germany, 1995

Marr, J.A., *PhD Thesis*, Massachusetts Institute of Technology, 1993

Marr, J.A., Giovane, L.M., Longwell, J.P., Howard, J.B., and Lafleur, A.L., *Combustion Science and Technology*, Volume 101, p. 301, 1994

Masonjones, M.J., *PhD Thesis*, Massachusetts Institute of Technology, 1995

Masonjones, M.J., Lafleur, A.L., and Sarofim, A.F., *Combustion Science and Technology*, Volume 109, pp. 273-285, 1995

Masonjones, M.J., Personal communication, 1996

Mauß, F., Schäfer, T., and Bockhorn, H., *Combustion and Flame*, Volume 99, 1994

Miller, J.A., and Melius, C.F., *Combustion and Flame*, Volume 91, pp. 21-39, 1992

Mukherjee, J., Sarofim, A.F., and Longwell, J.P., *Combustion and Flame*, Volume 96, pp. 191-200, 1994

Mulholland, J.A., *PhD Thesis*, Massachusetts Institute of Technology, 1992

Mulholland, J.A., Mukherjee J., Wornat M.J., Sarofim, A.F., and Lafleur A.L., *Combustion and Flame*, Volume 94, pp. 233-243, 1993

Müller-Dethlefs, K., and Schlader, A.F., *Combustion and Flame*, Volume 27, pp. 205-215, 1976

Nenniger, J.E., *PhD Thesis*, Massachusetts Institute of Technology, 1983

Neoh, K.G., *PhD Thesis*, Massachusetts Institute of Technology, 1980

Neoh, K.G., Howard, J.B., and Sarofim, A.F., "Soot Oxidation in Flames", from *Particulate Carbon Formation During Combustion*, Siegla, D.C., and Smith, G.W. (eds), Plenum Publishing Corp., p. 261, 1981

Page, F.M., Ates, F., *Evaporation-Combustion of Fuels*, ACS Advances in Chemistry Series, J.T. Zhang (ed.), ACS, Washington, DC, Number 166, pp. 190-197, 1978

Palmer, H.B., and Cullis, C.F., "The Formation of Carbon from Gases" in *Chemistry & Physics of Carbon*, P.L. Walker, ed., 1965

Penman, B.W., Chen, L., Gelboin, H.V., Gonzalez, F.J., and Crespi, C.L., "Development of a human lymphoblastoid cell line constitutively expressing human CYP1A1 cDNA: substrate specificity with model substrates and promutagens, *Carcinogenesis*, Volume 15, pp. 1931-1937, 1994

Plummer-Turano, E.F., Personal communication, 1997

Pope, C.A., Dockery, D.W., and Schwartz, J., "Review of Epidemiological Evidence of Health Effects of Particulate Air Pollution", *Inhalation Toxicology*, Volume 7, Number 1, Proceedings of the Colloquium on Particulate Air Pollution and Human Mortality and Morbidity, p. 1, 1995

Pope, C.J., *SM Thesis*, Massachusetts Institute of Technology, 1988

Pope, C.J., Marr, J.A., and Howard, J.B., *J. Phys. Chem.*, 1993

Pope, C.J., Personal communication, 1997

Prado, G., and Lahaye, J., in *Particulate Carbon Formation in Combustion*, Siegla, D.C., and Smith, G.W. (eds), Plenum Publishing Corp., p. 143, 1981

Procaccini, C., Personal communication, 1996

Ralston, S.L., Lau, H.H.S., Seidel, A., Luch, A., Platt, K.L., and Baird, W.M., *Cancer Research*, Volume 54, p. 887, 1994

Ritter, E.R., and Bozzelli, J.W., *International Journal of Chemical Kinetics*, Volume 23, Number 9, pp. 767-778, 1989

Samet, J.M., Zeger, S.I., and Berhane, K., "The Association of Mortality and Particulate Air Pollution", in *Particulate Air Pollution and Daily Mortality*. Health Effects Institute, Cambridge MA, 1995

Scott, L.T., and Agopian, G.K., *J. Am. Chem. Soc.*, Volume 99., pp. 4506-4507, 1977

Scott, L.T., Kirms, M.A., Berg, A., and Hansen, P.E., *Tetrahedron Lett.*, Volume 23, pp. 1859-1862, 1982

Scott, L.T., and Roelofs, N.H., *J. Am. Chem. Soc.*, Volume 109, pp. 5461-5465, 1987

Scully, D.B., and Davies, R.A., *Combustion and Flame*, Volume 9, p. 185, 1964

Schwartz, J., Dockery, D.W., Neas, L.M., "Is Daily Mortality Associated Specifically with Fine Particles?", *Journal of the Air and Waste Management Association*, Volume 46, Number 10, p. 927, 1996

Smyth, K.F., and Miller, J.H., *Science*, Volume 236, pp. 1540-1546, 1987

Stein, S.E., Walker, J.A., Suryan, M.M., and Fahr, A., *23rd Symposium (International) on Combustion*, The Combustion Institute, pp. 85-90, 1990

Stone, A.J., and Wales, D.J., *Chem. Phys. Lett.*, Volume 128, p. 501, 1986

Street, J.C., and Thomas, A., *Fuel*, Volume 34, p. 4, 1955

Sun, W.H., *PhD Thesis*, Massachusetts Institute of Technology, 1985

Thijssen, J.H., *PhD Thesis*, Massachusetts Institute of Technology, 1993

Thijssen, J.H., Toqan M.A., Beér, J.M., and Sarofim, A.F., *25th Symposium (International) on Combustion*, The Combustion Institute, pp. 1215-1222, 1994

Tompkins, E.E., and Long, R., *12th Symposium (International) on Combustion*, The Combustion Institute, pp. 625, 1969

Vaughn, C.B., *PhD Thesis*, Massachusetts Institute of Technology, 1988

Weisburger, J.H., and Williams, G.M., *Chemical Carcinogenesis*, Amer. Chem. Soc. Monogr. 182, ed. C.E. Searle, pp. 1323-1373, 1984

Welsch, C.W., *Cancer Res.*, Volume 45, pp. 3415-43, 1985

Westmoreland, P.R., *PhD Thesis*, Massachusetts Institute of Technology, 1986

Woods, I.T., and Haynes, B.S., Brief Communication, *Combustion and Flame*, Volume 85, pp. 523-525, 1991

Wornat, M.J., Sarofim, A.F., and Lafleur, A.L., *24th Symposium (International) on Combustion*, The Combustion Institute, pp. 955-963, 1992